Metabolic Brain-Computer Interfaces

Inaugural-Dissertation

zur Erlangung des Doktorgrades

der Humanwissenschaften

der Medizinischen Fakultät

der Eberhard-Karls-Universität

zu Tübingen

vorgelegt von

Ranganatha Sitaram

aus

Harihar/Indien

2010

Dekan:	Professor Dr. I. B. Auterieth
1. Berichterstatter:	Professor Dr. N. Birbaumer
2. Berichterstatter:	Professor Dr. B. Pichler

To my mother and late father.

Acknowledgements

Contents

Introduction

Brain-Computer Interfaces (BCI) utilise neurophysiological signals originating in the brain to activate or deactivate external devices or computers (Donoghue 2002; Wolpaw, Birbaumer et al. 2002; Nicolelis 2003; Birbaumer and Cohen 2007). The neuronal signals can be recorded from inside the brain (invasive BCIs) or outside (non-invasive BCIs) of the brain. Most BCIs developed so far have used operant training of direct neuroelectric responses, Electroencephalography (EEG) waves, event-related potentials and brain oscillations (Birbaumer, Weber et al. 2006; Birbaumer and Cohen 2007). Compared to neuroelectric studies on regulation of brain activity, there have been fewer studies with metabolic signals from the brain (Sitaram, Caria et al. 2007; Weiskopf, Sitaram et al. 2007; Sitaram, Weiskopf et al. 2008). Near Infrared Spectroscopy (NIRS) and Functional magnetic resonance imaging (fMRI) present themselves as attractive methods of acquiring hemodynamic activity of the brain for a developing a BCI. In this study, we exploit NIRS and fMRI for the implementation of BCIs for the investigation of regulation of hemodynamic signals in the brain and their behavioural consequences. We propose that these methods could be used not only for communication and control in paralysis, but also as powerful tools for experiments in neuroscience and rehabilitation and treatment of neurological disorders.

Research on operant training to self-regulate brain responses began with early studies on biofeedback of EEG and single cellular responses (Fetz 1969; Kamiya 1971). Subsequent to this work, many clinical applications were explored in human patients by the biofeedback of EEG oscillations and event-related potentials (Elbert, Rockstroh et al. 1980). In biofeedback, the subject receives visual or auditory on-line feedback of brain activity and tries to voluntarily modify a particular type of brainwave. The feedback signals contain both the information on the degree of success in controlling the signal and the reward. Self-regulation of brainwaves as described in the biofeedback literature was reported to have therapeutic effects on many psychiatric and neurological conditions but only a few studies passed rigorous clinical and experimental testing (Barber, Kamiya et al. 1971–78; Birbaumer and Kimmel 1979).

There are two broad approaches in neuroscience for studying the interaction between brain and behaviour. The first category involves the manipulation of neural substrate itself (Moonen and Bandettini 2000; Feinberg and Farah 2003). Such an intervention might activate a brain area, perhaps by a lesion. An example is the 1861 observation of the link between language and left frontal lobe damage. The effects of stimulation of brain areas can also be studied. An example is Harvey Cushing's study of human sensory cortex in the early 20th century. The second approach is observational in nature, relating a measure of neural function to behaviour. Hans Berger's work in the early 1920s on the human electroencephalographic response is a good example. Tremendous advances and refinements to both approaches have taken place over the last century. For example, beyond the static lesions that have been the mainstay of neuroscience for many years it is now possible to temporarily and reversibly inactivate areas of the human cortex using transcranial magnetic stimulation (TMS). The

branch of observational methodology has also grown impressively in the last few decades, with the development of functional neuroimaging.

Neurofeedback is in a unique position to combine these two approaches. It is in one sense a *manipulative* approach, as the subject is trained to voluntarily change the activity in a certain region of the brain to observe the ensuing changes in behaviour. However, it is in another sense an *observation* approach, as it incorporates the experimental paradigms routinely used in neuroimaging studies. To explain it in another way, traditionally neuroimaging studies treat brain activity as effect of stimulation on behaviour. For example, they evaluate the effects of stimuli (whether visual, auditory, tactile or a combination of these), motor execution, or a specified task performance on brain activity (Moonen and Bandettini 2000; Feinberg and Farah 2003). In that sense brain activity is a dependent variable. In contrast, in neurofeedback studies, one studies the effect of voluntary controlled brain activity on behaviour. In that sense brain activity becomes an independent variable. Using EEG neurofeedback as an approach, studies have been previously carried out on slow cortical potentials (SCP) and their behavioural effects on lexical processing, motor action, emotional responses and musical performance (Rockstroh, Elbert et al. 1990; Egner and Gruzelier 2003). Real-time NIRS and fMRI neurofeedback approaches have the added advantage of targeting a localized brain region, with high spatial resolution and a reasonable temporal resolution adequate for feedback

NIRS utilizes light in the near infrared range (700 to 1000nm) to determine cerebral oxygenation, blood flow, and metabolic status of localized regions of the brain providing a signal analogous to the BOLD signal (Villringer and Chance 1997; Villringer and Obrig 2002; Hoshi 2007). The degree of increases in regional Cerebral Blood Flow (rCBF) exceeds that of increases in regional cerebral oxygen metabolic rate (rCMRO2) resulting in a decrease in deoxygenated haemoglobin in venous blood. Thus, increase in total haemoglobin and oxygenated haemoglobin with a decrease in deoxygenated haemoglobin is observed in activated areas during NIRS measurement. NIRS uses multiple pairs or channels of light sources and light detectors operating at two or more discrete wavelengths. NIRS provides spatially specific signals at high temporal resolution. NIRS instruments could be potentially portable and less expensive than fMRI and Positron Emission Tomography (PET). Subjects can be examined under normal conditions such as sitting in a chair, without their motion being severely restricted, making it suitable for implementing BCIs. However, the depth of brain tissue which can be measured is only 1-3 cm restricting its applications to higher level cortical regions.

Functional magnetic resonance imaging (fMRI) relies on the measurement of task induced blood oxygen level-dependent (BOLD) response (Ogawa, Lee et al. 1990). Although BOLD is an indirect measure, there is growing evidence for a strong correlation between the BOLD signal and electrical brain activity. FMRI measures increases and decreases of paramagnetic load of blood-flow to activated poles of neurons, particularly to apical dendrites (Logothetis, Pauls et al. 2001; Logothetis 2002; Logothetis 2003; Logothetis and Pfeuffer 2004; Logothetis 2008). Studies have characterized the relationship between localized increases in neuronal activity and the corresponding increase in BOLD, making it possible to interpret positive functional

responses in terms of neural activity. Recently, Amir Shmuel, Nikos Logothetis and colleagues have reported a tight coupling between negative BOLD response and decreases in neuronal activity (Shmuel, Augath et al. 2006). In both cases of increase and decrease in BOLD, a correlation with similar changes in local field potentials and multiunit activity have been found.

Functional imaging offers non-invasive recording of the activity across the entire brain with high spatial resolution in the millimetre range. With innovations in high performance magnetic resonance scanners and computers, and developments in techniques for faster acquisition, processing and analysis of MR images, real-time fMRI has recently become a possibility. With improvements in real-time fMRI, a novel type of non-invasive BCI has emerged. Studies that have been reported so far (Posse, Binkofski et al. 2001; Yoo and Jolesz 2002; Weiskopf, Veit et al. 2003; deCharms, Christoff et al. 2004; Weiskopf, Mathiak et al. 2004; Yoo, Fairneny et al. 2004; deCharms, Maeda et al. 2005; Caria, Veit et al. 2007) have demonstrated that human subjects using fMRI-BCI can learn self-regulation of localized brain regions. However, most of these studies are based on conventional univariate statistical parametric mapping (SPM) by measuring brain activity from many thousands of locations repeatedly, but then analyzing each location separately. Furthermore, the previous approaches to fMRI-BCI have used feedback of BOLD activation from single regions of interest. However, it is often difficult to find individual sites where differences in BOLD activations corresponding to different brain states are large enough to allow for efficient decoding. In contrast, it has been shown that pattern-based methods integrate considerably more information for detecting the brain states from measurements of brain activity. In the present study, we incorporate multivariate pattern-based methods for real-time recognition of brain states from fMRI and NIRS signals. We have used this method to classify and feedback brain responses from motor imagery and execution with NIRS signals, and emotional states of the brain (such as happiness, disgust and so forth) with fMRI signals, respectively. Furthermore, the present study investigates self-regulation of brain activity of emotionally relevant brain areas such as the anterior insular cortex in both healthy individuals and psychopathic criminals, and motor related brain areas such as ventromedial prefrontal cortex in healthy individuals and stroke patients.

The fact that operant regulation of brain activity, even single cell responses is possible also in animals argues against the influence of cognitive factors such as explicit imagery on operant brain regulation. On the other hand in humans, imagery and cognitive processing is known to affect learning and physiological regulation. There are very few studies (Roberts, Birbaumer et al. 1989; Birbaumer, Elbert et al. 1990) evaluating the differential contribution of cognitive instructions on the effect of brain regulation. These studies suggest that instruction to imagine facilitates learning in the early stages, but feedback is more important for successful cortical regulation. Whether these results can be generalized to the regulation of subcortical structures, and additionally to the metabolic brain response remains an open question that will be investigated in this study.

Chapter 1 provides an introduction to functional Near Infrared Spectroscopy (fNIRS), considering the theoretical underpinning of fNIRS, practical issues with

regard to signal acquisition and analysis, and finally its applications to functional brain imaging.

Chapter 2 describes our study with fNIRS for implementing a BCI by online classification of the motor imagery signals. We describe in detail the signal acquisition, pre-processing, analysis, and comparison of online classification using two different machine learning approaches, namely, support vector machines (SVM) and hidden Markov models (HMM).

Chapter 3 provides an in-depth presentation of fMRI-BCIs in terms of the technological advance and our implementation, and the results of our preliminary studies on the regulation of anterior insula; regulation of the right inferior frontal gyrus and its effect on language processing; and the regulation of ventrolateral premotor cortex with motor imagery.

Chapter 4 presents our approach for online recognition of brain states by classifying fMRI signals using SVM, and the application of this approach to real-time detection and feedback of discrete emotional states of the brain.

Chapter 5 is a presentation of our experimental investigation of the effects of volitional regulation of left anterior insula both in terms of cerebral reorganisation and behavioural effects in healthy individuals as well as in psychopathic criminals.

Chapter 6 is the concluding chapter that contains a discussion of the Hemoneural hypothesis that could potentially explain how volitional regulation of BOLD signal from a circumscribed brain region could influence neural activation and behaviour.

Functional Near Infrared Spectroscopy

Introduction

Near Infrared Spectroscopy is emerging as a portable, affordable and non-invasive neuroimaging system suited for the development of brain-computer interfaces. Although fNIRS has been in use since the 1970s (Jobsis 1977) for clinical and scientific studies of tissue oxygenation, cerebral blood flow and metabolism, its use in BCIs has been more recent (Coyle, Ward et al. 2004; Sitaram, Hoshi et al. 2005; Naito, Michioka et al. 2007; Sitaram, Zhang et al. 2007). fNIRS technology has now progressed to an extent where a number of commercial instruments are available making it an accessible tool for functional neuroimaging, in general, and BCI development in particular. With exciting developments in portable fNIRS instruments incorporating wireless telemetry (Shiga, Yamamoto et al. 1997; Atsumori, Kiguchi et al. 2007; Kiguchi, Ichikawa et al. 2007), it is now possible to monitor brain activity from freely moving subjects (Hoshi 2007) thus enabling more dynamic experimental paradigms. The objective of this section is to provide an introduction to fNIRS.

Basic Theory of NIRS

It has been well known for many years in the field of medicine that the functional state of living tissue has influence on the properties of light passing through it. Since then, changes in optical properties of brain cells have been reported in cell cultures, brain cells and intact cortical tissue (Villringer and Chance 1997; Villringer and Obrig 2002). Recently, functional near infrared spectroscopy (fNIRS), which assesses the physiological changes associated with brain activity non-invasively has become possible. As an introduction to how functional maps of brain activity are generated, we need to look:

- the interaction of light with brain tissue which may be measured by optical methods (optical parameters), and
- the physiological events associated with brain activity (physiological parameters).

Interaction of light with brain tissue

Photons that enter tissue may undergo the following major types of interaction: absorption and scattering. An optical device that consists of one or more light sources by which the tissue is irradiated and one or more light detectors that receives light after it has been transmitted or reflected from tissue could be used to measure the interaction. Light that travels through tissue is attenuated due to absorption and scattering. By analogy with a photometer, the attenuation of light in tissue could be expressed mathematically in a modified Beer-Lambert law.

The Beer-Lambert Law states that the light attenuation is proportional to the concentration of the absorbing molecules. That is,

$$A = \varepsilon \times c \times d$$

Where A is the light attenuation, ε is the molar absorption coefficient of the absorbing molecules, c is the concentration of the absorbing molecules, and d is the optical pathlength.

However, this relationship assumes infinitesimal concentrations and disregards scattering. This assumption does not hold for spectroscopy in tissue. Scattering prolongs the pathlength of the light and thus the pathlength becomes longer than the distance between sending and receiving optodes. In order to account for the longer length, in a modified Beer-Lambert Law a differential pathfactor (DPF) B is introduced. Further, light may be lost due to scatter, not reaching the detector. Therefore, in second modification of the Beer-Lambert Law a term, G is introduced. Now, the modified law is:

$$A = \varepsilon \times c \times d \times B + G$$

Assuming constant B &G gives:

$$\Delta A = \varepsilon \times \Delta c \times d \times B$$

If the pathlength d x B can be determined, absolute changes in concentration can be calculated. For absolute measurements of the pathlength there are several types of optical approaches. One uses the measurement of the direct time of flight of a short (ps) light pulse traveling through tissue. In another approach the phase shift of a light source which is intensity-modulated at a certain frequency is measured. A third approach measures water absorption which, assuming a constant water concentration in tissue, should change with the pathlength of light. The above mentioned approaches for the determination of pathlength may also serve to measure light scattering (or changes in light scattering) as another optical parameter.

Physiological changes during brain activity

Regional brain activation is accompanied by increases in regional cerebral blood flow (rCBF) and the regional cerebral oxygen metabolic rate (rCMRO2). The degree of the increase in rCBF exceeds that of the increase in rCMRO (Fox and Raichle 1986) resulting in a decrease in deoxyhemoglobin (deoxy-Hb) in venous blood. Thus, increases in total hemoglobin (t-Hb) and oxyhemoglobin (oxy-Hb) with a decrease in deoxy-Hb are expected to be observed in activated areas in NIRS measurements. Studies have observed both no change in t-Hb with an increase in oxy-Hb and a reciprocal decrease in deoxy-Hb, and an increase or no change in deoxy-Hb accompanying increases in t-Hb and oxy-Hb (Hoshi 2007). Using a perfused rat brain model, Hoshi and colleagues, examined the direct effects of each change in CBF and CMRO2 on cerebral hemoglobin oxygenation to interpret NIRS signals. They reported that the directions of changes in oxy-Hb are always the same as those of rCBF, whereas the direction of changes in deoxy-Hb is determined by changes in venous blood oxygenation and volume. Small changes in CBF are not accompanied by those in t-Hb. Thus, oxy-Hb is the most sensitive indicator of changes in rCBF in NIRS measurements.

NIRS signal acquisition techniques

There are 3 techniques for NIRS signal acquisition: continuous wave spectroscopy, time-resolved spectroscopy and frequency-domain techniques (Villringer and Chance 1997; Villringer and Obrig 2002).

Continuous wave is the approach used in our current work. It uses a light source with discrete wavelengths. The light source may be a laser or a light emitting diode (LED). The optical parameter measured is attenuation. Commercially available CW-type instruments use a continuous wave of light as the source with discrete wavelengths – typically between 2 and 7, or a light source emitting across the entire spectrum. The only optical parameter measured is attenuation. The light source may be a laser or a LED (for the discrete wavelength approach) or a simple halogen lamp (for the continuous spectrum approach). The advantages of CW-approach are its simplicity and flexibility; also a very high signal-to-noise ration is achieved. A disadvantage is a strong contribution to the signal changes by superficial, extra cerebral structures. The separation of deep and superficial layers can be approximated by multiple source-detector separations.

Time resolved spectroscopy uses pulsed light source with a pulse duration in the order of picoseconds. In addition to the assessment of total light intensity, this technique assesses the distribution of photon arrival times. Based on this additional parameter, a multilayer depth resolution can be made. Further, by assessment of the individual differential path length factor, the quantification of the concentration changes can be improved.

Since time-resolved measurements require rather demanding technology, frequency-domain monitors have been developed to more easily assess the mean time of flight of photons. Instead of using pulsed light source the intensity of the injected light is sinusoidally modulated at a high frequency (100-150 MHz). The reflected light will also show this modulation. The phase delay of the modulation is proportional to the mean time of flight. This is called Phase-modulated Spectroscopy (PMS) or Frequency Domain NIRS System. All of the above-mentioned approaches may be performed over one single site (one channel) or many sites (multi-channel).

A portable NIRS instrument (for example: the HEO 200, from Omron Ltd. Inc., Tokyo, Japan) allows subjects to move about during measurement. It consists of a main unit and a probe unit. The main unit comprises a central processing unit (CPU), light emitting diode (LED) driver, amplifier, memory card interface, liquid crystal display, and power source. The probe unit moulded in black elastic silicon rubber, has a photodiode in the centre and two-wavelength (760 nm and 840 nm) near infrared LEDs on either side. A wireless system was combined with this portable NIRS system so that data could be seen in real time at a place distant from the subject. The instrument is connected to the transmitter of a wireless telemetry system by a RS232C cable. The NIRS instrument (8 x 16 x 4 cm) is as small as the transmitter of the wireless system. NIRS signals are sent by the wireless to the receiver, which is connected to a laptop computer on which data are displayed in real time. NIRS signals can be transmitted to a location at a maximum distance of 30 m outdoors and 10 m indoors.

NIRS signal analysis

Unlike fMRI signal preprocessing and analysis methods that have been standardized under univariate statistical parametric mapping (SPM), fNIRS analysis has not yet seen the unification of methods. In the majority of studies, comparison of fNIRS mean signals between the resting and activation states has commonly been performed using a paired *t-test* (Hoshi 2007). Recently, a number of different types of analyses including model-based, event related and a combination of these have been reported in literature (Schroeter, Bucheler et al. 2004; Huppert, Hoge et al. 2006), (Plichta et al., 2007). Hoshi (Hoshi 2007) suggests that model-based methods, as used in fMRI and PET signal analysis, may not be directly suitable for fNIRS data because of the varying pattern of hemodynamic data with each measurement and the difficulty in deriving a proper hemodynamic response function. Furthermore, even under resting conditions, the Hb oxygenation state fluctuates ((Toronov, Franceschini et al. 2000) (Schroeter, Bucheler et al. 2004)). These fluctuations are divided into two types: one is systemic fluctuations related to physiological activities such as the systemic arterial pulse oscillations (1 Hz) and respiration (0.2 to 0.3 Hz), and the other is the slower Hb wave fluctuation of frequency 0.05 Hz, with varying temporal patterns across brain regions. Due to these fluctuations fNIRS signals not return to the original levels immediately after the activation state. Novel signal correction and analysis techniques need to be developed to overcome the current limitations. While commercial manufacturers of fNIRS instrument provide custom-built analysis software packages, a freely available data analysis program written by the Photon Migration Imaging Lab at the Massachusetts General Hospital in Boston allows for basic signal processing, linear modeling and image reconstruction of fNIRS data of brain function (http://www.nmr.mgh.harvard.edu/PMI/resources/homer/home.htm).

Benefits and limitations of NIRS

NIRS is completely non-invasive and potentially portable. Subjects can be examined under normal conditions such as sitting in a chair, without their motion being severely restricted. NIRS does not have the disadvantages of motion related artifacts that EEG has. The portable, telemetric version of the NIRS instrument enables activation studies on freely moving objects. For all these reasons, NIRS could be expected to make significant contributions to functional neuroimaging and BCI development.

Currently, the major limitation NIRS concentration changes in Oxy-Hb cannot be quantified with CW-type instruments hindering NIRS from being widely employed in clinical medicine and research. Many different approaches to quantification have been tried, and the quantitative accuracy of time resolved spectroscopy (TRS) and of phase-resolved spectroscopy (PRS) has been established. However, the difficulty of quantification has not yet been completely overcome (Hoshi 2007). It is to be noted that it is not mandatory to know the absolute concentration changes for the development of BCIs, as relative changes can be used successfully in pattern classification of brain states and neurofeedback applications (Sitaram, Hoshi et al. 2005; Sitaram, Zhang et al. 2007).

Functional imaging with NIRS

The advantages of NIRS, namely, high temporal resolution (less than 1s), non-invasive measurement, portability and less motion restriction allowing monitoring in

natural environments, enable neuroimaging studies on subjects who have not been fully examined until now, such as children, the elderly, and patients with psychoneurological problems, as they are difficult to measure by other neuroimaging techniques, such as PET and fMRI.

NIRS has been applied, in neonates and infants, to investigate evoked responses to visual, olfactory, and auditory stimulation, and passive knee movement (Hoshi 2007). Several research groups have examined task-related hemodynamic changes in psychiatric patients and found task-dependent abnormalities in frontal hemodynamics in schizophrenia (Shinba, Nagano et al. 2004) and depression (Suto, Fukuda et al. 2004). Such task-dependent abnormalities were also found in patients with Alzheimer's disease (Fallgatter, Roesler et al. 1997; Hock, Villringer et al. 1997). Possibilities to monitor brain activity in the daily life environment open new dimensions in neuroimaging studies, as the study by Miyai colleagues (Miyai, Tanabe et al. 2001) showed by using 30-channel CW-type instrument to generate cortical activation patterns associated with human gait. This indicated that NIRS was useful for evaluating cerebral activation patterns during pathological movements and rehabilitation intervention.

A portable single-channel NIRS instrument combined with a wireless telemetry system allows subjects to move during measurements as with portable electrocardiogram (ECG) and EEG instruments. The details of the portable NIRS instrument (HEO 200, Omron Ltd. Inc., Kyoto, Japan) have been reported by (Shiga, Yamamoto et al. 1997). This NIRS system makes it possible to monitor brain activity of freely moving subjects outside of laboratories (Hoshi et al., 2006).

Since EEG, MEG, fMRI and PET measure different aspects of the brain function and have different merits and demerits, combined measurements with multiple modalities are expected to be complementary. As the optical characteristics of the NIRS system does not conflict with electrical or magnetic systems, a number of combined experiments have been reported. To investigate the neurovascular coupling in the human brain, NIRS is appropriate because its temporal resolution is high, and it can be combined with electrophysiological methods, such as EEG and MEG. Simultaneous measurements with NIRS and electrophysiological methods have also been employed for studies of higher brain functions (Horovitz and Gore 2004). NIRS can also be combined with TMS, much more easily than PET or fMRI, and has recently been employed this way to study the hemodynamic pattern due to stimulation (Noguchi, Watanabe et al. 2003; Mochizuki, Ugawa et al. 2006).

BCI development with fNIRS

The first experiments to use fNIRS for the purpose of developing BCIs was carried out separately by Sitaram and colleagues (Sitaram, Hoshi et al. 2005) Coyle and colleagues (Coyle, Ward et al. 2004), who studied the optical response to motor imagery in healthy subjects to demonstrate oxy-Hb concentration increases and deoxy-Hb concentration reductions in the contra-lateral hemisphere, as compared to the rest state. Sitaram and colleagues used overt and covert finger tapping of left and right hands to note that motor imagery produced similar but reduced activations in comparison to motor execution. Coyle and colleagues instructed subjects to imagine continually clenching and releasing a ball. The BCI system provided visual feedback

by means of a circle on the screen that shrunk and expanded with changes in hemoglobin concentration. An intensity threshold of the hemoglobin concentration from the contralateral optodes on the motor cortex (for comparison: near the C3/C4 electrodes in an equivalent 10-20 system) was used to determine if the brain was in a rest or activation state.

In a follow-up to the above experiments, Coyle and colleagues (Coyle, Ward et al. 2007) used their custom-built fNIRS instrument to demonstrate a binary switching control called the 'Mindswitch', while Sitaram and colleagues (Sitaram, Zhang et al. 2007) demonstrated that patterns of fNIRS signals during motor execution and imagery can be decoded with over 80% accuracy with two different machine learning algorithms. The Mindswitch operates in a synchronous mode, meaning that the system is active only during defined periods (Coyle, Ward et al. 2007), with the objective of establishing a binary yes or no signal for communication. The fNIRS signal used for this purpose was derived from a single channel on the left motor cortex elicited by imagined movement of the right hand. The protocol consisted of two options alternately presented to the user and highlighted by the controlling software. When the desired option is highlighted, the user performs motor imagery to enhance the oxy-HB signal in the motor cortex to indicate his choice. Subjects were instructed to imagine clenching a ball with their right hand while attending to the kinaesthetic experience of movement. Experiments with healthy subjects showed that the number of correct classifications to the total number of trials was on the average more than 80%.

Sitaram and colleagues (Sitaram, Zhang et al. 2007) used a continuous wave, multichannel fNIRS instrument (OMM-1000 from Shimadzu Corporation, Japan) to measure oxy-HB and deoxy-HB concentration changes from 20-channels on the motor cortex in each hemisphere during motor execution and imagery. Acquired signals were processed to remove artifacts from heart beat and high frequency noise from muscle activity, and the time series of amplitude changes of oxygenated hemoglobin and deoxygenated hemoglobin in the period 2–10 s after stimulation for the motor task to start for each trial were extracted from the preprocessed data and fed to two different pattern classification systems, namely, Support Vector Machine (SVM) and Hidden Markov Model (HMM). Typically, most channels on the contralateral hemisphere showed activation by an increase in oxygenated hemoglobin and decrease in deoxygenated hemoglobin, while the channels on the ipsilateral hemisphere either showed a similar response but to a smaller extent, or in a reversed manner (increase in deoxygenated hemoglobin and decrease in oxygenated hemoglobin) potentially indicating inhibition. Topographic images reconstructed from oxy-HB and deoxy-HB concentration changes showed distinct patterns of activations (yellow and red pixels) and inhibitions (green and blue pixels) to left-hand and right-hand motor imagery, although inter-subject variability in the patterns were observed (Sitaram, Zhang et al. 2007). Finger tapping data were classified with better accuracy compared to motor imagery data by both classification techniques for all the subjects. Between the two pattern classification techniques, HMM performed better than SVM for both finger tapping and motor imagery tasks. The authors hypothesized that inconsistencies in imagery create difficulties for robust generalization in a classifier, and hence a probability network of HMM could perform better in these circumstances.

The first direct investigation of fNIRS-BCI in locked-in patients suffering from amyotropic lateral sclerosis (ALS) was performed by Naito and colleagues (Naito, Michioka et al. 2007). The study included 40 male and female ALS patients, among whom 17 were in totally locked-in state. Naito and colleagues applied single-channel two-wavelength (770nm and 840nm) measurement on each patient's forehead to monitor changes in blood volume during the experiment. A simple 'yes' or 'no' binary communication method was employed where the subject was asked a question, and if the subjective answer to the question was 'yes' the patient indicated it by performing a mental calculation, singing fast or thinking. If the subjective answer was 'no', the patient indicated it by relaxing. Instantaneous amplitude and phase of the fNIRS signal was then calculated and used as input to a discriminant analysis to classify between the two answers. The discrimination of answers was reported to be successful for 70% of ALS patients not in the totally locked-in state, and 40% for totally locked-in patients. For the successful cases, the average rate of correct detection of answers was about 80%. The low applicability of the method to totally locked-in patients was attributed to the presence of only spontaneous low frequency oscillations with no brain responses specific to the questions. The authors suggested lack of motivation and low levels of brain activation as possible reasons for this problem, and highlighted the importance of maintaining a means of communication in ALS patients. In addition to its application for communication and control, fNIRS-BCI is considered to be a potential approach for movement restoration in stroke and paralysis due to neuroanatomical specificity in measuring activations from the motor cortex.

Chapter 2

Implementation of an fNIRS Brain-Computer Interface

Introduction

BCI can provide an alternative communication channel and environmental control capability to severely disabled persons. The quality of life depends on the possibility to communicate with the social environment. Disabled patients with appropriate physical care, and cognitive ability to communicate with a BCI, can continue to live with a reasonable quality of life over extended periods of time (Wolpaw, Birbaumer et al. 2000). Brain–computer interfaces have been developed with surface electroencephalogram (EEG), electrocorticogram (ECoG) and implanted electrodes (Birbaumer, Ghanayim et al. 1999; Wolpaw, Birbaumer et al. 2000; Nicolelis and Chapin 2002; Serruya, Hatsopoulos et al. 2002; Wolpaw, Birbaumer et al. 2002; Birbaumer, Hinterberger et al. 2003; Nicolelis 2003; Wolpaw 2004; Birbaumer 2006; Birbaumer 2006; Wolpaw, Loeb et al. 2006; Birbaumer and Cohen 2007). Surface EEG has many advantages: it is non-invasive, technically less demanding, and widely available at low cost. It has a long history of usage, and its mechanisms are well known. However, EEG has certain disadvantages: long-term application and fixation of electrodes are difficult, portable devices are artifact prone, and it has low spatial resolution. Other non-invasive methods of monitoring brain activity, such as magnetoencephalography (MEG), positron emission tomography (PET) and functional magnetic resonance imaging (fMRI) could in principle provide the basis for a BCI (Babiloni, Cincotti et al. 2001; Birbaumer and Cohen 2007; Sitaram, Caria et al. 2007; Weiskopf, Sitaram et al. 2007; Sitaram, Weiskopf et al. 2008).

More recently, near-infrared spectroscopy (NIRS) promises flexibility of use, portability, metabolic specificity, good spatial resolution, localized information, high sensitivity in detecting small substance concentrations and affordability (Villringer and Obrig, 2002). NIRS has no doubt certain disadvantages. It is slow to operate because of the inherent latency of the hemodynamic response. The signal strength is affected by hair on the head. Furthermore, relative motion of the optodes on the hair may introduce motion artifacts and drifts in the hemodynamic signal. Nevertheless, NIRS' ability to record localized brain activity with a spatial resolution in the order of centimeter (depending on the probe geometry) provides us with an excellent opportunity to control a variety of motor and cognitive activities in a BCI. The main goal of the present study was to ascertain the feasibility of using near-infrared spectroscopy for developing a BCI. We chose motor imagery of left-hand and right-hand as the paradigm of BCI control as it has been shown to work well in previous research on EEG-based BCIs (Pfurtscheller, Guger et al. 2000; Pfurtscheller, Neuper et al. 2000; Pfurtscheller, Graimann et al. 2004; Pfurtscheller, Muller-Putz et al. 2006). Our objective was to develop a viable set of methods for offline processing and classification of NIRS data, with the intention of incorporating them later on in an online BCI. To this end, we explored the use of two pattern recognition techniques,

Support Vector Machines (SVM) and Hidden Markov Model (HMM), for classifying NIRS signals.
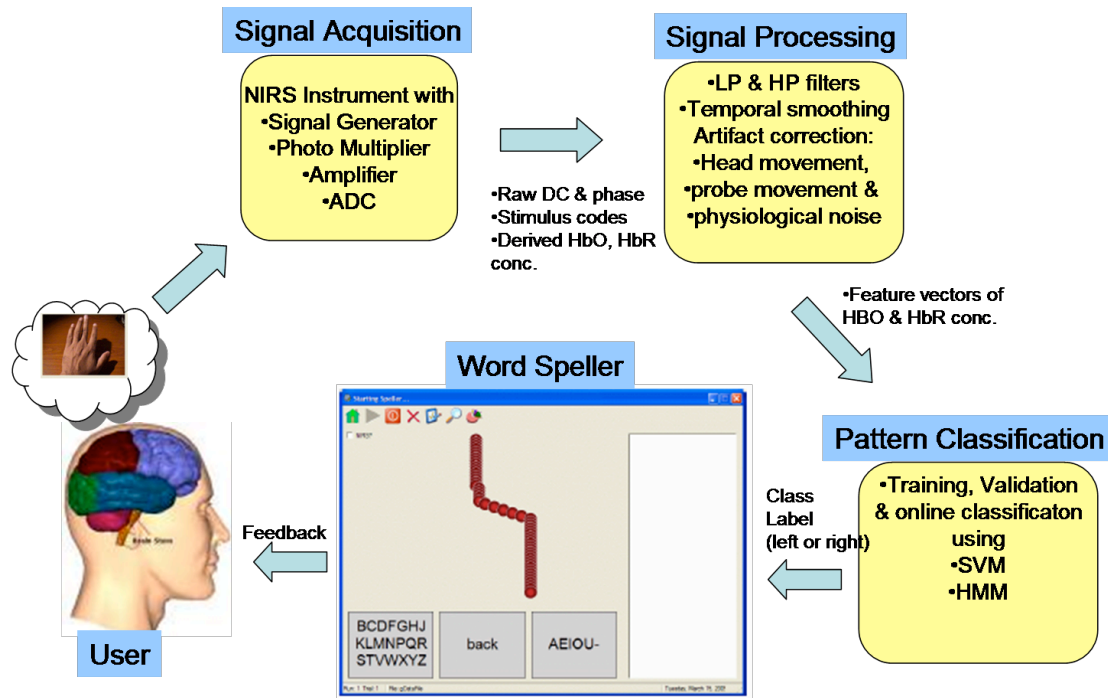
Figure 2.1: *Architecture of the Near Infrared Spectroscopy BCI (NIRS-BCI). Multi-channel NIRS signals from both hemispheres are acquired in real-time, processed, classified online by either a support vector machine (SVM) or a Hidden Markov Model (HMM), and translated for driving the word speller application.*

It has been shown in electrophysiological studies (Beisteiner 1995) that brain activation during motor imagery (imagination of left and right hand movement) is similar to the activation during actual execution of movement. In the above study, changes of DC potentials between task execution and imagination were localized in central recordings (C3, Cz, C4) with larger amplitudes during execution of the task than when only imagining to do so. Primary motor cortex was active in both the tasks. Benaron et al. (Benaron, Hintz et al. 2000) demonstrated optical response resulting in the contralateral hemisphere around 5-8 s after the onset of movement. Sitaram et al. (Sitaram, Hoshi et al. 2005) and Coyle et al. (Coyle, Ward et al. 2004) reported similar optical response using slow NIRS signals during overt and covert hand movements. Pfurtscheller's team have (Pfurtscheller, Guger et al. 2000; Pfurtscheller, Neuper et al. 2000; Pfurtscheller, Graimann et al. 2004; Pfurtscheller, Muller-Putz et al. 2006) reported a direct EEG-based BCI using motor imagery. It is important that for a BCI to be user-friendly, the mental task should be easy to learn. A BCI can be developed by classifying the NIRS response of the left hand motor imagery (or over movement) from that of the right hand imagery (or overt movement). In this way, a two-choice system can be developed, which can be used to develop a communication system, such as a word speller.

We applied both SVM and HMM to the classification problem. SVMs are learning systems developed by (Vapnik 1998). SVM has been demonstrated to work well in a number of real-world applications including BCI (Blankertz, Curio et al. 2001). A

Markov model is a finite state machine which can be used to model a time series. HMMs were first successfully applied for speech recognition, and later in molecular biology for modeling the probabilistic profile of protein families (Rabiner 1989; Rabiner and Juang 1993). HMM has been successfully used in a BCI application for online classification of EEG signals acquired during left-hand and right-hand motor imagery (Obermaier, Guger et al. 1999; Obermaier, Guger et al. 2001). To our knowledge, this is the first time that SVM and HMM techniques have been used to classify NIRS signals for the development of a BCI. Here, we describe the experimental paradigm of motor imagery; method of signal acquisition; preliminary signal analysis to test whether there are significant patterns in the hemodynamic response to motor imagery; offline classification of the NIRS signal using two classification techniques (SVM and HMM); and finally the results of signal processing, analysis and classification. We end with a discussion of the application of these techniques to the online classification problem towards developing a communication system for completely paralysed patients, and further applications of NIRS-BCI to movement restoration after stroke.

Materials and Methods

Subjects

Five healthy subjects (3 males and 2 females, mean age = 30) voluntarily participated in the study. None of the recruited subjects had neurological or psychiatric history, or was on medication. Each of them gave written informed consent for the experiment. The experiment was approved by the Ethical Committee of the Tokyo Institute of Psychiatry, Japan.

Experimental Procedure
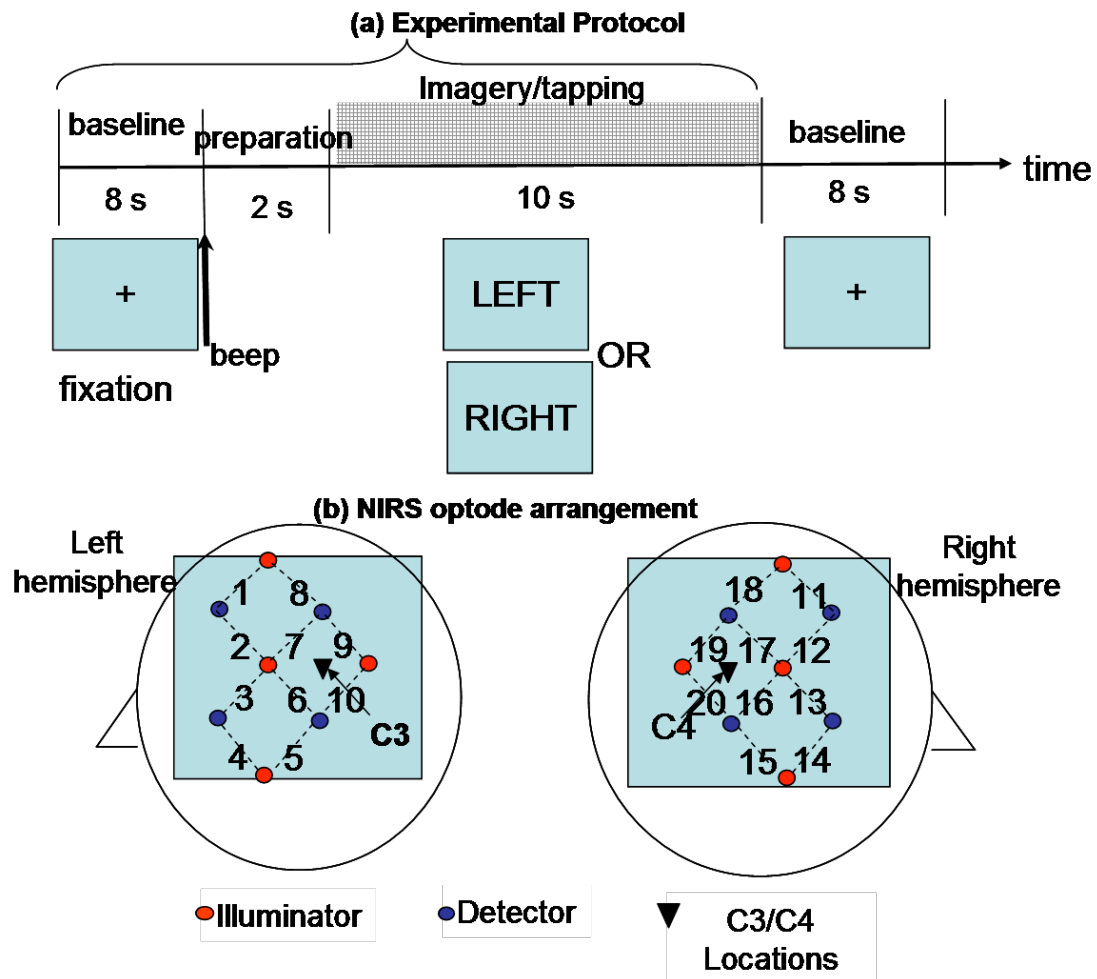
Figure 2.2: *(a) Experimental paradigm for finger tapping and motor imagery for collecting NIRS signals from subjects. Each trial consisted of a baseline block of 8 s, a preparation block of 2s and motor task block of 10 s. Finger tapping and motor imagery data were collected in separate sessions. The type of task (left or right hand) was specified on the computer screen, in a pseudo-random manner. During the task, subjects performed 3-4 number of self-paced overt execution or imagination (as specified) of finger tapping of the specified hand within the 10 s duration of the task. (b) Multichannel NIRS optode arrangement on the scalp. The optodes were arranged on the left and right hemisphere on the subject's head, above the motor cortex, around C3 (left hemisphere) and C4 (right hemisphere) areas (International 10-20 System). A pair of illuminator and detector optodes formed one channel. Four illuminators and 4 detectors in the arrangement resulted in 10 channels.*

NIRS signals were collected from each subject performing both overt motor execution (finger tapping) and covert motor imagery with left hand and right hand. Figure 2.2(a) shows the schematic diagram of the protocol. During the experiment, the subject sat on a chair in a quiet room in front of a computer screen which displayed the stimuli. A single trial comprised of a baseline block, a preparation block and a motor task block, in that order. Each trial started with a baseline block during which the subject fixated on the cross displayed on the screen for 8 s. This was followed by a beep indicating the subject to get ready for the motor task. The preparation phase lasted for 2 s. Following this, the subject performed the motor task as indicated on the screen for a

period of 10 s. The type of motor task to be performed was indicated by the text on the computer screen - 'LEFT' for left-hand motor task and 'RIGHT' for right-hand task. During the finger tapping task, subjects performed 3-4 number of self-paced tapping of fingers of the specified hand within the 10 s duration of the task. During the motor imagery task, subjects performed equal number of self-paced imagination of finger tapping.

Data for finger tapping and imagery were collected in two separate sessions. Each of left hand and right hand tasks for finger tapping and imagery was carried out for totally 80 trials, in four blocks of 20 trials each, with a rest period of 2 m between blocks.

Signal Acquisition

We used a multi-channel NIRS instrument (OMM-1000 from Shimadzu Corporation, Japan) for acquiring oxygenated hemoglobin and deoxygenated hemoglobin concentration changes during motor imagery. The system operated at three different wavelengths of 780nm, 805nm and 830nm, emitting an average power of 3 mW mm^{-2}.

The illuminator and detector optodes were placed on the scalp. The detector optodes were avalanche photodiodes fixed at a distance of 2 cm from the illuminator optodes. The optodes were arranged on the left and right hemisphere on the subject's head, above the motor cortex, around C3 (left hemisphere) and C4 (right hemisphere) areas (International 10-20 System). A pair of illuminator and detector optodes formed one channel. Four illuminators and 4 detectors in the arrangement resulted in 10 channels on each hemisphere, as shown by the dashed lines in the Figure 2.2(b). Near-infrared rays leave each illuminator, pass through the skull and the brain tissue of the cortex, and are received by the detector optodes. The photomultiplier cycles through all the illuminator-detector pairings to acquire data at every sampling period. The data were acquired at a sampling rate of 14Hz and digitized by the 16-bit analog to digital converter.

The NIRS instrument was capable of storing the raw signal intensity values for each of the 3 wavelengths, the stimuli codes (1 for left hand task and 2 for right hand task), as well as the derived values of oxygenated and deoxygenated hemoglobin concentration changes for all time points in an output file in a pre-specified format. The signal preprocessing, analysis and classification programs were implemented to read the data from the file either in an offline mode or in an online mode.

Preliminary Signal Analysis

Our objective, in carrying out this preliminary analysis, was to observe the responses of oxygenated hemoglobin and deoxygenated hemoglobin at different channels on both hemispheres due to left hand and right hand imagery tasks. The intention was to check if there were significant patterns or trends in the data. Offline analysis was performed using a custom Matlab NIRS data analysis program (HomER version 4.0, available for public download and use at http://www.nmr.mgh.harvard.edu/PMI/). A caveat was that, the HomER toolkit accepted only the raw intensity data as input to compute the oxygenated hemoglobin and deoxygenated hemoglobin concentration

changes using the modified Beer Lambert equation (Villringer and Obrig 2002). For this reason, we could not use the hemoglobin concentration changes obtained from the NIRS instrument directly in this analysis.

Preprocessing started with the raw intensity data from all channels being normalized to compute a relative (percent) change by dividing each value by the mean of the data.

$$NormIntensity(t) = Intesity(t) / MeanIntensity$$

The intensity normalized data were then low-pass filtered using the Chebyshev Type II filter of order 3 with a cut-off frequency of 0.7 Hz and Pass-band (ripple) attenuation 0.5 dB. After filtering, a value of 1.0 was added to make the mean of the data equal to unity. The change in optical density, called delta-optical density, was then calculated for each wavelength as the negative logarithm of the normalized intensity.

$$\Delta OD = -Log(NormIntensity(t))$$

Following the calculation of delta-optical density, two different principal component analysis (PCA) filters were applied to the data. The first PCA filter corrected for motion in the data, i.e., subject head movement. The second PCA filter used the principal components of the baseline data to project out systemic physiology. The resulting covariance reduced delta-optical density was used to calculate the change in concentration (delta-concentration) from the modified Beer-Lambert law. For each of the two wavelengths, Lambda#1 = 780nm and Lambda#2 = 805nm, 2 simultaneous equations can be written to equate delta-optical density to oxygenated hemoglobin (HbO$_2$) and deoxygenated (Hb) concentration changes as below:

$$\Delta ODLambda\#1 = \varepsilon_{Hb}^{Lambda\#1} * L * [Hb] + \varepsilon_{HbO_2}^{Lambda\#1} * L * [HbO_2]$$
$$\Delta ODLambda\#2 = \varepsilon_{Hb}^{Lambda\#2} * L * [Hb] + \varepsilon_{HbO_2}^{Lambda\#1} * L * [HbO_2]$$

where ε is the molar absorption coefficient for Hb and HbO$_2$ at the two wavelengths specified and L is the optical path length. Solving the two equations obtains the concentration changes for oxygenated and deoxygenated hemoglobin:

$$\Delta HbX = (e^T e)^{-1} e^T [\Delta OD]$$

We used a differential-pathlength factor of 6.0 and partial volume correction of 50, as can be set in the advanced filtering options of the toolbox. As the sampling rate for signal acquisition was 14 Hz, we obtained 140 delta-concentration values, each for oxygenated hemoglobin and deoxygenated hemoglobin, during a 10 s motor imagery task of each trial.

The data were then block averaged after specifying the pre- (5) and post-stimulus (140) time points for averaging, multiple stimulus conditions (1 for left hand imagery, and 2 for right hand imagery), and their timings. Block averaging was performed on each condition (left hand and right hand imagery) separately, first on a single run and later on across all data files. Statistical effects analysis based on Analysis of Variance (ANOVA) was conducted on the hemodynamic responses.

Following averaging, for each of the conditions (left hand and right hand imagery), images of hemodynamic activations superimposed on the probe geometry were constructed. Image reconstruction in HomER currently supports the back-projection methods and linear forward models created from semi-infinite (homogeneous) slab geometries. For details, please refer to the HomER User's Guide (available for public download and use at http://www.nmr.mgh.harvard.edu/PMI/). We used the following values for the image reconstruction constants in HomER: absorption and scattering coefficients (10 and 0.2), voxel dimensions (Y: 4.00:0.40:4.00, X: -4.00:0.65:9.00), and reconstruction depth (2:2:2). The results of the signal analysis will be discussed under the Results section.

Pattern Classification

Pattern classification was performed on the raw signals obtained from the signal acquisition process after the signal preprocessing operations described below. We did not re-use the processed signals from the preliminary analysis (section 2.4) for pattern classification, as the intentions of the two methods were quite different. However, in future, some of the artifact removal techniques used in HomER, such as principal component analysis (PCA) for head motion correction and systemic physiological changes, could be employed to potentially improve classification accuracy.

First, the acquired signals were processed to remove artifacts from heart beat and high frequency noise from muscle activity. We applied the Chebyshev type II filter (Parks 1987) (Parks 1987) that has a flat pass band, a moderate group delay, and an equiripple stop band. The filter was designed using "cheb2ord" and "cheby2" functions in Matlab (Mathworks, Inc., USA), using cut-off frequency at 0.7 Hz, stop frequency at 1 Hz, pass-band loss at no more than 6 dB, and at least 50 dB of attenuation in the stop-band.

Times series of amplitude changes of oxygenated hemoglobin and deoxygenated hemoglobin in the period 2-10 seconds after stimulation for the motor task to start for each trial were extracted from the preprocessed data and fed to the pattern classification system. In the following subsections, we shall describe the implementation of two different pattern classification techniques, namely, support vector machines and hidden Markov model.

Support Vector Machine (SVM)

The classification task is based on two separate sets of training data and testing data containing several instances of data. Each instance in the training set contains one *target value*, called the class label and several *attributes* or feature*s*. The goal of SVM is to produce a model which predicts target values in the testing set when only the attributes are given.
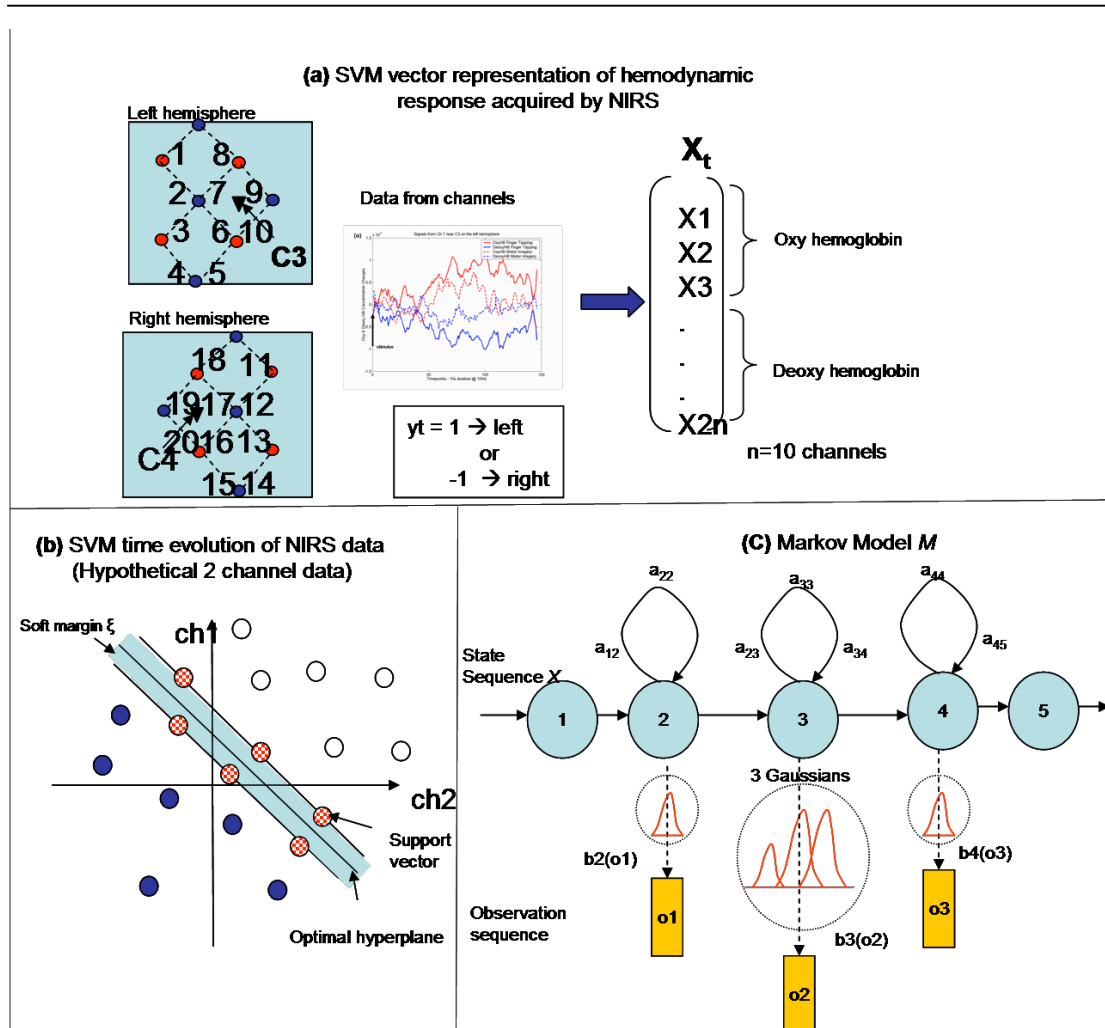
Figure 2.3: *(a) As input to the pattern classifier, a feature vector X_t, containing the concentration values of the oxygenated hemoglobin and deoxygenated hemoglobin from the 20 channels of optodes from both hemisphere, was created for each trial duration of interest of the motor task (2-10 s in this case). For each trial period t, y_t represents the type of task the subject performed, for example, left hand imagery (class = 1) and right hand imagery (class = -1). (b) In the formulation of the SVM, the input feature vector is mapped to a high dimensional feature space through a non-linear transformation function. The SVM algorithm attempts to find a decision boundary or a separating hyperplane in the feature space. (c) Schematic diagram representing the HMM model for motor imagery. The HMM is designed as a left to right model, transitions being allowed from a state to itself and to any right neighbour state. Arrows from left to right indicate the allowed transitions of states. States 1 and 5 were non-emitting, meaning that they do not result in any observations. Observations 2 and 4 were modelled using a single Gaussian while observation 3 was modelled using a mixture of 3 Gaussians.*

By formal notation, the classification problem involves determining a scalar class label y_t from a measurement vector X_t. For classification of the NIRS data from multiple channels from both hemispheres, X_t represents the concentration values of oxygenated haemoglobin and deoxygenated haemoglobin from all the numbered channels (1-20) for the duration of the trial, specified by T ($1 \leq t \leq T$), and y_t is the experimental value of the task for that time (Figure 2.3(a)). For each trial period t, y_t represents the type of task the subject was performing, for example, left hand imagery

(class = 1) and right hand imagery (class = -1). During the experimental procedure for collecting training data, as the subject performs alternating trials of left hand and right motor imagery, time-series of pre-processed oxygenated and deoxygenated haemoglobin concentration changes are organised as a vector $\mathbf{X_t}$, and the class label y_t is marked as + or − 1 according to the type of task. The present work is restricted to the binary classification problem ($y_t = \pm 1$).

In the formulation of the SVM, the input vector $\mathbf{X_t}$ is mapped to a high dimensional feature space, $\mathbf{Z_t}$, through a non-linear transformation function, g(.) so that $\mathbf{Z_t} = g(\mathbf{X_t})$. The SVM algorithm attempts to find a decision boundary or a separating hyperplane in the feature space, given by the decision function:

$$D(\mathbf{Z_t}) = (\mathbf{W} \cdot \mathbf{Z}) + w_0,$$

where $\mathbf{W}$ defines the linear decision boundaries (Figure 2.3(b)). The solution $\mathbf{W}$ that represents the hyperplane can be obtained by solving for the equation:

$$y_t[(\mathbf{W} \cdot \mathbf{Z}) + w_0] \geq 1$$

The solution is optimal when $\|\mathbf{W}\|^2 + C \cdot f(\xi)$ is minimised under this constraint, where the parameter C>0, termed the regularisation constant, is chosen by the user. A large value of C corresponds to higher penalty for errors.

We implemented the SVM classifier using the LibSVM package (Chang and Lin 2001). The LibSVM package is a C++ implementation, providing various features for SVM classification: C- and ν-classification, one-class-classification, ε- and ν-regression; linear, polynomial, radial basis function and sigmoidal kernels; and v-fold cross validation. Our implementation was carried out in the following steps:
Transform the NIRS data into the format of the LibSVM software,
Scale the data,
Choose the type of kernel,
Find the best penalty parameter and kernel parameters,
Use the above parameters in the SVM model in 8 runs of 5-fold cross-validation to determine the classification accuracy.

The training and testing sets were created as vectors of real numbers of oxygenated and deoxygenated haemoglobin concentration values from the 20 channels for each trial of left hand and right hand motor imagery tasks, as shown in Figure 2.3(a). The whole dataset was scaled before applying SVM. The main reason for scaling was to avoid attributes in greater numeric ranges from dominating those in smaller numeric ranges. As kernel values are obtained by the inner product of feature vectors, large attribute values may cause numerical problems. For these reasons, each attribute was scaled to a value in the range [-1, 1].

We used the linear kernel for the present study. We used the default value of 1 for the penalty parameter C as set in the LibSVM toolkit. Next, we performed a 5-fold cross-validation to determine the classification accuracy. The cross-validation procedure is also known to prevent the over-fitting problem. We conducted 8 runs of 5-fold cross-validation. In each run, the trials in the training dataset were randomly permutated and divided into 5 subsets of equal size. In each of the 5 folds, 4 subsets of data were used

for training, while one subset was used for testing (validation) and the classification accuracy was calculated based on it. After 8 runs of 5-fold cross-validation we obtained 40 test results (accuracy measures). We performed similar classification tests on overt finger tapping and covert motor imagery tasks, separately.

Hidden Markov Model

The HMM could be seen as a finite state automaton, containing s discrete states, emitting an observation vector (or output vector) at every time point that depends on the current state. Each observation vector is modelled using m Gaussian mixtures per state. The transition probabilities between states are defined using a transition matrix. The basic principles of HMM as applied to the NIRS signal classification problem will be discussed in this section. A detailed description of the method can be found in (Rabiner 1989).

We used the Hidden Markov Model Toolkit (HTK) from the Department of Engineering of Cambridge University, United Kingdom for our implementation (Young, Woodland et al. 1993). Written in ANSI C, HTK is an integrated suite of tools for building and manipulating continuous density HMMs.

Figure 2.3(c) is a schematic diagram representing our HMM model for motor imagery. Left hand and right hand motor imagery were identically modelled as depicted, and the model parameters were subsequently estimated separately with respective data. We chose 5 states for the model based on previous HMM models for motor imagery classification (Obermaier, Guger et al. 2001) and our own preliminary experiments with modelling. The HMM is designed as a left to right model, transitions being allowed from a state to itself and to any right neighbour state. Arrows from left to right indicate the allowed transitions of states. States 1 and 5 were *non-emitting*, meaning that they do not result in any observations. Observations 2 and 4 were modelled using a single Gaussian while observation 3 was modelled using a mixture of 3 Gaussians.

In this HMM model denoted by M, at each time t that a state j is entered, an observation vector o_t is generated from the probability density $b_j(o_t)$. Further, transition from state i to state j is also probabilistic and is governed by the discrete probability a_{ij}. The joint probability O generated by the model M moving through the state sequence X is calculated as the product of transition probabilities and output probabilities. For the state sequence X in Figure 2.3(c),

$$P(O|M) = a12b2(o1)a22b2(o1)a33b3(o2)...$$

The observation O is known and the state sequence X is hidden. Given that X is unknown, the required likelihood is computed by summing over all possible state sequences $X = x(1),x(2),x(3),....,x(T)$, that is

$$P(O, X \mid M) = \sum_{x} a_{x(o)x(1)} \prod_{t=1}^{T} b_{x(t)}(o_t) a_{x(t)x(t+1)}$$

where $x(o)$ is constrained to the model entry state and $x(T+1)$ is constrained to the model exit state. Using the training samples for left hand or right hand motor imagery, the parameters, the a and $\{b_j(o_t)\}$, of the model for the respective task are determined

by an estimation procedure. To determine the parameters of the HMM model, the HTK uses the Baum-Welch re-estimation procedure (Young, Woodland et al. 1993). To recognize an unknown trial data, the likelihood of each model generating the trial data (observation vector) is calculated using the Viterbi algorithm (Rabiner 1989; Rabiner and Juang 1993), and the most likely model identifies the data as resulting from left hand or right hand task.

Our implementation of the HMM classifier comprised of the following steps:
    Transform the NIRS data into the format of the HTK software,
    Scale the data,
    Train 2 models of HMMs, one for left hand task and one for right hand task by computing the model parameters using the Baum-Welch re-estimation algorithm,
    Use the above models in 8 runs of 5-fold cross-validation to determine the classification accuracies.

The training and testing sets were created as vectors of real numbers of oxygenated and deoxygenated haemoglobin concentration values, as per the format expected by the HTK software, from the 20 channels for each trial of left hand and right hand motor imagery tasks. With 80 trial examples of each pattern, viz., single trial data of left hand or right task, one HMM was trained for each type of task. For the purpose of comparison with SVM, we used the same evaluation methodology of 8 runs of 5-fold cross-validation. We performed similar classification tests on overt finger tapping and covert motor imagery tasks, separately.

Graphical user interface of the NIRS-BCI system

Graphical User Interface (GUI, implemented in the C# language) was designed as a central control system of NIRS-BCI experiment, stimulus presentation and synchronization. It also invokes the other internal subsystems of the software (Data Acquisition and Signal Analysis).

There are two GUIs – Training and Speller. At the start of the run, the experimenter will be able to choose one of the two options. (see Figure 2.4 (a).)

Training – Here the GUI instructs the user to imagine or move left or right hand in a certain order chosen by the experimenter and displays the NIRS feed back.
Speller – Here the trained user is presented with a moving cursor, which can be controlled to select letters and spell out a message.

(a)

(b)
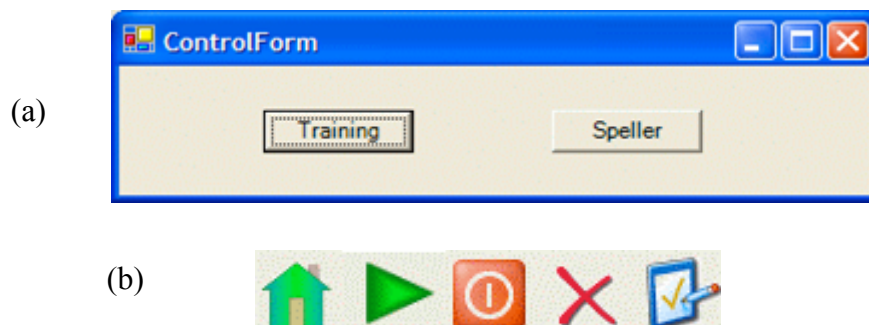
Figure 2.4. (a) Start screen of the program. (b) Control tool bar showing the options Home/Reset, Start, Pause, Quit and Edit Configuration options.

Once the Training or Speller GUI is started, the corresponding windows are opened. Common to both the windows is a tool bar (Figure 2.4(b)) which can be used to control the program. The Configuration file, System.cfg, can be edited by clicking on the last button. If the file doesn't exist in the working directory, it will be created with default values, and then the experimenter will be prompted to edit it right away.

The Training Mode has the following functions
Read in the configuration
Send a Beep to indicate start/end of a trial
Display Right or Left stimulus on the screen.
Control the Data Acquisition thread.
Control the Signal Analysis subsystem and display the feedback results.
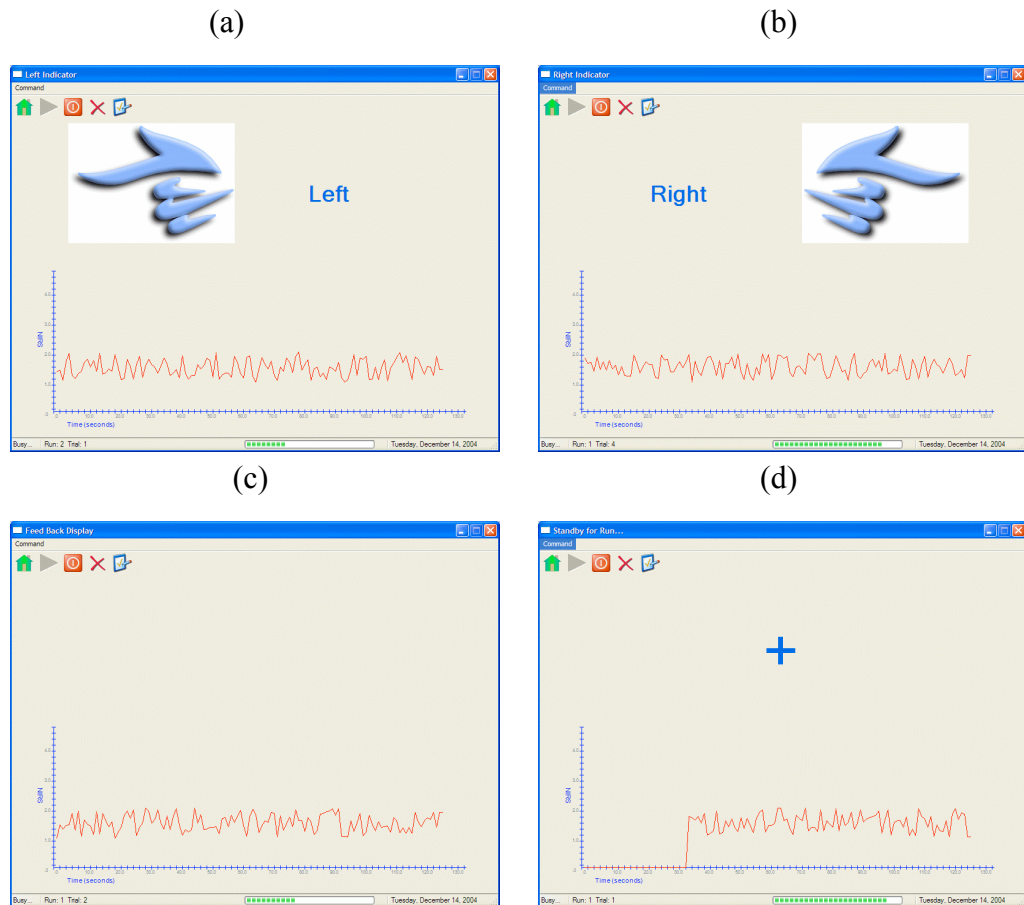
Figure 2.5. Graphical user interface for the training stage. Screen indications. (a,b) Right/Left hand indication, (c) Feedback display during task, and (d) Rest indication.

Results

(a) Comparison of hemodynamic response for overt & covert finger movement
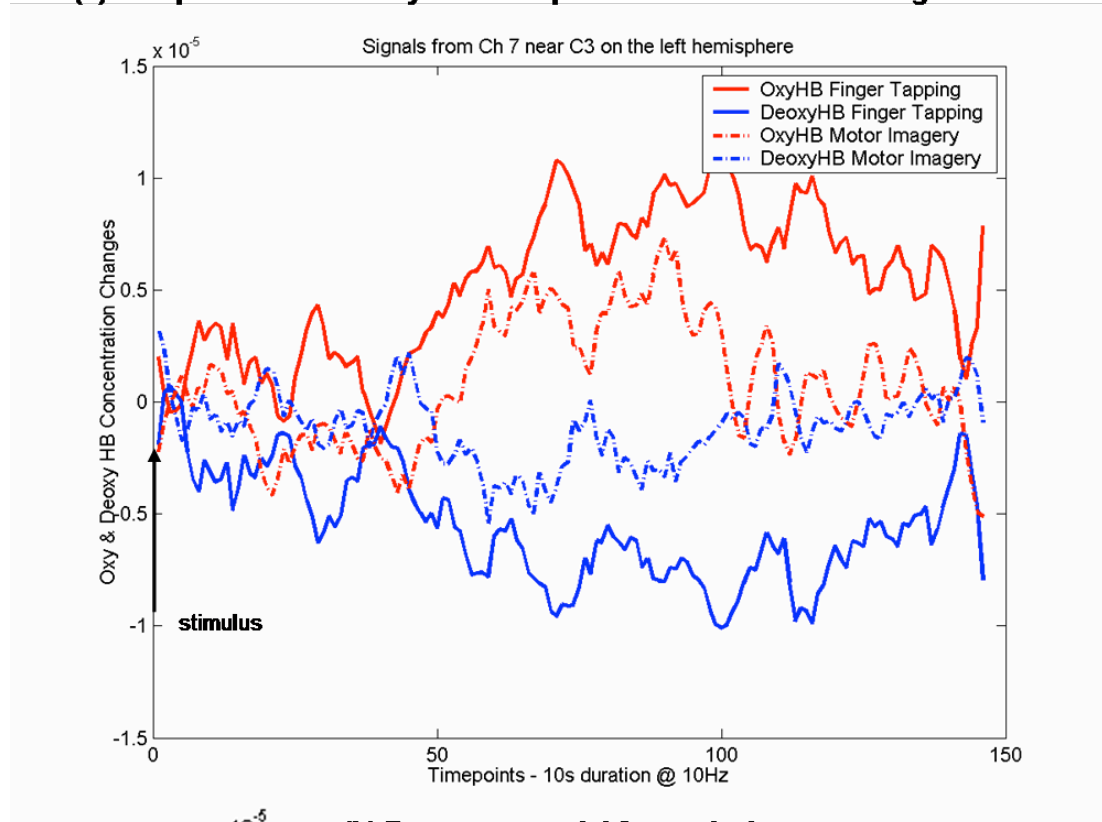
(b) Regressor model for analysis
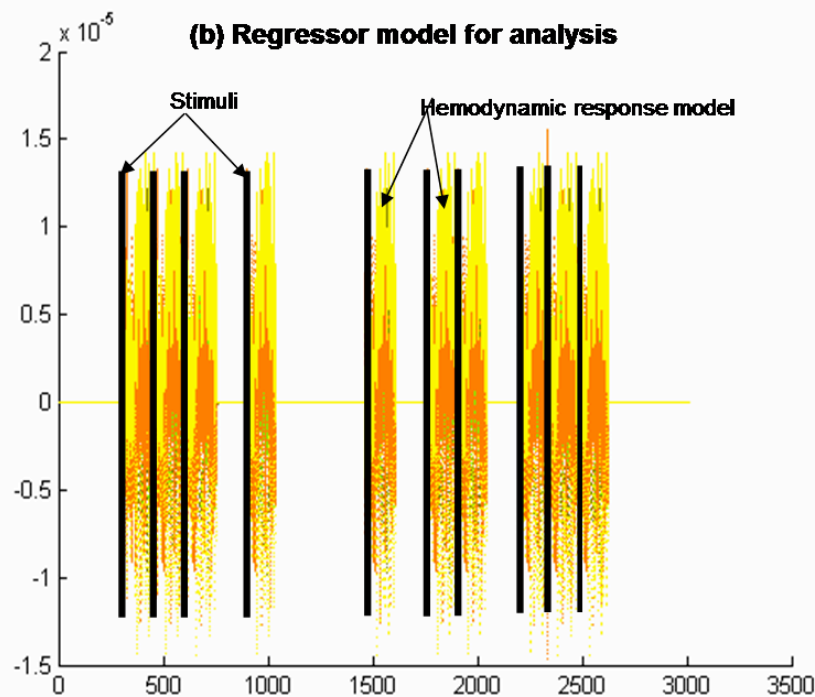
Figure 2.6: (a) Exemplary data from Subject-1 performing right hand finger tapping and motor imagery. Data displayed are averaged signals across a full session from channel 7 on the contralateral (left) hemisphere (close to the C3 electrode position as per the 10-20 system) for the duration 0-140 time points after stimulus presentation. Note that 140 time points are equal to 10 s of execution of the motor task at a sampling rate of 14 Hz. (b) Regressor model for right hand motor imagery task, based

on the timings of onset of stimuli for the task. The model was used for computing the Analysis of Variance (ANOVA) statistics and other measures in the HomER toolbox.

To start with, we wanted to check if overt finger tapping and covert motor imagery produced qualitatively similar responses. Figure 2.6 (a) shows exemplary data from Subject-1 performing right hand finger tapping and motor imagery. Data displayed are averaged signals across a full session from channel 7 on the contralateral (left) hemisphere (close to the C3 electrode position as per the 10-20 system) for the duration 0-140 time points after stimulus presentation. Note that 140 time points are equal to 10 s of execution of the motor task at a sampling rate of 14 Hz. Typically, concentration of oxygenated hemoglobin (red lines) increased and concentration of deoxygenated hemoglobin (blue lines) decreased during both finger tapping (continuous lines) and motor imagery (dashed lines) tasks. However, changes in concentration, both for oxygenated hemoglobin and deoxygenated hemoglobin, for finger tapping were greater than those for motor imagery. Applying the Analysis of Variance (ANOVA) on the data based on the regressor model (Figure 2.6 (b)) in the HomER toolbox obtained significant activation for oxygenated and deoxygenated hemoglobin values, both for finger tapping and motor imagery, with P<0.001 and correlation coefficient R^2=0.9.
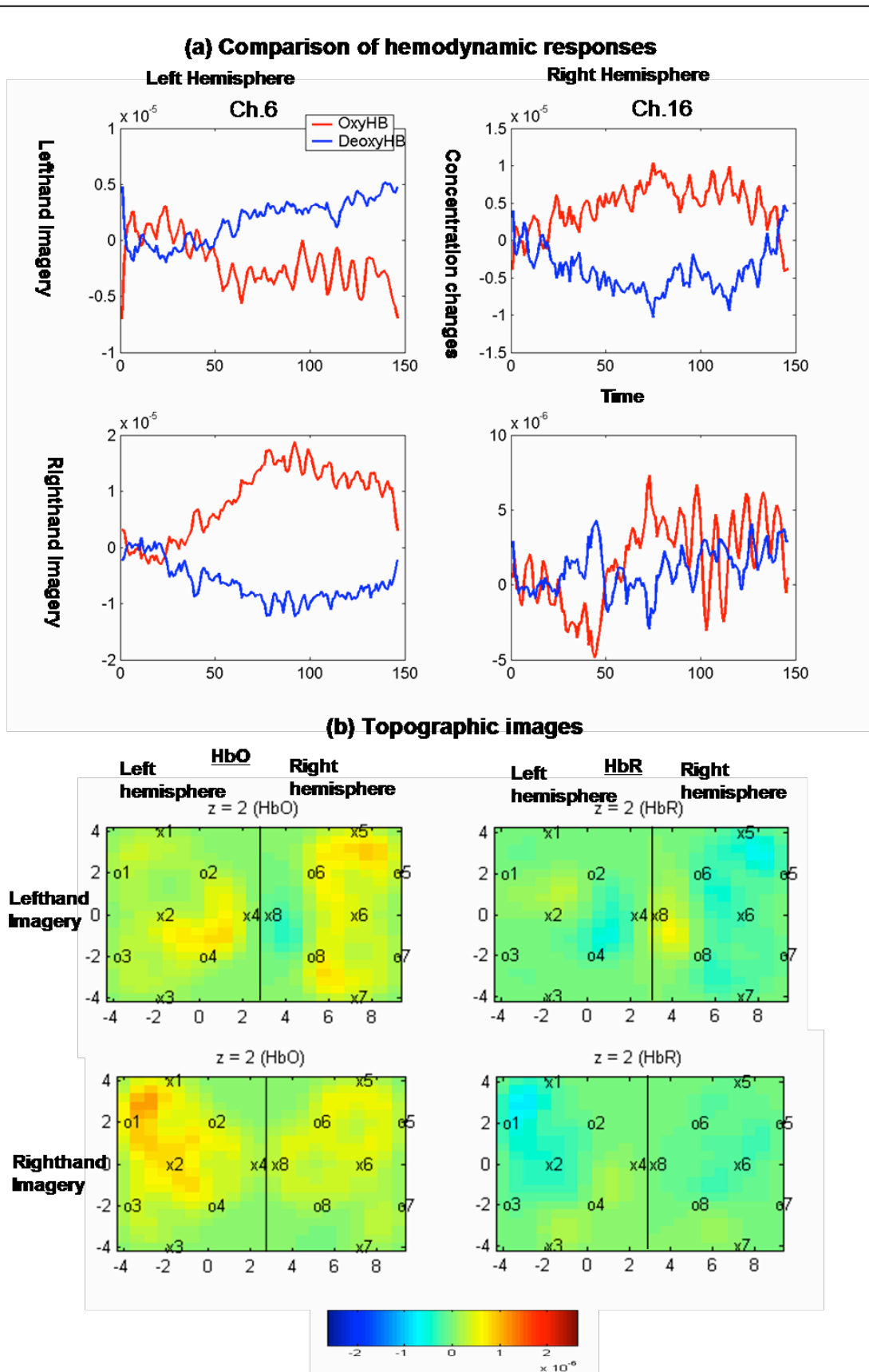
Figure 2.7: *(a) Hemodynamic response during motor imagery tasks at the ipsilateral hemisphere has substantial difference from that of the contralateral hemisphere. Exemplary data of averaged oxygenated and deoxygenated concentration changes for Subject-1, from channels on the left hemisphere (Ch 6) and right hemisphere (Ch 16),*

while performing left hand and right hand motor imagery. Typically, channels on the contralateral hemisphere showed activation by an increase in oxygenated hemoglobin and decrease in deoxygenated hemoglobin, while the channels on the ipsilateral hemisphere either showed similar response but to a smaller extent, or in a reversed manner (increase in deoxygenated hemoglobin and decrease in oxygenated hemoglobin) potentially indicating inhibition. (b) Exemplary topographic images from Subject-1. Images were reconstructed by back-projection methods and linear forward models in the HomER toolkit from the averaged hemodynamic responses from both left and right hemispheres while Subject-1 performed left hand and right hand motor imagery tasks. The reconstructed images for oxygenated hemoglobin and deoxygenated hemoglobin are superimposed on the probe geometry, with x1-x8 representing illuminator optodes and o1-o8 representing detector optodes.

Next, we wanted to check if hemodynamic responses during motor imagery tasks in ipsilateral and contralateral hemispheres have substantial differences. Figure 2.7(a) illustrates exemplary data for Subject-1, from channels on the left hemisphere and right hemisphere, while performing left hand and right hand motor imagery. Typically, most channels on the contralateral hemisphere showed activation by an increase in oxygenated hemoglobin and decrease in deoxygenated hemoglobin, while the channels on the ipsilateral hemisphere either showed similar response but to a smaller extent, or in a reversed manner (increase in deoxygenated hemoglobin and decrease in oxygenated hemoglobin) potentially indicating inhibition.

Figure 2.7(b) shows images reconstructed from the averaged hemodynamic responses from both left and right hemispheres while Subject-1 performed left hand and right hand motor imagery tasks. The reconstructed images for oxygenated hemoglobin and deoxygenated hemoglobin are superimposed on the probe geometry, with x1-x8 representing illuminator optodes and o1-o8 representing detector optodes. Activations are shown by yellow and red pixels and inhibitions by blue and green pixels. We found inter-subject variability in activation, illustrated by the variability between reconstructed images for different subjects.

The above analyses illustrated that there exist distinct patterns of hemodynamic responses as measured by NIRS to left hand and right hand motor imagery tasks which could be utilized in a pattern classifier towards developing a BCI. Table 2.1 lists the mean and standard deviation of accuracy of classification of left hand motor task from right hand motor task, using SVM and HMM techniques, on the data collected from 5 healthy volunteers. For the purpose of comparison, we classified both finger tapping and motor imagery data, although the proposed BCI was intended to be operated by motor imagery alone.

Subject	% Accuracy BY SVM (avg ~ STD)		% Accuracy BY HMM (avg ~ STD)	
	Finger Tapping	Motor Imagery	Finger Tapping	Motor Imagery
Subject-1	94.27~4.99	75.62~3.42	94.76~3.01	91.29~8.88
Subject-2	78.44~10.31	69.84~8.23	91.44~8.71	89.7~8.58
Subject-3	79.37~10.85	71.45~8.11	92.78~4.93	91.76~6.53

Subject-4	93.81~5.63	74.87~3.56	93.83~4.94	79.14~12.36
Subject-5	91.68~8.15	73.94~7.45	94.43~5.41	93.76~5.95
TOTAL	87.5	73.1	93.4	89.1

Table 2.1: *Accuracy of Support Vector Machine (SVM) and Hidden Markov Model (HMM) classification of finger tapping and motor imagery tasks for 5 healthy volunteers.*

Finger tapping data were classified with better accuracy compared to motor imagery data, by both classification techniques for all the subjects. Average accuracy of classification across all the subjects for finger tapping, by SVM and HMM, were 87.5% and 93.4%, respectively, as against 73.1% and 89.1% for motor imagery. Between the two pattern classification techniques, HMM performed better than SVM, for both finger tapping and motor imagery tasks. The accuracy of classification by HMM in comparison to SVM was greater by 5.9% for finger tapping, while the improvement was a striking 16% for motor imagery.

Discussion

Preliminary analysis of the NIRS signals collected during left hand and right hand motor imagery tasks indicated variation of the profile of the oxygenated and deoxygenated concentration changes from trial to trial. The dynamic nature of the signal could be due to inconsistency in the execution of motor imagery, especially when performed without any form of feedback. During overt finger tapping, the subject gets somatosensory and visual feedback of his/her own movement, while this is not so for the motor imagery task. A subject may start an imagination task at a different point in time in each trial. Further, he may perform the imagination at different tempos in different trials, creating considerable difficulties to the pattern recognition of the signal. This could be one of the reasons for the higher classification accuracy of finger tapping compared to motor imagery for both the classification techniques (SVM and HMM). With this consideration, we anticipated that a probability network like the HMM might model the dynamic nature of the hemodynamic time-series more effectively. Interestingly, this was confirmed by the greater improvement in classification accuracy by HMM for motor imagery (16% increase) compared to the improvement in accuracy for finger tapping (5.9% increase). Recently, Haihong and Cuntai (Haihong and Cuntai 2006) developed an improved method to address the above variations in the NIRS signal in response to motor imagery. The proposed technique uses a kernel-based model to represent variations in the hemodynamic signals of interest. Furthermore, a mathematical procedure was developed to locate the signals by estimating the parameters of the model. SVM was used on the located signals to differentiate left hand imagery from right hand imagery. The authors validated the method on simulated data as well as real data to obtain an error reduction of as much as 13%. This method can be potentially employed with HMM to improve classification accuracy even further.

By foregone results, we have established that there exist distinct patterns of hemodynamic responses between left hand and right hand imagery, and that such patterns can indeed be classified offline with substantially greater than chance accuracy. Our results of high accuracy of offline pattern classification of NIRS signals

during motor imagery tasks, especially with the HMM classifier, indicate the potential use of such techniques to the further development of an online BCI system. Towards this end, we have implemented a NIRS-BCI system incorporating a word speller as a language support system for the disabled. The system is written as a stand-alone application in C/C++, with C# used for development of the graphical user interface (GUI). The system comprises of four online modules: signal acquisition, signal processing, signal classification and word speller application with online feedback to the user. The signal acquisition module currently supports real-time data acquisition from 2 commercially available NIRS systems: OMM-1000 (Shimadzu Corporation, Japan) and Imagent System (ISS Inc., USA), through a serial port connection and two pluggable software components to support the differences in the data formats of the two instruments. The signal processing module implements low and high pass filtering and temporal smoothing. The pattern classification module currently supports SVM and HMM techniques. The SVM classifier is based on the LibSVM C++ library (Chang and Lin), while the HMM classifier is based on the HTK library (Young, Woodland et al. 1993). The word speller interface provides a means to use NIRS responses created by left and right hand motor imagery to spell words by a 2-choice cursor control paradigm. The user has to use left or right hand imagery to move the cursor to the left or right respectively to select a box that contains the letter of choice. Feature vectors of oxygenated and deoxygenated hemoglobin values from all channels in a moving window of 4 s is used as input to the pattern classifier. The length of the moving window can be increased or decreased depending on the performance requirements of execution and the expertise of the user. In terms of operation, the word speller is quite similar to the language support system of the Thought Translation Device (TTD) (Kotchoubey, Strehl et al. 1999; Anokhin, Lutzenberger et al. 2000).

A suitable training protocol needs to be developed to extend the offline pattern classification system to an active, online BCI system that drives the word speller application. In this regard, a 2-step procedure is being used. First, for each subject, parameters of the classifier (SVM or HMM) are estimated during offline training, and stored as a subject-specific model. This is necessary, as we have seen that there is great deal of variability between subjects in their hemodynamic response patterns. Next, subject-specific model parameters are loaded as the initial parameters of the classifier for online training. During online training on the word speller, the subject uses motor imagery to learn to control the cursor for selection of letters. At the end of each online training session, his model parameters are re-estimated based on the newly acquired data. This way, with each new training session the BCI would be re-tuned to operate in an online mode.

Until now, we have only considered a 2-choice BCI system operated by classifying left hand and right hand motor imagery. Potentially, such a system can be extended to 3- or 4-choice operation by imagery of the legs, and simultaneous imagery of hands and legs. Furthermore, other paradigms of BCI control, such as the P300 hemodynamic response could also be explored. Kennan et. al (Kennan, Horovitz et al. 2002) reported simultaneous recording of event-related auditory oddball (P300) response using NIRS and surface EEG. A peak signal of oxygenated hemoglobin was observed around 6 s after the onset of the oddball stimulus. Many other studies that assessed motor and cognitive functions using NIRS (Hoshi and Tamura 1993; Kato, Kamei et al. 1993; Kleinschmidt, Obrig et al. 1996; Hoshi and Tamura 1997; Okada

1997; Hoshi, Oda et al. 2000; Hoshi, Kobayashi et al. 2001) may indicate how future BCIs could be developed.

A major drawback of NIRS is the long time constants of the hemodynamic response making NIRS-BCI potentially very slow to operate. A fast NIRS signal (Franceschini, Toronov et al. 2000; Wolf, Wolf et al. 2002; Wolf, Wolf et al. 2003; Wolf, Wolf et al. 2003) is reported to appear in the range of milliseconds after stimulation. The signal is generated by rapid changes in the optical properties of the cerebral tissue. These changes presumably are due to an alteration of the scattering properties of neuronal membranes, which occur simultaneously with electrical changes, cell swelling, and increased heat production. Thus the fast signal is believed to be directly related to neuronal activity, as EEG or MEG, in contrast to functional NIRS, fMRI (BOLD signal), PET detecting only the slow hemodynamic response to neuronal activity. However, the fast signal is more difficult to detect, because the optical changes are small and other physiological signals, such as the hemodynamic pulsativity due to the heart beat dominate. Therefore, the system has to be highly noise resistant. Many trials of the fast signal need to be averaged to improve signal-to-noise ratio. When the above limitations and problems have been sufficiently overcome, the fast signal could prove beneficial to BCI development.

In this study, we have demonstrated the feasibility of a BCI using near infrared spectroscopy. Further work needs to be carried out to develop and test an online BCI system for the disabled. Novel signal processing methods need to be developed to exploit the NIRS signal. NIRS avoids the noise prominent in the electrical signals. It is less cumbersome to use, as there is no need to apply conductive gel. NIRS is non-ionizing, and so suitable for long-term use. However, NIRS also has certain drawbacks. It is slow to operate because of the inherent latency of the hemodynamic response. The signal strength is affected by hair on the head (especially if the subject has thick dark hair). Furthermore, if the probes are not secured well, the relative motion of the optodes on the hair may introduce motion artifacts and drifts in the hemodynamic signal. In spite of these limitations, NIRS's ability to localize brain activity 1-3 cm below the surface of cortex, with a spatial resolution in the range of cm could be an advantage in BCI development. NIRS provides us with an excellent opportunity to use a variety of motor and cognitive activities to detect signals from specific regions of the cortex for the development of future BCIs.

Chapter 3

Functional Magnetic Resonance Imaging Brain-Computer Interface

Introduction

Functional Magnetic Resonance Imaging (fMRI) is a non-invasive technique which measures the task induced blood oxygen level-dependent (BOLD) changes correlating with neuronal activity in the brain (Logothetis 2007; Logothetis 2008). Further progress has been made in real-time fMRI since the first description of the method by Cox et al., (Cox, Jesmanowicz et al. 1995). In contrast to conventional fMRI which allows analysis of images only after the scan is finished, real-time fMRI allows simultaneous acquisition, analysis and visualization of whole brain images. With progress in real-time fMRI due to higher field MRI scanners, fast data acquisition sequences, improved real-time pre-processing and statistical analysis algorithms, and improved methods of visualization of brain activation and feedback to the subject, implementation of fMRI-BCI and neurofeedback became feasible.

Architecture of fMRI-BCI

An fMRI-BCI system is a closed loop system (figure 3.1), with the following major subsystems: signal acquisition, signal preprocessing, signal analysis and signal feedback. The subsystems are usually installed and executed in separate computers for optimising system performance, and are connected via a local area network (LAN). Whole brain images from healthy subjects or patients are acquired slice by slice employing an echo planar imaging (EPI) sequence. Greater the number of slices the brain is divided into, the longer is the time for acquisition of the images. As the real-time nature of fMRI-BCI requires rapid acquisition of whole brain images (typically in 1-2s), a tradeoff needs to be made between spatial and temporal resolution. In most of our studies, we have used 16-20 slices (Caria, Veit et al. 2007). An fMRI voxel of size ~3x3x5 mm^3 contains millions of neurons. When neurons in an area become active, blood rich in oxygen flows to the area. The source of the fMRI signal is the difference in the magnetic properties of oxygenated blood from deoxygenated blood. The measured hemodynamic response due to the BOLD effect, which is the neurovascular response to brain activity, lags behind the neuronal activity by approximately 3-6s (Logothetis 2007; Logothetis 2008). Higher static magnetic field (B0) strengths and more sophisticated MRI pulse sequences are often used to increase the signal-to-noise ratio (SNR). The acquired images are then preprocessed to correct for head motion, compensate for signal dropouts and magnetic field distortions, and apply spatial smoothing. The signal analysis subsystem performs statistical analysis and generates functional maps using any of the following methods: subtraction of active and rest conditions, correlation analysis, multiple regression, General Linear Model (GLM) and pattern classification. Feedback can be presented to the subject by different modalities, including, acoustic

and visual; and with a variety of visualization methods, such as, functional maps, continuously updated curves of the mean activity in one or more selected region-of-interest (ROI), varying activity levels in one or more ROIs using a graphical thermometer, and augmented interfaces such as Virtual Reality (VR). Feedback is presented at an interval that depends on the time involved for image acquisition and processing, based on the computational resources available and the efficiency of the algorithms with which they are implemented, thus directly affecting the performance of the system. A short interval is critical for learning voluntary control of brain activity (for example, 1.5s, (Caria, Veit et al. 2007)).

Signal Acquisition
- Echo Planar Imaging (EPI)
- Field Strength
- Spatial Resolution
- Temporal Resolution
- Relaxation Time
- Magnetic Inhomogenities

Feedback approaches
Virtual reality
Thermometer
Time series
Video feedback

Signal Analysis
- Head Motion Artefact Correction
- Breathing Artefact Correction
- Correlation Maps
- Anatomical Co-registration
- ROI Selection and Analysis

Participant
- Background
- Healthy Volunteer/Patient
- Naïve/Experienced
- Mood
- Motivation for Learning
- Prior Instructions
- Operant Learning

Signal Feedback
- Physiological Measure
- Pattern Classification
- Feedback Modality
- Temporal Delay

Figure 3.1: *An fMRI-BCI system is a closed loop system, with the following subsystems: signal acquisition, signal preprocessing, signal analysis and signal feedback. Whole brain images from healthy subjects or patients are acquired employing a conventional Echo Planar Imaging (EPI) sequence or any of its variants. The measured hemodynamic response due to the BOLD effect is preprocessed for correction of different artifacts, including, for head motion. The signal analysis subsystem performs statistical analysis and generates functional maps. Feedback can be presented to the subject by different modalities, including, acoustic and visual; and with a variety of visualization methods, such as, functional maps, continuously updated curves of the mean activity in one or more selected*

region-of-interest (ROI), varying activity levels in one or more ROIs using a graphical thermometer, and even augmented interfaces such as Virtual Reality (VR).

In the following subsections we will elaborate on each of the subsystems, explaining different algorithms and methods developed so far. We will consider technological and psychophysiological factors that affect and influence the performance and efficiency of the system.

Signal Acquisition

Conventional MRI has been a slow imaging modality where increases in imaging speed result in signal losses (Cohen 2001). The reason is that the MR signal is derived from the conversion of tissue magnetization to a radio signal, and the magnetization recovers rather slowly. This had limited the possibility of implementing a real-time MRI. Fortunately, over the last 20 years technical advances in imaging have enabled substantial reduction in acquisition time. The most significant speed advance came with the development of echo-planar imaging (EPI). EPI is capable of imaging the entire brain in 1-2s. At this sampling rate, fMRI can accurately follow the time course of brain activation.

In a traditional fMRI experiment, images are reconstructed offline only after the experiment has been completed. Real-time fMRI, on which fMRI-BCI is based, requires the simultaneous reconstruction of the images with the acquisition of the MR signal. Cox's group reported the first implementation of a real-time fMRI system using a whole-body 3T scanner (Bruker Instruments) (Cox, Jesmanowicz et al. 1995). In their implementation, the analog signal from the signal acquisition system was sent to a workstation for analog-to-digital conversion and image reconstruction. In our laboratory, we have modified the Siemens MR scanner's image reconstruction software to allow online reconstruction of whole-brain images at the end of every repetition time (TR), and storage of these images in a pre-specified folder to be immediately retrieved for further processing, analysis and feedback by the fMRI-BCI system. The online image reconstruction software program was written in C++ based on the Image Reconstruction Environment (ICE) provided by Siemens. The RTExport system runs both on the 1.5T (Vision) and 3T (TIM Trio) Siemens scanners.

Many factors influencing signal acquisition have important consequences for real-time performance of fMRI-BCI: static magnetic field (B0) strength, spatial resolution, temporal resolution, echo time and magnetic field inhomogeneities. Although high spatial resolution is desired, increasing the spatial resolution decreases the SNR and increases the acquisition time, and hence a compromise needs to be made among these variables. Commonly in fMRI-BCI, 64x64 image matrices resulting in 3-4 mm in-plane resolution, and slice thickness of around 5 mm are used. For online processing after image acquisition, spatial filtering or averaging across a ROI helps improve SNR. Reduced spatial resolution could be beneficial, compensating for head motion, data complexity and inter-subject variability (Weiskopf, Scharnowski et al. 2004). A repetition time (TR) of 1500 ms has been used (Weiskopf, Veit et al. 2003; deCharms, Christoff et al. 2004) in real-time fMRI with single-shot EPI. It is advisable that fMRI-BCI studies choose the echo time (TE) close to the relaxation time (T2*) of the gray matter in the brain to maximize

functional sensitivity (Moonen and Bandettini 2000). This value is about 70 ms at 1.5 T and 45 ms at 3 T.

At the interface between tissue and air in the brain, in areas such as orbitofrontal cortex and temporal pole, a significant change in the local magnetic field is present over a short distance. Artifacts such as signal dropouts and geometric distortions (local shifts and compressions in the image) caused by magnetic field inhomogeneities potentially affect the performance of fMRI-BCI. Several methods have been developed for reducing susceptibility related signal losses in fMRI (for an overview see (Weiskopf, Hutton et al. 2007)). Weiskopf et al., (Weiskopf, Hutton et al. 2007) developed a theory supported by experimental evidence showing that susceptibility-induced gradients in the EPI readout direction cause severe signal losses. They have proposed a model to simulate EPI dropouts to make informed choice of scan parameters depending on the field inhomogeneities in a region. Based on this insight, they developed an optimized EPI sequence for maximal BOLD sensitivity using a specific combination of an increased spatial resolution in the readout direction and a reduced echo time.

Signal Preprocessing

This component of the fMRI-BCI system retrieves the reconstructed images from the signal acquisition component via the LAN, and performs data preprocessing. Methods of signal preprocessing can be head motion artifact correction, respiratory and cardiac artifact correction, and spatial smoothing.

Head Motion Correction

Head motion is one of the largest sources of artifacts in fMRI. If two neighboring voxels differ in intrinsic brightness by 20%, then a motion of 10% of a voxel dimension can result in a 2% signal change – comparable to the BOLD signal change at 1.5T subsequent to neural activation (Bandettini, Wong et al. 1992). The motion artifacts can interfere with and reduce the detection of signal changes due to neural action or even simulate signal changes. Head motion can be reduced by padding and a bite bar to some extent only. Real-time fMRI feedback profits from robust online motion correction. Because the head moves as a whole, rigid body transformations (3 for translation, 3 for rotation) can be estimated from a number of volume data points for motion correction. The short response latency (tens of seconds) of real-time fMRI makes it particularly sensitive to motion artifacts (Mathiak and Posse 2001). Motion correction in real-time requires efficient algorithms that can be executed on fMRI data sets within a single repetition time (TR). For neurofeedback applications, feedback of motion artifacts to the subjects and omitting rewards may discourage head movement. Two major types of head motion correction have been developed: retrospective and prospective methods. Both methods can be potentially applied to fMRI-BCI, when real-time adoptions of the methods are made feasible and implemented. Retrospective motion correction for real-time fMRI involves image registration soon after every volume of the fMRI data is acquired. Prospective methods correct for subject head motion even before image acquisition.

Retrospective methods realign the time-series data to a reference image collected during the fMRI session. Conventional retrospective correction uses rigid body transformation normally consisting of 3 translational and 3 rotational parameters. Realignment parameters are typically estimated by optimizing a similarity measure

based on voxel signal intensity values, quantifying the difference between a specific image in the time-series, and the reference (Tremblay, Tam et al. 2005). As an adaptation for real-time fMRI, Mathiak et al.,(Mathiak and Posse 2001) developed a real-time retrospective algorithm which performs a rigid body motion correction of a complete multislice EPI dataset within a single TR cycle. In this method, one of the first images is chosen as the reference image, and all subsequent images are realigned separately with respect to this image. The optimization criterion is to minimize the quadratic difference between the reference image and shifted image. In the 3-stage implementation of this technique, the reference gradient maps are first calculated, motion parameters are then estimated, and finally images are corrected for the estimated movement using re-slicing with linear interpolation. For selecting gradient maps, a set of estimation equations are used for the translational and rotational components for the 3 axes.

Retrospective motion correction has a few drawbacks, including blurring due to interpolation and image transformations, potential misregistration due to local intensity changes from the BOLD signal, and the potential for introducing false-positives or for false-negatives in the activation statistics (Ward, Riederer et al. 2000). The retrospective motion correction method has been incorporated into a number of public-domain postprocessing software packages, including SPM, AIR, and AFNI. Turbo Brain-Voyager (TBV, Brain Innovation, Maastricht, Netherlands), a commercial software for real-time fMRI which is incorporated in our fMRI-BCI, has implemented a real-time version of retrospective motion correction. Figure 3.2 shows estimated values of head motion in the 3 translational directions and 3 rotational directions, as computed by TBV.
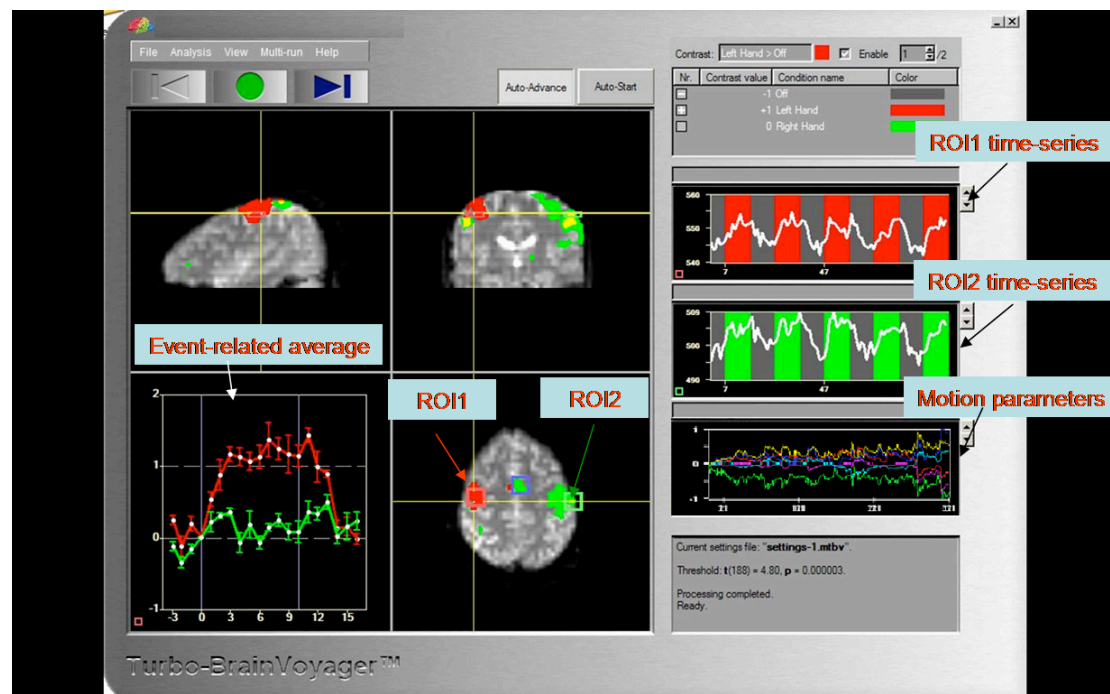

Figure 3.2: *Real-time functional maps during motor imagery of left and right hands. The functional maps are displayed using the Turbo Brain Voyager software (TBV; Brain Innovations, Maastricht). The TBV software allows orthographic and slice-based display of functional activations. On the left panel, statistical maps of brain*

activation are superimposed on the orthographic images (sagittal image – top-left, coronal image – top-right, axial image – bottom-right) acquired by an EPI sequence. In this example, self-paced motor imagery of left hand and right hand resulted in activation in the right and left primary motor areas (ROI1- red rectangle and ROI2- green rectangle respectively), somatosensory areas, and supplementary motor area (SMA). The upper and middle right panels show the BOLD time courses in the ROI1 and ROI2, respectively. Blocks of left hand imagery are colored red, right hand imagery green, and baseline grey. The lower right panel displays head motion parameter (3 translations and 3 rotations).

Prospective methods correct for subject head motion before image acquisition by adjusting scanning parameters by tracking the moving anatomy (Tremblay, Tam et al. 2005). Ward et al., (Ward, Riederer et al. 2000) developed such a method by measuring rotation and translation for each of the sagittal, axial and coronal planes. This was achieved by incorporating a special type of sequence called orbital navigator echo sequence, a separate process applied before each cycle of acquisition of multislice fMRI signals. Immediately after their acquisition, the navigator signals are processed to determine motion in three degrees of rotation and three degrees of translation. The values of the rotations and translations detected are then used to adjust the gradient rotation matrix and the RF excitation frequency prior to the excitation of the subsequent imaging sequence. Any motion relative to the baseline determined from the navigator acquisitions at the start of the multislice cycle is used to correct all the images of that cycle. The time from the acquisition of the first navigator echo to alteration of the EPI acquisition can be less than 160ms. The results of applying the technique to volunteers demonstrated the feasibility of in-vivo correction of head-motion for real-time fMRI (Ward, Riederer et al. 2000).

Physiological Noise Correction

The magnetic field in the head changes during breathing because of the bulk motion of the thorax. Breathing patterns may change the fMRI signal more than the desirable BOLD response. Changes in the respiratory rhythm and volume can also change the CO_2 level in the blood and cause BOLD signal fluctuations (Birn et al., 2006). The pulse is also known to cause artifacts. Techniques have been developed to remove cardio-respiratory artifacts during offline analysis (Josephs, Howseman et al. 1997; Glover, Li et al. 2000; Birn, Diamond et al. 2006), but they have not been adapted to online processing for real-time fMRI. Recently van Gelderen et al., (van Gelderen, de Zwart et al. 2007) reported a real-time shimming method to compensate for respiration induced fluctuations in the main magnetic field (B0 field). Future implementations of fMRI-BCI could potentially explore the use of these methods for correction of physiological artifacts and noise. This becomes even more important at higher static magnetic fields, because the relative contribution of physiology to the noise increases (Triantafyllou, Hoge et al. 2005).

Signal Analysis

While majority of work in fMRI-BCI have used conventional neuorimaging methods of univariate analysis, there is a growing interest in incorporating multivariate methods of pattern analysis using machine learning techniques in the emerging field of brain state detection. In this section, we will consider both methods as applied to fMRI-BCI.

Univariate Analysis

Univariate methods seek to find out how a particular perceptual or cognitive state is encoded by measuring brain activity from many thousands of locations repeatedly, but then analyzing each location separately (Haynes and Rees 2006). If the responses at any brain location differ between two states, then it is possible to use measurements of the activity at that location to determine or decode the state. A commonly used method for detecting neuronal activity from fMRI time-series is correlation analysis. The method computes correlation coefficients between the time-series of the reference vector representing the expected hemodynamic response and the measurement vector of each voxel. A primary advantage of this method is that the reference vector can have an arbitrary shape best reflecting the hemodynamic response. Gembris et al., (Gembris, Taylor et al. 2000) presented a computationally efficient algorithm, implemented in the analysis software Functional Magnetic Resonance Imaging in Real-time (FIRE), which generates correlation coefficients on a "sliding-window" of the fMRI time-series. The basic concept of this method is to restrict the correlation computation to only the most recent data sets. According to this method, definition of the correlation coefficient in combination with detrending is given by the equation:

$$\rho = \frac{\vec{x}\vec{r}_s}{|\vec{x}_s||\vec{r}_{\vec{s}}|}$$

where $\vec{x}$ is the measurement vector of one voxel that is updated at every time step, $\vec{r}_s$ is the reference vector, and $\vec{x}_s$ and $\vec{r}_{\vec{s}}$ are detrending vectors. (For further details on implementation of this method the reader is referred to the article (Gembris, Taylor et al. 2000). Each new data set replaces the data set of the previously acquired sliding-window buffer. This method reduces the load on memory and computational time, two important factors that critically affect the performance of fMRI-BCI. The authors tested the method in an experiment with 20 healthy participants in a paradigm comprising alternating baseline and visual stimulation blocks. The sliding window correlation method successfully identified the visual areas as being significantly active with voxels in this region crossing the threshold correlation coefficient of 70%. The method offers greater sensitivity of the correlation coefficients to changes in the signal response shape and amplitude with passing measurements. Another advantage of the sliding-window technique is its capability for quantifying physiological variability when combined with a technique called reference vector optimization (Gembris, Taylor et al. 2000). This method takes into account a realistic model of the hemodynamic response function to adapt the reference vector to the measured data and thus increases functional sensitivity.

The general linear model (GLM) provides by far the most unified framework in the analysis of the fMRI data (Friston, Holmes et al. 1995). GLM can model multiple experimental and confounding effects simultaneously. Bagarinao et al., (Bagarinao, Matsuo et al. 2003) presented a method for real-time estimation of GLM coefficients. The observed fMRI data are considered a linear combination of L explanatory functions $f_i(.)$ and an error term:

$y_{k,s} = b_{k,1}f_1(t_s) + \ldots + b_{k,1}f_L(t_s) + \varepsilon_{k,s}$

where $y_{k,s}$ is the observation of kth voxel at time t_s, $s=1..n$ are scan numbers, $f_s(.)$ are basis functions that span the fMRI responses for a given experiment, b_k are

coefficients that need to be estimated and $\varepsilon_{k,s}$ is the residual error or noise term. The method converts the basis functions or explanatory variables of a GLM into orthogonal functions using an algorithm called the Gram-Schmidt orthogonalization procedure. The coefficients of the orthogonal functions are then estimated using the orthogonality condition. (For further details on implementation of this method the reader is referred to the article (Bagarinao, Matsuo et al. 2003). In a conventional GLM analysis of fMRI data, multiple trials are required to identify significantly activated voxels with sufficient consistency. However, it is not possible to obtain many trials in an fMRI-BCI setting with its very need for identifying significantly active voxels in real-time. The advantage of the real-time GLM implementation is that estimates can be updated when new images data are available, making the approach suitable for fMRI-BCIs. Furthermore, with this approach it is not necessary to store the data as it is immediately used in computing the estimates, thus reducing the memory requirements. A similar approach is taken by the analysis software (TBV) running on our local fMRI-BCI setup at the University of Tuebingen which uses the recursive least squares regression algorithm (Pollock 1999) to incrementally update the GLM estimates.

After identification of the significantly active voxels, either by the method of real-time correlation or GLM analysis, their values are passed to the Signal Feedback subsystem at every time point for computation and presentation of the feedback to the participant.

Multivariate Analysis

Using univariate analysis it is often difficult to find individual locations where the difference between conditions are large enough to allow for efficient decoding. In contrast to the conventional analysis, recent work shows that the sensitivity of human neuroimaging may be improved by taking into account the spatial pattern of brain activity (Mitchell, Hutchinson et al. 2003; Davatzikos, Ruparel et al. 2005; Polyn, Natu et al. 2005; Norman, Polyn et al. 2006). Pattern-based methods use considerably more information for detecting the current state from measurements of brain activity. In the previous studies with fMRI-BCI, brain signals from only one or two regions of interest (ROI) were extracted for providing neurofeedback to the subject. A major argument for moving away from deriving feedback signals from single ROIs is that perceptual, cognitive or emotional activities generally recruit a distributed network of brain regions rather than single locations. Pattern-based methods not only use voxel-intensities but also their spatiotemporal relationships.

Several studies have previously reported offline classification of fMRI signals using various pattern based methods such as multilayer neural networks (Norman, Polyn et al. 2006), Fisher Linear Discriminant (FLD) classifier (Mourao-Miranda, Bokde et al. 2005) and Support Vector Machines (SVM). LaConte et al., (Laconte, Peltier et al. 2006) recently reported probably the first implementation of a real-time pattern classification system that could be applied to neurofeedback and BCI. The aim of the study was to first train a classification model based on early fMRI data, and thereafter to use the classifier to predict the brain state with each acquired image and alter the stimulus based on the estimated brain state. The authors modified the Siemens scanner's Image Calculation Environment (ICE) to perform Support Vector Machine (SVM) classification during training and testing, and then transmitted the classification results to a stimulus display computer. To improve the efficiency of

classification the authors implemented a method for segmenting brain regions from non-brain regions with a combination of intensity thresholded mask and an additional variance mask to remove signals from the eye regions. For SVM classification, images from each scan were represented as a vector whose components were intensity values for each brain voxel at that time. The experimental condition associated with each vector was represented as a scalar class label. The SVM algorithm attempts to find a decision boundary as a separating hyperplane to discriminate between the two class labels. Once the SVM model was determined from the training images, independent testing images were classified into the specified labels. Percentage classification accuracy was reported as the ratio of number of correctly classified scans to the total number of scans. To test this approach the authors used an experimental task consisting of rapid button press blocks that alternatively used the left or right portion of the visual display. During the training runs an arrow in the center of the display pointed toward the left or right target acted as the cue. During the subsequent testing run, each acquired image was classified by the SVM model, and the arrow was updated in terms of its position and orientation based on the classifier's left or right decision. With additional subjects, task instructions were changed to further examine pattern classification of mood, language and imagined motor tasks. The authors concluded that real-time pattern classification of brain states using fMRI data is possible; high prediction accuracies are attainable during sustained activation; and stimulus feedback based on pattern classification can respond to changes in brain states much earlier than the time-to-peak limitations of the BOLD response. The above approach is limited to two-class classification of brain states.

We have recently implemented in our fMRI-BCI a multiclass pattern classification system offers the experimenter the flexibility of selecting either an SVM or a multilayer neural network classification algorithm (Sitaram 2007). Mourao-Miranda et al., (Mourao-Miranda, Bokde et al. 2005) carried out a comparison of two methods, SVM and Fisher Linear Discriminant classifier (FLD), for classifying multisubject data from an experiment involving a face matching and location matching task. They demonstrated that SVM outperforms FLD in classification accuracy as well as in the robustness of the spatial maps obtained. Further work needs to be carried out to rigorously compare the performance of existing pattern classification approaches to assess their suitability and efficacy for fMRI brain state classification.

Signal Feedback

Training to self-regulate a brain activity can be implemented by feedback of this specific brain signal (Schwartz and Associates 1995). In fMRI-BCI, feedback provides reward and information of the BOLD signal. Contingent feedback following the response with a minimum lag and at a high probability improves learning. FMRI-BCI can operate both in a feedback mode for applications involving self-regulation and non-feedback mode for applications involving brain state detection (e.g., lie detection). In this section, we elaborate on the techniques used to date in identifying the feedback, in computing the feedback signal and eventually in presenting the feedback to the subject.

Feedback Identification

fMRI-BCI can take advantage of the high spatial resolution and whole brain coverage of fMRI to derive feedback from specific anatomical locations called regions of interest (ROI) (Weiskopf, Scharnowski et al. 2004). Feedback from circumscribed

brain regions necessitates the delineation of the target ROI by anatomical landmarks or by identifying functional activation elicited in a functional localizer experiment by presenting the subject a stimulus or instructing the subject to perform a mental task. Motor areas can be localized by overt finger tapping, covert movement imagery and observation of movement. Primary and higher visual areas can be localized by presenting distinct visual stimuli. For example, the higher visual areas like fusiform gyrus (FFA) and parahippocampal place area (PPA) can be localized by presenting images of faces and houses, respectively. Functional localizers can also be used to identify brain areas involved in higher cognitive and affective processing such as anterior cingulated cortex (Weiskopf, Veit et al. 2003) or the insula (Caria, Veit et al. 2007). ROI is chosen by drawing a rectangular area on the functional map computed by the signal analysis software (e.g., TBV). To improve selection of ROIs, functional maps could be co-registered with previously acquired anatomical scans of the subject for accurate localization of ROI, when the region is too small to be located using the EPI images alone or too hard to localize consistently by functional localizers (e.g., amygdala). In contrast to selecting circumscribed brain regions by the ROI method employing univariate analysis, pattern-based methods (Laconte, Peltier et al. 2006) are able to extract brain activity from spatially distributed regions which dynamically interact while the subject learns to regulate a motor, cognitive or affective behavior.

Feedback Computation

After the feedback signal is identified, further processing needs to be carried out to arrive at a suitable representation of brain activity to be presented as feedback. By conventional univariate methods, effective signal change from an ROI is usually computed as a difference of the average BOLD signal between the activation block and the baseline block. Specificity of the signal can further be improved by designing a protocol that includes bidirectional control, that is, both up and down regulation of the activity in the ROI. Studies have used differential feedback (Weiskopf, Scharnowski et al. 2004) between two ROIs to subtract global signal changes. General effects of arousal and attention caused by the demands of the task or the state of the subject are thus canceled out leaving only the effects of increasing or decreasing the signal. A potential problem related to differential regulation of two ROIs is that subjects may learn to regulate only one ROI while keeping the second ROI constant. We have recently incorporated a correlation coefficient in the computation of feedback of two ROIs to prevent the above undesirable effect. We used the following equation to compute the magnitude of feedback when subjects were trained to increase BOLD in ROI1 while decreasing BOLD in ROI2 simultaneously (i.e., negative correlation of the two time-series):

*Magnitude of feedback = (BOLD$_{ROI1}$ – BOLD$_{ROI2}$) * (1 –R)*

where R is the correlation coefficient of BOLD time-series in the two ROIs computed from a sliding window of past n (example, n=10) time points. If the subject learns to maintain a high BOLD in ROI1 compared to ROI2 and a negative correlation of the two ROIs he receives higher reward through feedback. However, the subject receives lesser reward if the difference between the BOLD values in the ROIs is negative, or if there is a positive correlation between the BOLD values in the two ROIs, or both.

In designing the experimental protocol for fMRI-BCI, the time constants of the hemodynamic response and the time required for task switching need to be kept in mind. Most studies reported so far have used block designs with alternating rest

periods and regulation tasks. Duration for rest periods and regulation tasks is in the range of 15-60s. Shorter periods could be used for overt execution of motor tasks (like finger tapping) as they can be started and stopped quickly. Longer periods need to be used for mental imagery and emotional regulation tasks. A delay between brain activation and feedback of that activation in range of seconds is inevitable due to the hemodynamic delay and delay in image acquisition and processing. Hemodynamic coupling introduces a delay between neuronal activation and the BOLD signal changes (Moonen and Bandettini 2000), with the onset of signal changes delayed by around 3s and the peak signal change by 6s. Due to signal acquisition and processing an additional delay of around 1.5s is introduced. Fortunately, the delay in acquisition allows for temporal averaging of fMRI data to increase SNR and hence the reliability of feedback (Weiskopf, Scharnowski et al. 2004).

The benefits of the high spatial resolution of the fMRI is lost if the feedback signal is obtained from too large an ROI that encompasses multiple disparate areas involved the target function. By averaging signals from individual voxels in a large ROI, the spatial information across the circumscribed region would be lost. To overcome this problem and to be able to compare results across subjects, we used small rectangular ROIs of a uniform size of 6x6 voxels (36 voxels) in our studies on self-regulation of interior insula (Caria, Veit et al. 2007). Another advantage of using smaller ROIs is in reducing the computational bottleneck in processing statistical information in a reduced number of voxels. The newly emerging real-time pattern-based feedback (Laconte, Peltier et al. 2006) is able to circumvent the necessity of specifying anatomical ROIs, thus providing a flexible method to account for inter-subject variability in brain size, shape and neural network.

Feedback Presentation

Although many feedback modalities (verbal, visual, auditory, olfactory and tactile) are possible, visual feedback has been the most frequently used method. A variety of visual stimuli have been employed by different researchers to indicate the required level of activation at different time points. Scrolling time series graphs and curves of BOLD activation of the ROI provide immediate information to the subject (Weiskopf, Veit et al. 2003; deCharms, Christoff et al. 2004). Yoo and Jolesz (Yoo and Jolesz 2002) used functional maps of the brain as feedback. Sitaram et al. (Sitaram, Caria et al. 2005) introduced the thermometer type of feedback (see figure 3.1 for an illustration of different types of feedback) that shows varying levels of ROI activity as changing bars of a graphical thermometer. Positive BOLD activity with respect to baseline activity is shown in one color (red) to differentiate from negative BOLD activity (blue). We introduced virtual reality (VR) for feedback (Sitaram, Caria et al. 2005; Sitaram, Caria et al. 2006) which provides a playful and engaging environment to encourage the subject to continue with self-regulation training. In a recent application of fMRI-BCI, we used video-based feedback to train stroke patients to self-regulate ventromedial premotor cortex (Sitaram 2007). Laconte et al., (Laconte, Peltier et al. 2006) implemented a visual feedback updated from results of real-time pattern classification of left hand and right finger tapping (also see section on Multivariate Analysis). A target stimulus located about 10° to the left or right of the center indicated the fingers (left or right) to be tapped. The feedback consisted of an arrow in the central visual field oriented towards the target. The arrow position and orientation were updated after classification of the images as left or right from the volumes collected for previous 2s. Based on the brain-state classification, the

arrow either continued in the current orientation or flipped its left-right orientation. After 30s, the target position was alternated and the arrow was re-centered, pointing to the new target.

Preliminary Investigations

Regulation of Anterior Insula in Healthy Individuals

Background

In the present group study we investigated whether healthy subjects can voluntarily gain control over right anterior insular activity by using fMRI-BCI. Cortical representation of smell and taste (Rolls 1996; Francis, Rolls et al. 1999; Rolls 2004), viscerosensation (Craig 2002), and pain perception (Coghill, Sang et al. 1999; Peyron, Laurent et al. 2000) converge in the insula and surrounding operculum. The activity of the insulae correlates with the subjective perception of emotional states (Craig 2002; Craig 2003). Studies on emotional perception showed that insula activity is correlating with the aversive valence of stimuli (Anders, Birbaumer et al. 2004). A review of PET and fMRI studies investigating the neuroanatomy of emotion (Phan, Wager et al. 2002) revealed that the anterior cingulate and insula were recruited during induction by emotional recall/imagery and during emotional tasks with cognitive demand. Awareness of salient emotionally stimuli increases right insula cortex activity (Critchley, Wiens et al. 2004) suggesting that this area is critical for the representation of bodily responses and interoception (Adam 1998). Therefore, volitional modulation of insula activity may be a valuable exploratory approach to study emotion regulation. Modulation of the insular activity with fMRI-BCI training might be relevant for the development of novel approaches for clinical treatment of social phobia or antisocial behaviour which have shown hyper-activity and hypoactivity, respectively, in the insular region (Veit, Flor et al. 2002; Birbaumer, Veit et al. 2005).

Methods

Fifteen healthy right-handed subjects participated in this study. Nine of them were trained to voluntarily control the local BOLD signal of the right anterior insular cortex using the fMRI-BCI system. The remaining six subjects participated in two different control conditions: 1) mental imagery of emotional episodes without any feedback, 2) non-contingent feedback.

The selection of ROI1 – the right anterior insula– was anatomically based on the high resolution T1 structural scan. This ROI was a rectangular area encompassing 4×5 voxels (~15×20 mm) on a single slice (5 mm). The reference ROI2 was a large background region of interest selected from a reference slice positioned distant from ROI1 encompassing the whole brain with the intent to cancel global effects and to average out any unspecific activation. During training, the mean BOLD signal from the regions of interest ROI1 and ROI2 was extracted. The first ten volumes of each session were excluded from statistical analysis to account for T1 equilibration effects.

For the feedback presentation the difference between the two ROI time-courses was calculated and normalized to the baseline.

The training consisted of four feedback sessions followed by a 'transfer' session performed in 1 day. One feedback session consisted of four regulation blocks (22.5 s each) during which the subjects had to learn to increase the BOLD signal in insula alternating with five baseline blocks (22.5 s each) during which they had to return the activity to the baseline level. Each session lasted about 4 min and was repeated five times including the transfer session. During the feedback session the normalized average BOLD signal from the right anterior insula was presented to the subjects by means of thermometer bars. The thermometer was displayed during regulation and rest period. The regulation blocks were cued with a red arrow at the thermometer display while during rest blocks a cross hair was presented in the same position. Additionally, two different control experiments were conducted to verify that the effects of the self-regulation of the insular activity were due to fMRI feedback. Three subjects participated to each of the control experiments. The first control condition aimed to verify the specificity of the feedback information; the control group performed three sessions of the same experimental paradigm but received sham feedback. This sham feedback was not specific to any particular brain area but consisted of information from a large background ROI from the same subjects not encompassing the anterior insulae. The second control condition assessed the effects of repetitive use of mental imagery. Subjects were provided with the same instructions and same general strategies as before, the thermometer frame was present but no fMRI-BCI information was available (no bars were shown). Subjects performed three consecutive sessions during which they were asked to recall and evoke memories and imagery of personally relevant affective events.

Results

All participants were able to successfully regulate the BOLD signal in the right anterior insular cortex. Training resulted in a significantly increased activation cluster in the anterior portion of the right insula across sessions. Subjects reported the use of both positive and negative mental imagery. Positive strategies were focused on recalling themselves playing music, playing with daughter, engaging in sport activities, recall of holidays; while negative strategies were focused mostly on bringing back themselves in dangerous situations, anger states and while taking examinations. Linear regression across all sessions performed on the individually selected region of interest showed significant increase of activity in the target area [$y=0.174+0.127$, $P<0.012$]. The success of training is observed by comparing the time course of the selected area during the last session (see Figure 3.4, lower image) with the first session (see Figure 3.4, upper image). Percent signal change calculated in the ROI as difference between task and rest for each subject and then averaged across all the participants resulted in a clear monotonic increase across the first three sessions [repeated measures ANOVA, $F_{(2,7)}=10.32$, $P=0.001$].
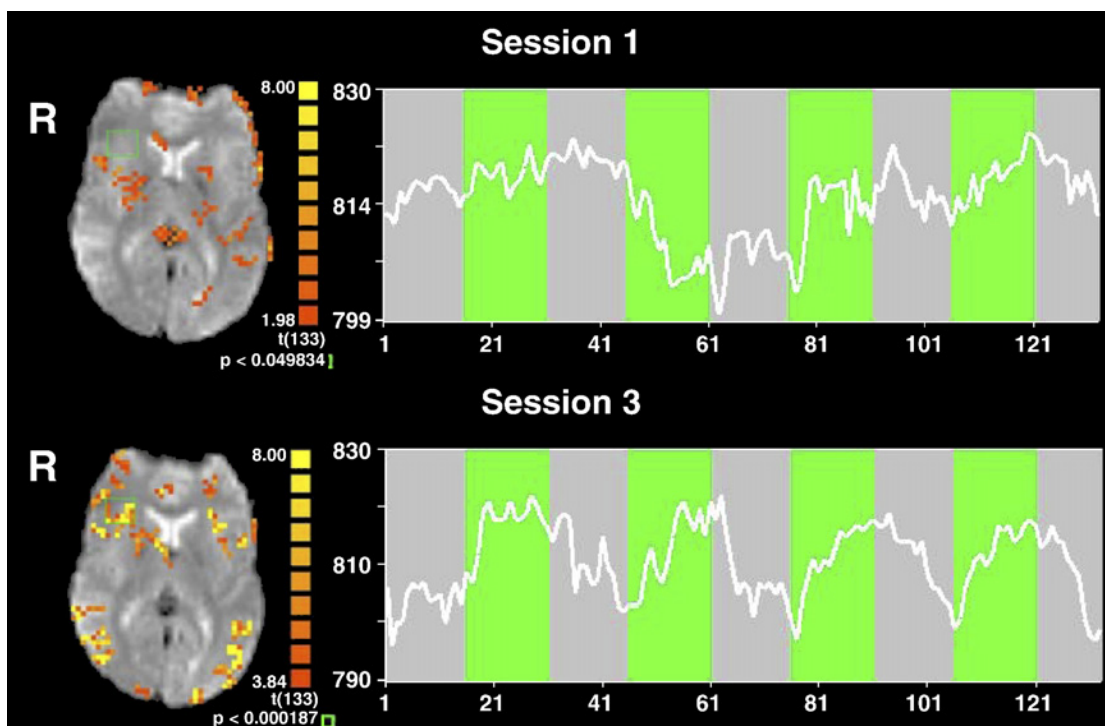
Figure 3.4. Single subject statistical maps (left) and BOLD time-courses (right) of the right anterior insula in the first (top) and in the last session (bottom). The selected ROI is delineated by the green box. Functional images are in the radiological convention and are not normalized. Statistical significance was based on t test comparing activation on each voxel during the regulation blocks with respect to the baseline blocks, with a threshold of P<0.05 false discovery rate (FDR) corrected for multiple comparisons. The time course of the BOLD activity (white line) is related to the ROI selected and is showing the progress during the regulation blocks (green) and the baseline blocks (gray). Number of volumes is in the x axis and magnitude signal in the y axis; these values are the raw output from the scanner.

Random effects analysis on the experimental group confirmed an increased BOLD-magnitude in the right anterior insular cortex over time (see Figure 3.5).
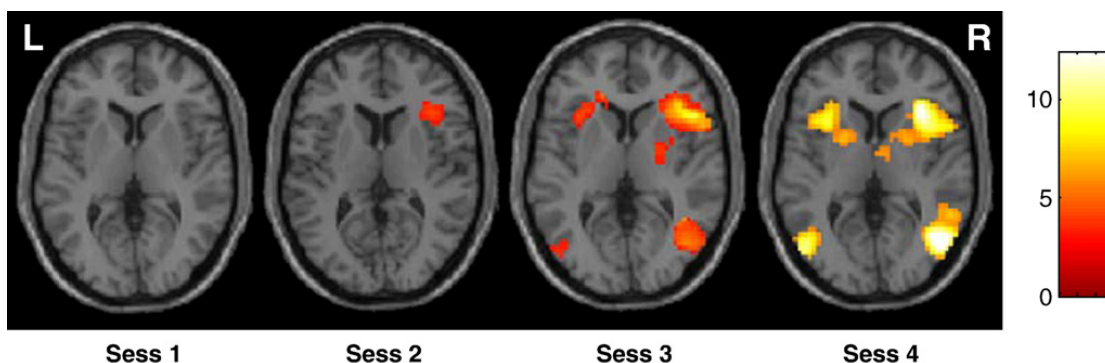
Figure 3.5. Random effects analysis on the experimental group confirmed an increased BOLD–magnitude in the right anterior insular cortex over time course. SPM2 of the single sessions showed no significant activation during the first session in the target area; a significant activation cluster (t=4.50; P=0.001, uncorrected) during the second session (MNI coordinates: 39, 33, 0); and a highly significant activation cluster (t=10.23; P<0.001, uncorrected) during the third session located

(MNI coordinates: 36, 26, 6). Fixed effect analysis was also performed on the six subjects who completed the fourth session reporting a higher significant cluster (t=12.47, P<0.001, FEW-corrected; MNI coordinates: 36, 23, 5). All activation maps are projected on a single-subject T1 template at the coordinate z=5.

Our results show that with fMRI-BCI a specific modulation of the right anterior insula is possible. This was achieved after a short training time. BOLD signal in the target ROI increased with the number of feedback sessions, indicating training effects and learning.

Regulation of Ventrolateral Premotor Cortex in Healthy Individuals & Stroke Patients

Background

Stroke is a principal cause of long-term disability. Although various treatment options are available there is currently no universally accepted treatment, especially for those patients who show little or no functional recovery of upper limb motor function. The aim of this study was to assess the feasibility of fMRI-BCI feedback training as a new tool in stroke rehabilitation. Four healthy young adults and two chronic subcortical stroke patients participated in three days training by using fMRI-BCI based neurofeedback. Healthy subjects and patients were trained to learn to regulate their brain activity in the ventral premotor cortex (PMv). PMv is a secondary motor area that contributes to the control of upper limb and head movements, particularly for grasping and manipulating objects. Therefore, it could play a significant role in functional recovery after stroke. We investigated real-time feedback using virtual hands and video showing first-person perspective of arm movement to guide self-regulation (unplublished).

Methods

Participants
Two right-handed chronic stroke patients (both male, 63 and 68 years old) and four right-handed healthy young adults (3 male, 1 female, mean age 25.3 years) participated in the study. The stroke patients had a history of a single subcortical stroke in the left hemisphere at least 1 year before the study and showed good recovery of hand function. Written informed consent was obtained from all subjects according to the Declaration of Helsinki and the University of Tübingen Ethics Committee.

Functional Localizer
The fMRI setup used for real-time data processing was the same previously described earlier. In order to determine the location of the PMv, all subjects underwent two localizer sessions. These sessions consisted of a block-based paradigm in which blocks of rest (15s) were alternated with blocks of action observation or movement execution (30s). The region of interest was selected on-line, based on functional maps generated by Turbo-BrainVoyager during localizer sessions. In the first localizer session subjects were shown a video of a hand holding a coffee cup and moving it to

the mouth. The video showed a right hand in first-person perspective (Figure 3.6). The right hand was chosen as the effector performing the action because all participants (healthy young adults and stroke patients) were right-handed and the right hand was also the paretic hand in the stroke patients. Therefore left PMv was the target ROI. First-person perspective was preferred based on the study by Jackson and colleagues (Jackson, Mavoori et al. 2006) suggesting that brain activity from the first-person perspective is more tightly coupled to the sensory-motor system than from the third-person perspective. Participants were instructed to observe the presented action carefully. The second localizer was run in order to compare the activation induced by the video with activation related to executing a similar hand movement. Participants saw the instruction "Please move your right hand towards your mouth" and had to execute the movement repeatedly. Due to limited space within the MR scanner and also in order to avoid head movement, participants were instructed to make a short movement using their forearm only.
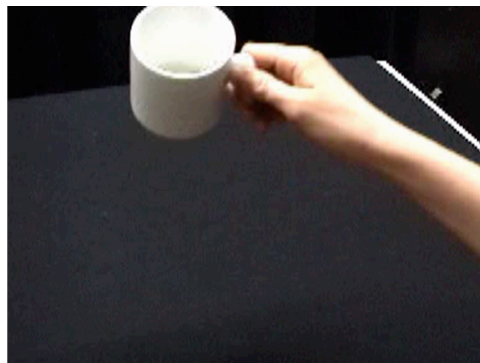

Figure 3.6: *Action observation localizer. First-person perspective.*

Feedback Training Protocol
All participants underwent three sessions of fMRI-BCI feedback training. The healthy young adults were trained on three consecutive days. The stroke patients had one day of rest in between the second and the third training session due to restricted access to the MR scanner. Each fMRI-BCI feedback session consisted of 4 runs of self-regulation training. During each run six activation blocks (45s) were alternated with baseline blocks (30s). The training was performed using a two different feedback scenarios: (1) a video feedback scenario with the same object-related hand movement as in the localizer (hand moving a coffee cup to the mouth, (Figure 3.7) and (2) as a control condition a feedback scenario showing a thermometer on which degree bars had to be increased. During the video feedback scenario participants saw a fixation cross on a static picture of a hand holding a coffee cup during the baseline. The beginning of a self-regulation block (activation block) was indicated by the disappearance of the fixation cross. In the thermometer feedback scenario subjects saw a fixation cross next to the thermometer during the baseline blocks and a red arrow (pointing upwards) next to the thermometer during the activation blocks. Participants were instructed on mental imagery strategies that potentially would have promoted self-regulation of the PMv. Instructions included kinesthetic feeling of the hand movement towards the mouth, lifting weights, moving an object from one place to another. During the first feedback training session participants were encouraged to explore different imagery strategies in order to find their own successful strategy. They were then asked to use this strategy throughout the remaining fMRI-BCI

feedback training. A further transfer session was also performed during which participants were instructed to perform the same task as during feedback but fMRI information was not provided and bars were not shown. The transfer session was performed to verify the efficacy of the feedback and to check whether training effects might persist beyond the experimental situation.
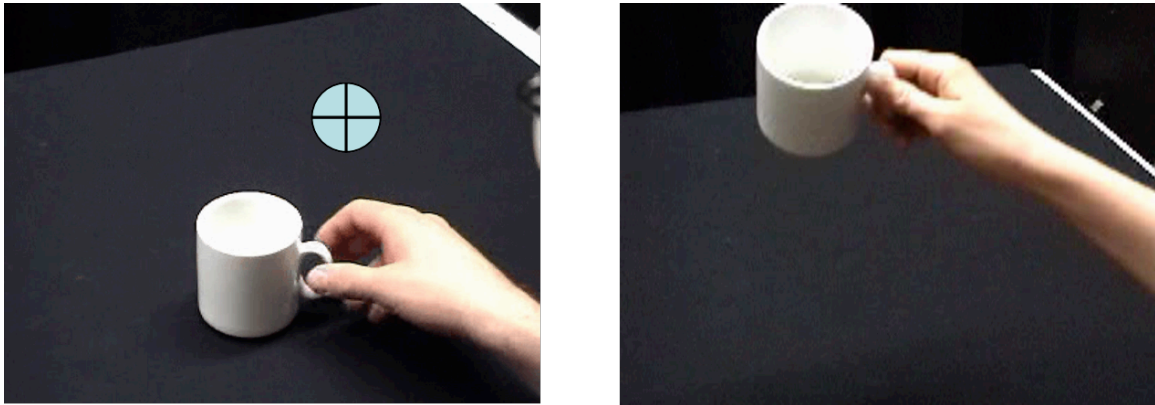
Figure 3.7. *Video feedback scenario. Left: baseline condition showing a static action observation picture with a fixation cross. Right: activation condition. Start of the feedback video is indicated by the disappearing of the fixation cross.*

Results

We present exemplary data from a healthy subject and a stroke patient.

Healthy young adult: Subject FB
During the video feedback sessions FB showed brain activations in bilateral PMv, bilateral SMA, bilateral somatosensory cortex, bilateral medial frontal gyri, bilateral inferior frontal gyri (BA44), bilateral superior temporal gyri, bilateral superior medial and inferior temporal gyri, bilateral inferior parietal lobe and bilateral medial and superior occipital gyri (**Figure 3.8a**). Local maxima of brain activity in the left PMv were identified at Talairach coordinates [x, y, z] [-42, -3, 48] and [-51, 6, 18]. Mean signal changes (%) for these two local maxima are depicted in Figure 3.8b-c. At both maxima the BOLD signal increased in all sessions compared to baseline and these signal changes (%) were quite stable over the 3 feedback training days.

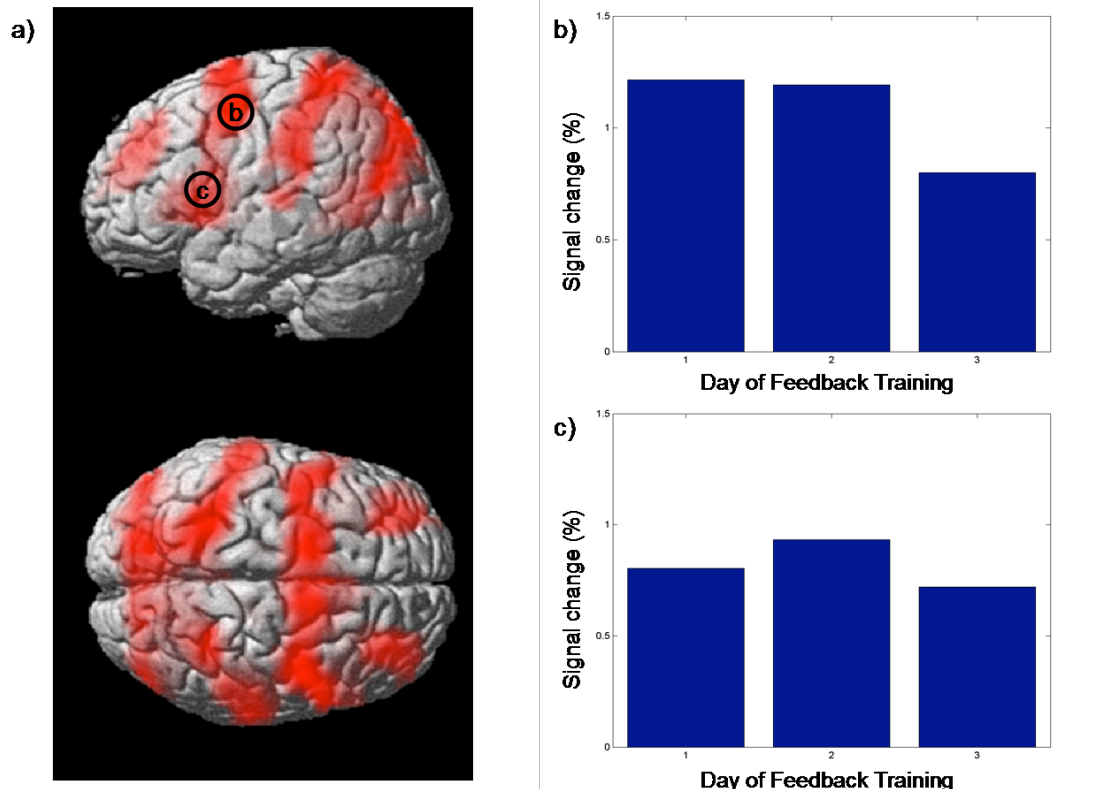*Figure 3.8: a) Brain activations during video feedback sessions (main effect). b) Mean signal change (%) in the left PMv (-42 -3 48) for each of the 3 training days. c) Mean signal change (%) in the left PMv (-51 6 18) for each of the 3 training days.*

During the thermometer feedback sessions FB showed brain activations in the same areas as during the video feedback scenario: bilateral PMv, bilateral SMA, bilateral somatosensory cortex, bilateral medial frontal gyri, bilateral inferior frontal gyri (BA44), bilateral superior temporal gyri, bilateral superior medial and inferior temporal gyri, bilateral inferior parietal lobe and bilateral medial and superior occipital gyri. Local maxima of brain activity in the left PMv were identified at Talairach coordinates [-54, 3, 48] and [-48, 6, 21]. At both maxima the BOLD signal increased for all sessions compared to baseline and these signal changes (%) were quite stable over the 3 feedback training days.

During the transfer scenario FB showed brain activations in bilateral PMv, bilateral PMd, bilateral SMA, bilateral primary motor cortex, bilateral somatosensory cortex, bilateral medial frontal gyri, bilateral inferior parietal lobe, bilateral superior temporal gyri, bilateral superior medial and inferior temporal gyri, and left medial and superior occipital gyri. A local maximum of brain activity in the left PMv was identified at Talairach coordinates [-48, 3, 15]. At this maximum the BOLD signal increased during both feedback training sessions compared to baseline. However, the signal change (%) was greater during the training session on day 2.

Stroke patients. Patient WS
During the video feedback scenario WS showed brain activations in bilateral PMv, bilateral PMd, left M1, bilateral somatosensory cortex, bilateral SMA, bilateral medial frontal gyri, bilateral inferior frontal gyri (BA44/BA45), bilateral inferior parietal lobe

(Figure 3.9a). Local maxima of brain activity in the left PMv were identified at Talairach coordinates [-57, -3, 21] and [-45, 3, 42]. Mean signal changes (%) for these local maxima are depicted in Figure 3.9b-c. At local maximum [-57, -3, 21] the BOLD signal increased substantially from the second to the third feedback training session. At [-45, 3, 42] a different pattern emerged: the largest BOLD signal change (%) occurred on day 2 of the feedback training.
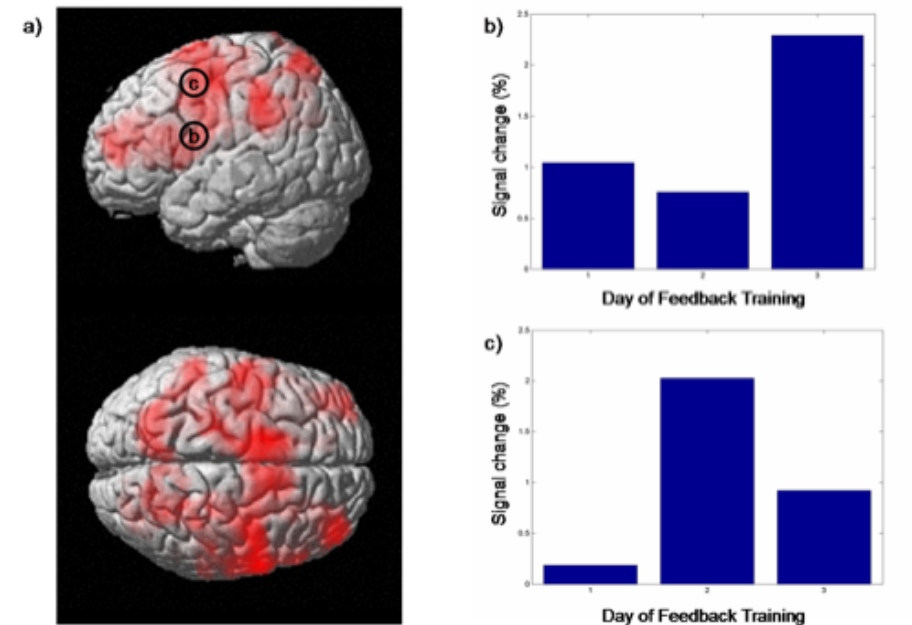

Figure 3.9: a) Brain activations during video feedback scenario (main effect). b) Mean signal change (%) in the left PMv (-57 -3 21) for each of the 3 training days. c) Mean signal change (%) in the left PMv (-45 3 42) for each of the 3 training days.

During the thermometer feedback scenario WS showed brain activations in the same areas as during the video feedback scenario: bilateral PMv, bilateral PMd, left M1, bilateral somatosensory cortex, bilateral SMA, bilateral medial frontal gyri, bilateral inferior parietal lobe. Local maxima of brain activity in the left PMv were identified at Talairach coordinates [-57, -3, 21] and [-48, 0, 36]. All training sessions showed increases of the BOLD signal compared to baseline. At [-57, -3, 21] the BOLD signal change (%) was lower during the second session than during the first session but was large during the third session. At [-48, 0, 36] the BOLD signal increased from session to session.

During the transfer scenario WS showed brain activations in bilateral PMv, left M1, bilateral SMA, bilateral medial frontal gyri, bilateral inferior frontal gyri (BA44/BA45), left inferior parietal lobe, right middle and superior occipital gyri. A local maximum of brain activity in the left PMv was identified at Talairach coordinates [-51, 3, 45]. The BOLD signal increased during both transfer sessions compared to baseline but the increase was greater on day 3 of the training.

Discussion

This pilot study provided first evidence that it is possible to learn to modulate brain activity in PMv. Participants learned to up-regulated PMv activity. However, the individual time courses of the self-regulation training followed different patterns. Some subjects learned to regulate PMv activity immediately, as indicated by a large BOLD percent signal change in the PMv during the first session of the feedback training. Other subjects showed a progressive increase of the BOLD signal in PMv over the three following training sessions. Design of future fMRI-BCI feedback studies must take into account the inter-subject variability during regulation training. The length of the training might be calibrated individually in order to achieve maximal benefit, especially for stroke patients. It is noteworthy that additional factors such as attention and fatigue can strongly influence neurofeedback training.

Comparison of the patterns of mean BOLD percent signal change of different regions in the left PMv within each subject shows that the mean percent signal change is not homologous across slocal maxima in a single subject. This might be explained by the notion that PMv is somatotopically organized (Buccino, Binkofski et al. 2001). Whether differential BOLD signal modulation within PMv itself has any impact on behavioral and neurophysiological effects of the feedback training is currently unclear.

Interestingly, almost all subjects showed bilateral PMv activation, and right PMv sometimes showed even a stronger activation. This result, even though at first glance might appear contradictory as the subjects were specifically instructed to image right hand actions only, in fact it is consistent with findings of previous neuroimaging studies. Bilateral PMv activation was found during precision grasping (Ehrsson, Fagergren et al. 2000; Ehrsson, Fagergren et al. 2001) and object manipulation (Binkofski, Buccino et al. 1999). Additionally two other studies demonstrated the existence of ipsilateral finger representations in PMv (Cramer 1999; Hanakawa, Parikh et al. 2005). Recently bilateral activation of PMv during precision grasping was confirmed by a TMS study. Davare et al. (Davare, Andres et al. 2006) found that both left and right PMv code hand posture during grasping movements with the right hand. They suggest that both PMv are active during an early phase of movement preparation. According to this suggestion the persistent bilateral PMv activation observed throughout the fMRI-BCI feedback training could be due to an early planning/programming component of the imaged action. Using a block design with repeated imagery of the action within a certain time period this early planning/programming component can show up as persistent activation. The relevance of the observed bilateral PMv activation for the outcome of the feedback training is unclear.

These results might be also remarkable in the light of a number of behavioral studies demonstrating interference between action observation and action execution (Brass, Zysset et al. 2001; Castiello 2003). It has also been shown that observation of an action facilitates its subsequent execution (Craighero, Bello et al. 2002). Action observation is a prerequisite for the imitation of actions. Based on the large amount of evidence that action observation recruits the motor system in a similar fashion as action execution it has been suggested that action observation may be used to promote recovery of hand function after stroke by affecting cortical reorganization (Buccino, Solodkin et al. 2006). Overall the results of this pilot study, combining both a

sophisticated technique to directly enhance PMv activation and an 'action observation' strategy due to the peculiar feedback used, are promising and stimulating but more subjects need to be tested before conclusions can be drawn and furthermore specific behavioral tests might corroborate and confirm the efficacy of this novel approach. In chapter 2, we have demonstrated the application of NIRS for the development of BCIs. As NIRS is a more portable and affordable system, and as NIRS can access the premotor and motor cortical regions, future work should explore the application of NIRS-BCI for neurorehabilitation of stroke victims.

Self-regulation of Right Inferior Frontal Gyrus and Language Processing

Background

There is evidence in favour of a central role of the left inferior frontal gyrus (IFG) in a number of linguistic tasks. Known as Broca's area, this brain site has been postulated to be a crucial structure for syntactic and semantic processing (Friederici, Kotz et al. 2003; Heim 2005). While the significance of the left hemisphere has been highlighted by a considerable amount of evidence, the functional role of the contralateral site of Broca's area in speech processing still needs to be clarified. Some studies have indicated the recruitment of the right hemisphere during processing of emotional prosody (Kotz, Frisch et al. 2003; Friederici and Alter 2004). Clinical evidence has suggested that impairments of the left temporal-frontal network might allow contralateral areas to take over functions previously carried out by the homologues left-sided brain structures (Thulborn, Carpenter et al. 1999; Fernandez, Cardebat et al. 2004). Based on the above consideration, we used fMRI-BCI to train subjects to achieve control over the level of activation recorded in the right IFG, aiming to investigate short-term effects of operant BOLD-training on linguistic performance (Rota, Sitaram et al. 2008).

Methods

Participants
Twelve matched males, German native speakers (aged 24-30 years, mean age = 27), right handed according to the Edinburgh Handedness Inventory (Oldfield, 1971), participated in this study. Seven of them were trained to acquire control over the BOLD signal in the right IFG by means of real-time fMRI feedback. The remaining five were recruited as control subjects.

Experimental procedure and data analysis
The pars triangularis of the right IFG was chosen as the target region of interest (ROI$_{target}$) for the experimental group, and it was individually selected by means of a functional localizer run. The ROI$_{target}$ was selected as a square region (6x6 voxels, ~ 20x20 mm) centred on the area of activation. The mean location across subjects in MNI coordinates for the centre of the selected ROI$_{target}$ was $x = 51$, $y = 18$, $z = 6$. A large reference slice (ROI$_{control}$) was used as control area in order to account for global changes of activity, and cancel out effects due to task-unspecific activation. During training, mean BOLD signal was extracted from the ROIs. The differential BOLD

response $[(ROI_{target} - ROI_{control})_{\text{activation blocks}} - (ROI_{target} - ROI_{control})_{\text{baseline blocks}}]$ was transformed into the visual feedback of varying graduations of a thermometer and presented in real-time (interval of 1.5s) to the subjects by means of video projection.

The functional localizer

We employed a linguistic task which was previously shown to reliably activate the pars triangularis of the right hemisphere (Dogil, Frese et al. 2004). This "prosody-unrelated" task was adopted to avoid the risk of a facilitation effect, which might have been induced by performing a similar or strictly related task during both the localizer and the performance-evaluation phases. This task was carried out by the participants before the beginning of the training. The localizer session consisted of four activation blocks, separated by five baseline blocks, beginning and ending with a baseline block. Every block lasted for 50 s. The stimuli consisted of 20 balanced German sentences with three syntactic constituents and were presented visually as lines of text by means of video projection. During each activation block, 10 sentences (5 s each) were presented without an inter-stimuli interval. A total of 40 sentences were presented for the whole localizer session (total length of the session = 7.5 minutes). The subjects were instructed to read each sentence silently, to manipulate its word order, and to replace the subject noun phrase (NP) with a hyperonym (for details on this task see Dogil, Frese et al. 2004).

Neurofeedback-training

The training consisted of 4 BOLD-feedback sessions, each of which encompassed six activation blocks (50 s each) separated by five baseline blocks (30 s each), beginning and ending with a baseline block (length of each session = 8.5 minutes). During activation blocks, the subjects had to increase the level of activation recorded from the right IFG (BA 45). During baseline blocks, they were instructed to relax by performing mental imagery that could help them to relax, e.g., imagining themselves being on a beach with a vast expanse of blue water. For both types of blocks, subjects from the experimental group received real-time visual feedback of the differential BOLD signal detected in the ROI_{target} (BOLD detected in the ROI_{target} minus BOLD detected in the $ROI_{control}$). Control subjects received sham feedback based on signals taken from a different brain area that did not correlate with the cognitive processes engaged by the subjects. Areas that were used to extract sham-feedback included the parahippocampal place area (PPA) and the posterior cingulate cortex. The symbols "↑" and "+" were presented on the left side of the thermometer to signal the beginning of each activation or baseline block, respectively.

Behavioural tasks

Stimuli belonging to two behavioural tasks were divided into two balanced sets, each of which was performed either before or after the training, in a random way across subjects. At the end of the training-phase, subjects were instructed to focus on the same cognitive strategies previously successfully adopted, and to continuously up-regulate BA 45 while carrying out the two tasks. No feedback on brain self-regulation was provided to the subject in this phase. Identification of emotional prosody was used to test short-term training effect on prosodic processing. This task consisted of four sets of German sentences belonging to the Tübingen Affect Battery (Breitenstein, Daum et al. 1996), describing happy, sad, angry or neutral scenarios, for a total of 16 samples. Each sentence was read by a professional actress with sad, happy, angry and neutral emotional intonations, producing a total of 64 samples. The strings lasted 2 s

and were randomly presented. The participants listened to a sentence at once and were instructed to identify its emotional intonation in the shortest time possible, within a 4 s limit. Prosody judgments were performed by button pressing (i.e. selecting from a four-button device the key corresponding to the intended emotional intonation). A fixed inter-trial interval of 12 seconds was chosen. At the end of the session, subjects were debriefed, and their ability to reliably hear and understand the aurally presented stimuli was confirmed.

Speeded grammaticality judgments were used to test short-term training effects on syntactic processing. The stimuli consisted of 48 balanced German sentences belonging to three sets: ambiguous, incorrect and correct sentences. The sets of sentences were approximately the same length, and were randomly presented. In order to control for reading strategies the strings were provided to the subjects in a segmented and successive manner, and each word was presented visually for 400 ms by means of a video projection. The subjects could view just one word at a time and were instructed to perform grammaticality judgements (Meng and Bader 2000). The critical segment for deciding about grammatical correctness always appeared at the end of each string. After the presentation of the last segment, a question mark signalled to the subjects that they should judge the correctness of the preceding sentence. The judgment task was carried out by button pressing (i.e. right button for correct or pressing the left button for incorrect sentences). Subjects were instructed to carry out grammaticality judgment in the shortest time possible, within a 4 s limit. An inter-trial interval of 12 seconds was chosen.

Results

All experimental-group subjects achieved voluntary differential up-regulation of the activation-level recorded in the ROI_{target}, as required by the task. A progressive increase of the level of activation in the right BA 45 (mean center of activation in MNI coordinates = 51, 18, 6) across training sessions suggests a learning effect (r = 0.98; N = 4 sessions, P = 0.01 one-tailed; linear regression). A similar but not significant trend was observed for the control group (r = 0.82; N = 4 sessions; P = 0.08 one-tailed, linear regression). Please see figure 3.10.

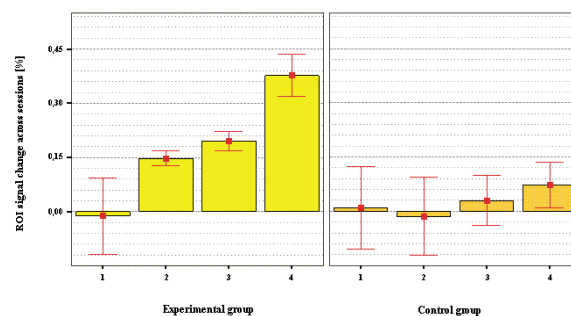*Figure 3.10*. *Percentage of signal change locally recorded from the right BA 45 (MNI = 51, 18, 6) across training-sessions for both experimental and control groups. Bars show mean and error bars indicate mean+/- 1.0 standard error (SE). A significant increase of BOLD signal in the ROI (r = 0.98, N = 4 training-sessions, P = 0.01 one-tailed, regression analysis) across sessions was detected for the experimental group*

only, and suggests a learning effect. Significant differential activation of the ROI_{target} for session 4 versus session 1 was observed for the experimental group only (two-tailed paired t test, N = 7, P = 0,021).

Increased differential activation (calculated for up-regulation blocks versus rest) in the ROI_{target} across sessions was observed for the experimental group [repeated measures ANOVA, $F(3,18) = 6.379$, $P = 0.004$], but not for the control group [repeated measures ANOVA, $F(3,12) = 0.216$, $P = 0.883$]. Fixed-effects analyses on the experimental group showed an increased level of activation from session 1 for the experimental group only (N = 7, FWE corrected, no activation observed, $P < 0.001$) to session 4 (N = 7, FWE corrected, $t = 6.96$, $P < 0.001$). Random effects analyses on the experimental group confirmed the results of the fixed-effects analyses by showing an increased level of activation for the ROI_{target} from session 1 (ROI analysis, ROI = right BA 45, N = 7, no activation observed, $P < 0.05$, FDR corrected) to session 4 (ROI analysis, N = 7, $t = 3.43$, $P < 0.05$ FDR corrected). Subjects reported strategies connected to speech, such as imagination of lecturing before a class of students, arguing scenes with colleagues, and debates. Other strategies included imagined singing, imagined recitation of poems, and recalling old conversations with friends.
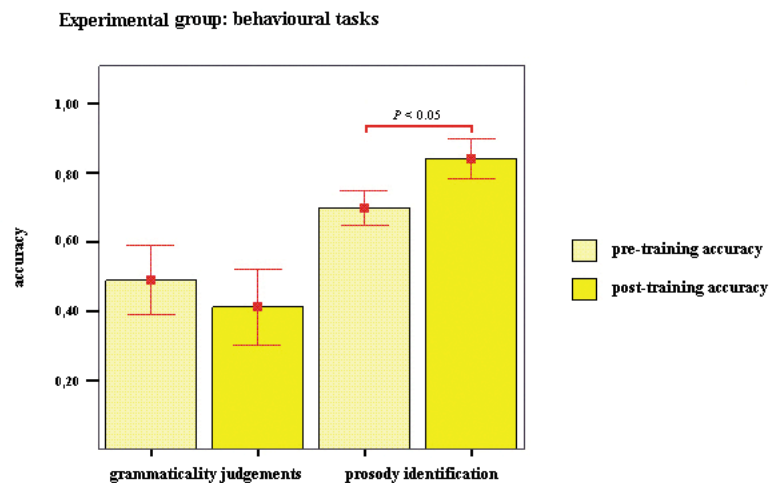
Figure 3.11. Behavioural effects of up-regulation of the right BA 45: experimental group. The figure shows mean levels of accuracy for grammaticality judgments and identification of prosodic intonations preceding and following fMRI-BCI training. Significant improvement was observed for detection of affective intonations only (two-sided Wilcoxon signed-rank test, P < 0.05). Bars show mean accuracy level, and error bars indicate mean +/- 1.0 SE.

Experimental subjects succeeded in correctly identifying 70 ± 13 % (mean ± SD) of the affective prosodic stimuli before the beginning of the training, and 84 ± 15 % (mean ± SD) after it. Statistical analysis showed a significant difference between the two sets of scores (two-sided Wilcoxon signed-rank test, $P = 0.017$, see figure 3.11). Pre-training RTs were 3455.7 ms ± 317,2 ms (mean ± SD), and post-training RTs were 2926,3 ms ± 548.5 ms (mean ± SD)]. Statistical analyses showed a significant difference between the two sets of scores (two-sided Wilcoxon signed-rank test, $P =$

0.043). With respect to the grammaticality judgment task, experimental subjects achieved 49 % ± 26% (mean ± SD) of accuracy before the training and 41 % ± 29 % (mean ± SD) after it. Statistical analysis revealed no significant difference between the two levels of accuracy (two-sided Wilcoxon signed-rank test, $P = 0.55$). Pre-training RTs were 1547.6 ms ± 357.4 ms (mean ± SD) and post-training RTs were 1186.7 ms ± 558.9 ms (mean ± SD). Statistical analyses showed no significant difference between the two sets of scores (two-sided Wilcoxon signed-rank test, $P = 0.091$).

Discussion

In this study (Rota, Sitaram et al. 2008), we tested the hypothesis that humans can learn to volitionally increase the BOLD-responses locally recorded in the pars triangularis of the right IFG. In all experimental subjects the level of activation restricted to the right BA 45 increased across training sessions. This result indicates a progressive learning effect, and suggests that real-time fMRI-biofeedback is a promising tool for non-invasively manipulating localized brain activity. Even though both control and experimental subjects were provided with the same strategy guidelines, their efficacy in up-regulating the ROI_{target} greatly differed. The unavailability of genuine feedback information made it impossible for the control group to evaluate the efficacy of the ongoing regulation process, thus presumably impeding the learning process. The comparison of performances in the two tasks pre and post-training suggests that up-regulation of BA 45 correlates to a specific improvement in detecting and identifying emotional prosodic intonations. This effect was not observed for the control group. No significant differences in performance were measured for syntactic processing. These findings suggest that the right IFG plays an important function in mediating the understanding of a speaker's emotional state and intentions. So far, the role played by the right hemisphere, and specifically by the right BA 45, with respect to language processing has been only marginally explored. The findings of our experiment are consistent with a number of studies that indicate the involvement of the right IFG in the processing of prosodic features for auditorily presented stimuli (Friederici and Alter, 2004; Kotz et al. 2003). Following these lines, fMRI-BCI training could potentially be used to stimulate and strengthen linguistic abilities connected to emotional processing. The possibility of facilitating the cognitive processing of emotional speech appears of particular interest for a number of clinical applications. Clinical studies have shown that the identification of affective prosody is strongly impaired in schizophrenic patients. As reported by Hoekert and colleagues (Hoekert, Kahn et al. 2007), deficits in processing of emotional cues conveyed by speech are among the most pervasive disturbances in psychosis. Other clinical studies have shown that schizophrenia correlates with an abnormally reduced cerebral blood volume (Brambilla, Cerini et al. 2007), and hypofunctioning of the prefrontal cortices (Snitz, MacDonald et al. 2005). Furthermore, the recognition of emotion from prosodic stimuli is also compromised in patients suffering from major depression. As reported by Kan and co-workers (Kan, Mimura et al. 2004), depressed patients are biased in their interpretation of neutral emotions (for both prosody and faces), and tend to attribute a negative valence to them. Presumably, these brain sites could be targeted as loci of self-regulation, and neurofeedback aids could be employed as therapy to normalize hypofunctioning cortical networks.

Chapter 4

Decoding Emotion States of the Brain from fMRI Signals

Introduction

An important question that confronts current research in neuroscience as well as in the treatment of neuropsychological disorders is whether it is possible to determine the emotional state of a person based on the measurement of his/her brain activity. Related questions are: 1) is it possible to perform such emotion detection automatically, by a computer or a machine, with minimal or no human intervention? and 2) is it possible to do this online, in real-time (milliseconds or seconds after the acquisition of the brain signals) as against after several minutes or days of offline processing? Development of techniques that answer the above questions in the affirmative help not only to further the progress of affective neuroscience but also in the development of technologies, commercial products and services such as brain-computer interfaces (BCIs), neurofeedback systems, clinical treatment of mental disorders including but not restricted to depression, schizophrenia, anxiety, psychopathy and social phobia, automatic detection of deception in criminals and persons endangering security, development of affective and socially competent computers, intelligent machines and robots that recognize and express emotions.

Conventional neuroimaging methods seek to find out how a particular perceptual, motor, cognitive or emotional state is encoded in brain activity by measuring brain activity from many thousands of locations repeatedly, but then analyzing each location separately (Univariate analysis). If the responses at any brain location differ between two states, then it is possible to use measurements of the activity at that location to determine or decode the state. This is the basis of the Statistical Parametric Mapping (SPM) techniques currently in vogue in analyzing fMRI signals. In practice it is often difficult to find individual locations where the difference between conditions are large enough to allow for efficient decoding. The limitations extend to current fMRI-BCI and neurofeedback methods which use univariate methods albeit in real-time. In contrast to the conventional analysis, sensitivity of neuroimaging can be improved by using multivariate, pattern-based methods. Pattern-based methods use advanced machine learning techniques, such as multilayer neural networks, support vector machines and so forth to discriminate spatial, temporal and spectral patterns in a system, methods that have been previously successfully used in character recognition, speech recognition and image recognition applications. Such pattern-based multivariate analysis has several advantages over conventional univariate analysis:

❋ Weak information available from single locations can be accumulated

across many spatial locations.

* Interaction between brain regions, as can be determined by simultaneously analyzing activity in multiple locations could have important information for decoding brain states.

* Temporal evolution of activity in different regions and their interactions can be different for different brain functions thus providing information for recognizing them.

* Conventional Neuroimaging uses preprocessing methods such as spatial smoothing, that might remove important information about the brain state. Multivariate methods which simultaneously analyse pattern of brain activity across multiple locations are able use this information more effectively.

* Conventional methods typically average brain activity across multiple trials to improve statistical sensitivity. However, by computing average activity, information about the state of the brain at any given point in time is lost. In contrast, the pattern-based methods incorporate this temporal information in the analysis.

* In summary, pattern-based methods use considerably more information for detecting the current state from measurements of brain activity.

Another disadvantage of the existing fMRI-BCIs is in the method of selecting single regions of interest for providing feedback of activation to the participant or patient. In the previous studies with fMRI-BCI, brain signals from one or two regions of interest (ROI) were extracted for providing neurofeedback to the subject. While this approach has shown convincing evidence that volitional control of circumscribed brain regions results in behavioral changes, the system needs to be further improved for clinical applications. A major argument for moving away from deriving feedback signals from single ROIs is that perceptual, cognitive or emotional activities generally recruit a distributed network of brain regions rather than single locations. Furthermore, while activity in certain locations of the network could be facilitatory, activity in certain other locations could be inhibitory, thus maintaining a complex temporal interaction among the regions. As such representation of activity from one or two ROIs, merely combined with additive and subtractive contrasts, does not completely model the network dynamics of the desired brain state.

Secondly, there is variation among individuals with regard to brain structure and activity. Extracting signals from spatially localized regions may lead to sub-optimal or even discordant feedback information for the desired behavioral training.

An improved method for employing the whole network of activity with no assumption on the inhibitory or excitory effects of single ROIs needs to be implemented. Our proposed method makes no assumption about the functional localization and performance strategy used by the subject.

Recently, there have been studies on the offline pattern-classification of brain states from fMRI signals using multilayer neural networks (MNN) (Norman, Polyn et al. 2006), Fisher Linear Discriminant (FLD) classifier (Mourao-Miranda, Bokde et al. 2005), Support Vector Machines (SVM) (LaConte, Strother et al. 2005). However, because they are computationally intensive and need constant human input during

modeling and analysis, they can not be directly applied to real-time fMRI including fMRI-BCI and neurofeedback applications. Until now only one implementation (Laconte, Peltier et al. 2006) of real-time fMRI pattern classification system using SVM has been reported. However, this implementation has 2 main drawbacks that limits its application to fMRI-BCI and neurofeedback systems. Firstly, the above method works based on spatial pattern of brain activity alone as input in discriminating different states of the brain and ignores the temporal pattern or time evolution of brain activity. The BOLD activations from previous time points were not used during classification or were averaged out removing useful information. This was done to reduce the large dimension of fMRI input. Greater the dimension of data input to the classifier, greater would be the time involved during training and online operation. To give an example, an Echo Planar Imaging (EPI) (used normally in real-time fMRI measurements) employing Field of View (FOV) of 212x 212 in the X and Y dimensions, and having 64x64 image matrix and 16 slices (thickness = 5mm) has in total 65,536 voxels (64x64x16), each voxel of resolution 3.3x3.3x5mm in the X,Y,Z directions. Data input of such a large dimension (>65,000) for every time point to an SVM for a real-time classification would be daunting in terms of memory and computational resources. BOLD signal has its onset after about 3s of the neural activity and reaches its peak after 6s of onset of activity, and comes down to zero after 10-12s of the onset. Considering the above, from 6-10s of past BOLD values could be useful brain state discrimination. However, if voxel activations from previous n time points are included, the size of input then increases n-fold increasing training time of the classifier and adversely affecting online performance even further.

Method

To overcome the above limitations, we have recently developed a real-time brain state detection system (Sitaram, Lee et al. 2008) based on the support vector machine (SVM) classification of whole-brain fMRI signals for each repetition time of acquisition (TR). The aim of the experiment was to investigate for the first time if a brain state detection system can be built to recognize emotional states of the brain from fMRI signals and whether the output from the real-time classifier could be used for providing feedback to the participant. The experiment was conducted in 3 stages:

Stage 1: Acquisition of fMRI signals when participants are presented: **a)** Standard pictures from International Affective Picture System (IAPS) known to elicit discreet emotions: neutral, happy and disgust emotions. **b)** instructions to recall emotional episodes belonging to categories: neutral, happy and disgust. Classifier parameters are then estimated for each participant by using our custom developed SVM toolbox for fMRI data.

Stage 2: Testing the classifier for each participant on new fMRI data acquired during a similar paradigm (as above) involving viewing of emotional pictures or recall of emotions.

Stage 3: Neurofeedback training of emotional regulation using a thermometer feedback based on real-time brain state classification.

Figures 4.1 and 4.2 show the experimental paradigm for emotional picture presentation and instructions for recall of emotional episodes.
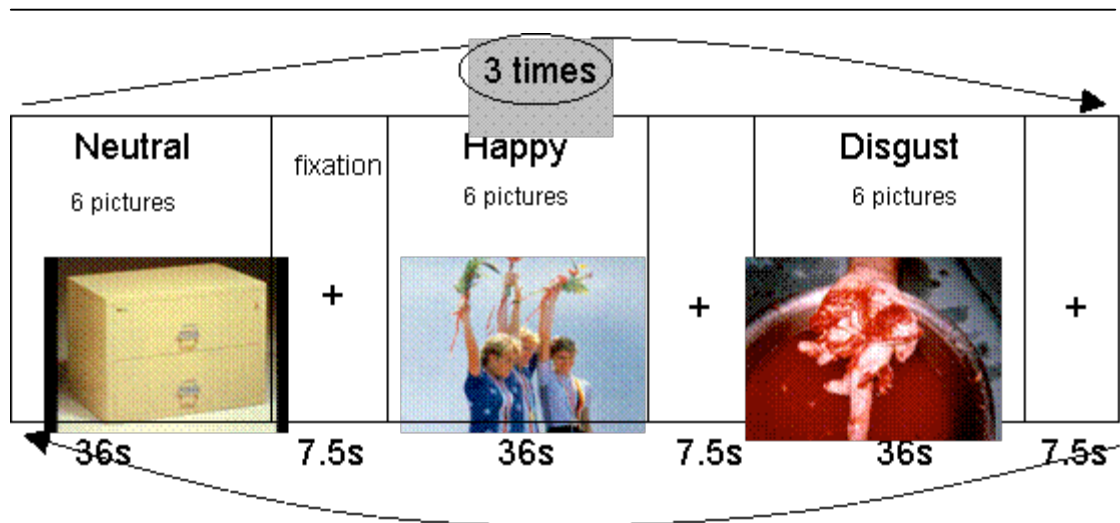
Figure 4.1: *Each run has 3 blocks of emotional picture presentation alternating with a fixation cross. Six pictures are presented in each block of emotion. Each picture will be shown for 6s. Students were asked to attend to each picture without moving their head and body. During fixation block students were required to count back from 100 to 1.*
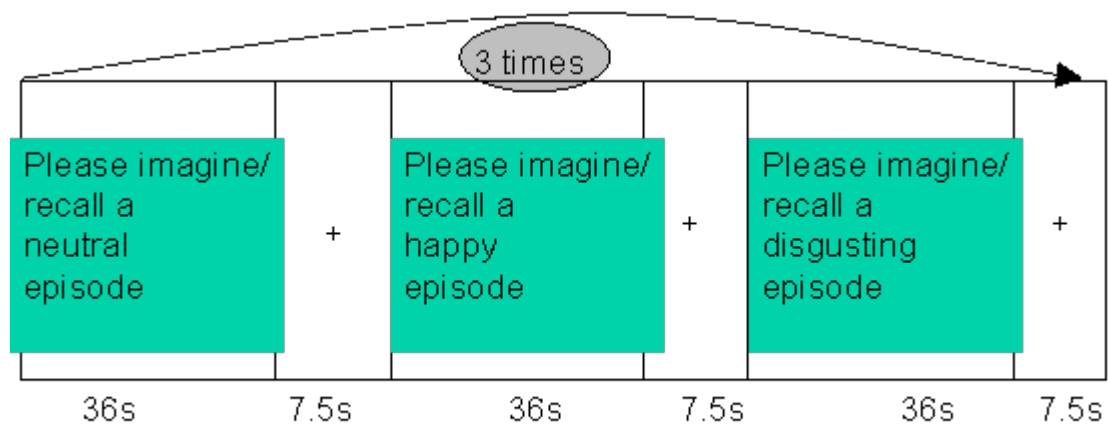

Figure 4.2: *Each run has 3 blocks of emotional recall instructions alternating with a fixation cross. Instructions were given in English and German. In each recall block students were instructed to recall corresponding emotions (neutral, happy and disgust). During fixation block students were required to count back from 100 to 1.*

FMRI data acquired during the above experimental paradigm from each participant was corrected for head motion in real-time by performing realignment and smoothed to reduce noise. To reduce the large dimension of input to the classifier due to large number of voxels in the brain (64 x 64 x 16 = about 65,000), a feature extraction step was performed. First, non-brain voxels were excluded with a thresholding method. Secondly, the Fisher Criterion (FC) (as shown in equation below) was used to select voxels which had higher discriminability for different emotional states compared to other voxels. This voxel selection method would reduce computational time and make the classifier more robust in the presence of noisy signals.

$$score_F(X) = \frac{(mean(X_1) - mean(X_2))^2}{var(X_1) + var(X_2)}$$

Classification was based on multivariate SVM to investigate which brain areas are associated in discriminating between different emotional states. SVM was used to discriminate between the following emotional states: neutral vs. happy, neutral vs. disgust, and happy vs. disgust. In addition, 5-fold cross validation was performed by dividing the whole data set into 5 separate permutations of a *training set* and a *testing set*, to each time test the accuracy of classification. In this process, the threshold of FC was selected which showed the lowest error rate and the lowest standard deviation of error.

A new measure was developed to determine the discriminability of each voxel as obtained by the SVM method. This new measure was defined as the ratio of mutual information between a weighted voxel value and the designed label to the mutual information between the weighted sum of other voxels without the voxel in question and the designed label (as shown in the equation below). The weighting used in the above definition is obtained from the weight vector obtained due to SVM model training.

$$MI(w_i x_i ; y) / MI(w_{-i} x_{-i} ; y)$$

where,

$w_{-i} x_{-i}$: is the weight vector multiplied by the voxel vector for the i-th component,

$\hat{y} = \text{sgn}(wx + b)$: is the the predicted output of SVM.

To test the reliability of the SVM classification on new data, subjects were shown new sets of IAPS pictures invoking the different emotional states, and fMRI signals were collected in real-time using a custom-written Echo Planar Imaging (EPI) sequence developed in our institute for the purpose of real-time acquisition (1.5 s interval) and feedback for an fMRI Brain-Computer Interface. The real-time SVM classifier then determined the emotional state of the brain. Based on the classification result, a visual feedback was provided to the subject in the form of graphical thermometer with changing bars (see figure 4.3).
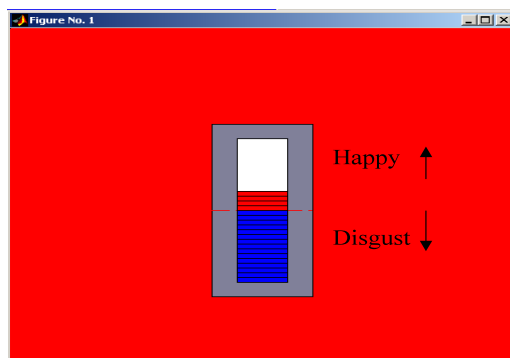
Figure 4.3. Graphical thermometer that provides real-time feedback of the emotional state detected by multivariate SVM.

Results

The SVM offline pattern classifier could classify brain states from the participants with an average accuracy of around 90% (figure 4.4), while the real-time version tested on 4 participants showed an average accuracy of above 70% and maximum accuracy of 90%. The following bar chart shows the performance of the classifier. Remarkably, on a few participants, a classifier that was trained to discriminate emotional states elicited by pictures could also discriminate emotional states realized through recall with about ~70% accuracy. This result suggests that there are common areas of activation between picture-based and recall-based emotion induction.
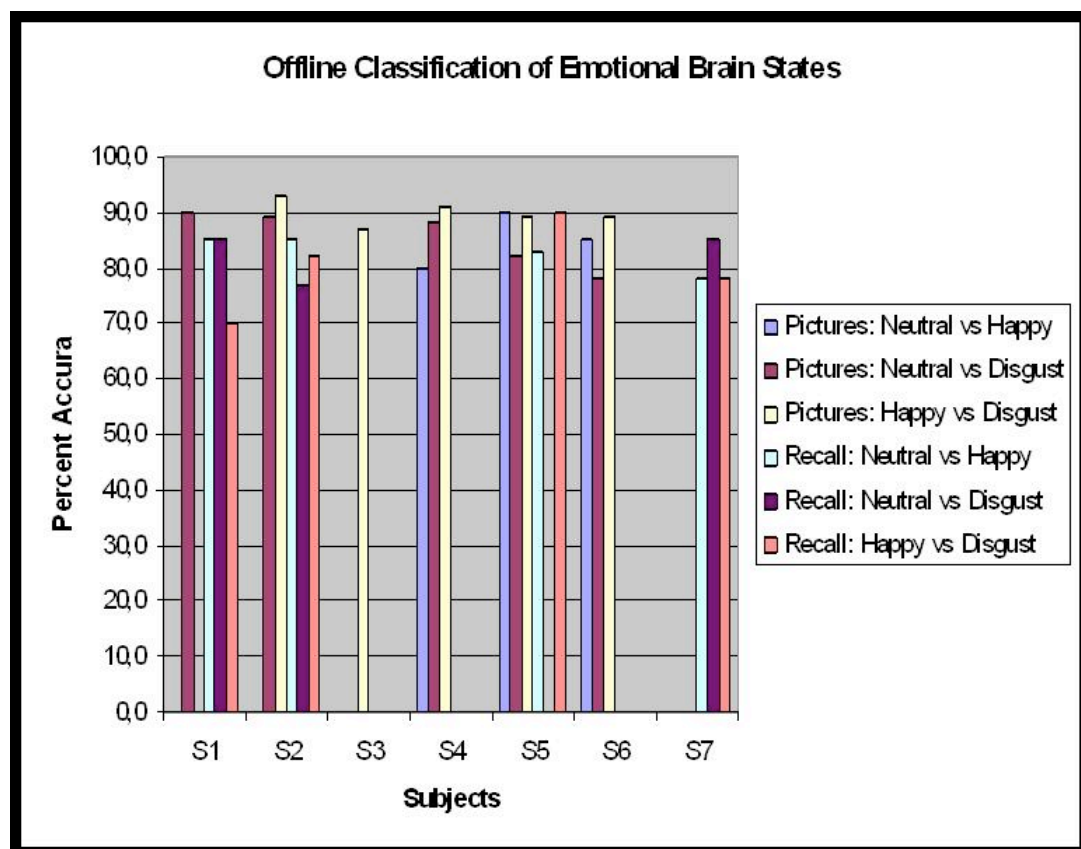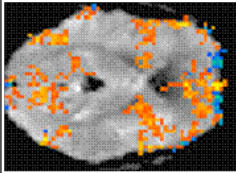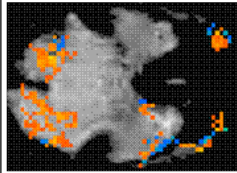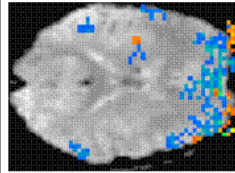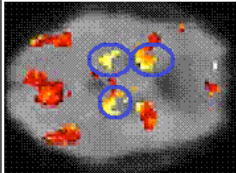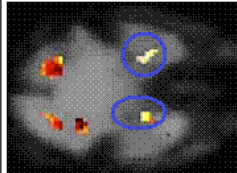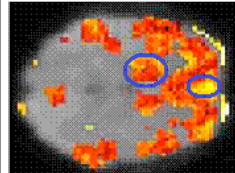
Figure 4.4: Performance of the brain state classifier.

We compared the activation patterns obtained using the univariate (GLM) method and multivariate (SVM) method of analysis. Figure 4.5 shows the difference of activations between the two methods. With the GLM maps, yellow/red voxels show significant activations and blue/green voxels show significant deactivations at the given contrast (e.g., Happy vs Neutral). With the SVM maps, yellow/red voxels show significant voxels that discriminate between the emotional states. Notice the different activation clusters that SVM uses for discrimination of emotional states. These areas might be coding the spatiotemporal information representing the brain state in a way that the voxel-wise GLM is not sensitive enough to detect.

	Happy vs Neutral	Disgust Vs Neutral	Disgust Vs Happy
Univariate (GLM)			
Multivariate (SVM)			

Figure 4.5. Differences in brain activation as obtained by the conventional univariate GLM analysis and the multivariate SVM analysis.

This work shows for the first time that multiple emotional states elicited in an individual's brain (either by viewing emotional pictures or by recall of emotional episodes) can be recognized and discriminated in real-time from fMRI signals. Furthermore, this work demonstrates that a BCI can be developed using a pattern classifier to provide feedback from an entire neural network involved in a cognitive/emotional activity in contrast to previous single ROI methods. Most importantly, this work shows the difference between multivariate SVM based method and univariate GLM based method in identifying discrimating voxels between brain states. We anticipate clinical applications of this emotion brain state detection technique, examples: neurorehabilitation of emotional disorders, in brain computer interfaces, and lie detection.

Discussion

Our work (Sitaram, Lee et al. 2008) demonstrates the application of real-time classification of emotion states in the brain from fMRI signals, and subsequently using the classification to provide feedback information to the subject to modulate his brain activity to enhance or reduce the effect or intensity of the brain state. Although, the method described below is limited to 3 discrete emotional states, the method is not inherently limited to these states, and could be extended to many more discrete and complex emotional states.

Further, the method is not limited to classification training based on emotion inducing pictures or recall of personal emotional episodes. The method can be extended to include emotions induced by auditory, audio-visual, olfactory, gustatory, touch and pain stimuli.

Chapter 5

Volitional Regulation of Anterior Insula in Healthy Individuals and Psychopathic Criminals

Introduction

The traditional approach to investigate neural processes underlying emotions involves the presentation of emotional stimuli to elicit brain activity. By using this approach, neuroimaging studies (Murphy, Nimmo-Smith et al. 2003; Wager, Phan et al. 2003; Phan, Fitzgerald et al. 2006) have provided increasing evidence for a role of the insula in a variety of brain processes such as viscerosensation, pain, motivation, emotion and cognition. However, the inverse question, which emotional response is elicited when a brain region is modulated, is not much explored. From this perspective, in order to verify the functional specificity of the anterior insula in emotional processing fMRI-BCI presents itself as a novel method.

Neurobiology of Insula

The areas of the insula, lateral orbitofrontal cortex and cingulate cortex represent the transition from allocortex to granular cortex identified as paralimbic cortex (Mesulam and Mufson 1982; Mesulam and Mufson 1982). The insula, named as limbic integration cortex (Augustine 1985) along with other paralimbic structures due to their localization in the brain between neocortex and limbic areas would integrate the internal and external milieu (Mesulam and Mufson 1982; Mesulam and Mufson 1982). Anatomical evidences show that insula has connections with areas in the frontal parietal temporal lobes, cingulate gyrus, basal nuclei, amygdala, dorsal thalamus and other structures of the limbic system (Augustine 1985; Augustine 1996; Rolls 1996). Due to the multiplicity of its cortical and subcortical connections the insula is posited to have a manifold function as a visceral sensory, visceral motor, vestibular, somatosensory area. It has been hypothesized to have a key function in evaluating the emotional state of the organism (Reiman, Lane et al. 1997; Damasio, Grabowski et al. 2000). Specifically, it would be critical to the evaluation of the interoceptive emotional significance through the functional representation of homeostatic changes (Reiman, Fusselman et al. 1989; Craig 2002; Craig 2003). The anterior part of the insula is reported to be directly implicated in emotional processing, specifically during emotional recall, self-generated emotions (Reiman, Fusselman et al. 1989; Reiman, Lane et al. 1997; Damasio, Grabowski et al. 2000) and self induced anxiety (Kimbrell, George et al. 1999). Correlation between insula activity and perception of emotional stimuli has been extensively described in healthy people (Phillips, Young et al. 1997; Anders, Birbaumer et al. 2004; Critchley, Wiens et al. 2004; Singer, Seymour et al. 2004; Wright, He et al. 2004; Jackson, Meltzoff et al. 2005). Neuroimaging studies reported bilateral but

asymmetric activation of the anterior insula with a bias to the left hemisphere both during self-induced negative emotion (Damasio 2000) and when participants were asked for verbal ratings of emotional valence during observation of negative emotional pictures (Anders, Birbaumer et al. 2004). Anticipatory anxiety, which is a combination of future-oriented cognitive state, negative affect and autonomic arousal was correlated with increased regional cerebral blood flow in the left insula and at a lower threshold in the right homologous area (Reiman, Fusselman et al. 1989; Chua, Krams et al. 1999). It has been shown that anticipation and observation of aversive stimuli is associated with increased insula activation in normal subjects (Reiman, Fusselman et al. 1989; Phillips, Young et al. 1997; Schienle, Stark et al. 2002) and recently in anxiety-prone subjects (Simmons, Strigo et al. 2006; Stein, Simmons et al. 2007). These data suggested the hypothesis that insula hyperactivity might be a common feature in persons with elevated trait anxiety and therefore it might represent a neuroimaging marker for anxiety proneness (Paulus, Feinstein et al. 2004; Paulus and Stein 2006). Furthermore, anterior insula hyperactivity is observed in social phobia (Birbaumer, Veit et al. 2005) and panic disorders (Reiman, Fusselman et al. 1989) while its hypoactivity is associated with lack of aversive anticipatory arousal in criminal psychopaths (Birbaumer, Veit et al. 2005).

The insular cortex has been rarely investigated in humans using direct electrical cortical stimulation because of its anatomical localization covered by frontal, parietal and temporal opercular cortices and separated by a dense wall of vessels. The few studies conducted during the presurgical assessment of epilepsy reported somaesthethic symptoms, cardiovascular effects as well as viscero-motor, viscero-sensitive sensations (Penfield and Faulk 1955; Wieser 1983; Oppenheimer, Gelb et al. 1992; Ostrowsky, Isnard et al. 2000) and nociceptive responses (Ostrowsky, Isnard et al. 2000). The observed elicited sensations were mainly caused by the stimulation of the posterior part of the insula while the few stimulation sites in the anterior insular did not induce exteroceptive pain sensations but only viscerosensitive, visceromotor and autonomic reaction (Oppenheimer, Gelb et al. 1992; Ostrowsky, Isnard et al. 2000). Furthermore, the few lesional studies in humans available reported impairment in recognizing both facial and vocal signals of disgust, and impaired experience of disgust as a consequence of left hemisphere damage affecting the insula and basal ganglia, including the striatum (Calder, Keane et al. 2000). Similar findings have been observed in patients affected by the Huntington's disease which also afflicts the insula and the striatum (Sprengelmeyer, Young et al. 1996). Therefore, the question, which emotional response is induced by stimulation of anterior insular activity in healthy individuals is still a challenging open issue.

Psychopathy

Psychopathy is a personality disorder described by a constellation of affective, interpersonal and behavioral characteristics such as callousness, lack of empathy, egocentricity and impulsivity. Psychopaths engage in more criminal behavior and institutional misconduct than their non-psychopathic counterparts. Central to psychopathy is the deficient processing of emotions. These include shallowness and profound lack of remorse or empathy. Hare et al., (Hare, Hart et al. 1991) subsumed those features under the factor "emotional detachment". Lykken (Lykken 1957), using questionnaires and electrodermal responses, investigated the hypothesis that psychopaths fail to develop anxiety. Lykken found reduced anxiety levels in the

subjective evaluations and low electrodermal responses to conditioned stimuli that were previously associated with shock in the autonomic indices. Cleckley (Cleckley 1951, 1976?) suggested that psychopaths exhibit discordance in the linguistic and experiential components of emotion. Empirical evidence indicates that psychopathic individuals have less intense emotional reactions to many everyday situations than do non-psychopaths (Day and Wong 1996). Other investigators suggested that the inability of psychopaths to anticipate the negative consequences of their behavior results from an insufficient capacity to develop anticipatory fear (Hare 1978). Hence, psychopathy may be characterized by a faulty modulation of associative links between external stimuli and internal reactions (Patrick 1994; Patrick, Cuthbert et al. 1994). Neuroimaging studies investigating the affective processing of psychopathy will potentially lead to an understanding of mechanisms and elements that maintain this disorder (Porter, 1996).

The amygdala plays a central role in emotional processing, particularly in fear conditioning (Kim and Jung 2006). However, fear retention is not necessarily at the same site as fear learning, and hence it is unclear whether the amygdala is the permanent storage site for long-term fear memory. For example, fear retention is abolished if the amygdala is lesioned one day but not many days after inhibitory avoidance training, suggesting that long-term fear memory is not stored in amygdala (Liang, McGaugh et al. 1982; McGaugh, Martinez et al. 1982). From the point of view of efficacy of human neuroimaging studies, amygdala is a particularly difficult region as it is highly vulnerable to magnetic susceptibility artifacts including distortions and signal dropouts (Weiskopf, Scharnowski et al. 2004; Weiskopf, Klose et al. 2005; Weiskopf, Hutton et al. 2006). In addition to the amygdala, a network of structures that includes insula, anterior cingulate gyrus and medial prefrontal cortex is suggested as important in identifying the emotional significance of the stimulus, and regulate the affective state (Philips ML et al 2003; (Adolphs 2003; Adolphs 2003). The insula has afferent and efferent connections to the medial and orbitofrontal cortices, anterior cingulate and amygdala (Augustine 1996). Stein et al., (Stein, Simmons et al. 2007) maintain that insula may have been relatively neglected compared with amygdala, and suggest including insula within the sphere of inquiry.

As mentioned earlier, Insula activation is associated with many emotional processes, including differential positive versus negative emotion processing (Buchel, Morris et al. 1998), (Morris, Ohman et al. 1998), (Morris, Friston et al. 1998), pain perception (Gelnar, Krauss et al. 1999; Peyron, Laurent et al. 2000), anticipation and viewing of aversive images (Phan, Fitzgerald et al. 2006), (Simmons, Matthews et al. 2004), and the making of judgements about emotions (Gorno-Tempini, Pradelli et al. 2001). The IES model of psychopathy (Blair, Peschardt et al. 2006) proposes that psychopathic individuals receive markedly reduced augmentation of the representation of the conditioned stimulus (CS) from the reciprocal connections of the amygdala and insula. This means that if the CS is the target stimulus, performance will be impaired in individuals with psychopathy relative to comparison individuals (i.e., a weaker representation should be less able to control behaviour). On the other hand, if the CS is a distracter to ongoing behaviour, performance will be superior in individuals with psychopathy relative to comparison individuals (i.e., a weaker representation will be a less of a competitor for the stimulus that should be controlling behaviour). Furthermore, human studies strongly suggest that the insula is instrumental in the detection and interpretation of certain internal bodily states (Crichley 2003; Crichley

2005). The construct of interoceptive awareness shares many features with anxiety sensitivity and phobia. Insula activity is elevated in persons prone to anxiety disorders (Simmons, Strigo et al. 2006) and social phobia (Veit, Flor et al. 2002), and as such may be a neuroimaging marker of these disorders. In contrast, a hypoactivity of insula is observed in psychopathic individuals (Veit, Flor et al. 2002, Birbaumer, 2005 #25), and could in turn act as a marker of psychopathy.

Study Objectives

In view of the above line of argument, we asked the following questions: could healthy individuals and psychopathic criminals be trained to regulate activity the BOLD activity in the insula using an fMRI-BCI, and does volitional increase of activity in insula have any effect on emotional processing? In addition, we investigated whether training to regulate the insular cortex changes the functional connectivity of the emotional network. Studying the functional interactions between brain regions involved in the regulation of emotion and the directions of these interactions will provide a deeper understanding of this brain function. Comparing the functional interactions between healthy individuals and those with psychopathology could give new insights in developing treatment.

Methods

Participants

Two groups of participants took part in experiments carried out separately. Healthy individuals were first investigated to assess the behavioral effects of volitional regulation of anterior insula. In a second experiment, psychopathic criminals underwent a similar experimental protocol. As we could not match healthy individuals and psychopathic criminals for age, sex and background, we are not able to compare results across the two groups in any form of random effects or group analysis. As such, we would present the results of the two experiments separately.

Experiment 1: Healthy Individuals

Sixteen healthy right-handed subjects (9 female and 7 male; age range 23-40 years; mean age 27.50 years) participated in this study. Volunteers of both groups, namely, the experimental group (5 female and 4 male; age range 23-40 years; mean age 26.86 years) and the control group (4 female and 3 male; age range 23-40 years; mean age 28.0 years), had no history of neurological or psychiatric disorders including substance abuse/dependence and psychotropic medications. All were naive to neurofeedback and fMRI experiments. Written instructions were provided to all participants and informed written consent was obtained. This study was approved by the ethics committee of the Faculty of Medicine of the University of Tübingen.

Experiment 2: Psychpathic Criminals

Six psychopaths (Birbaumer, Sitaram et al. 2008) with criminal records participated in the study. The psychopaths consisted of offenders out on bail and waiting for their

trial or those out of jail and on parole, all of whom were screened from a larger sample using the Psychopathy Checklist-Revised (PCL-R) (Hare, 1991). The mean emotional detachment score was 14.25 (SD = 10.3, range = 7-21. These values are much lower than the scores for the American population of psychopaths but are in accordance with the lower values for the German norms (Ullrich 2003).

None of the participants was taking psychoactive drugs. The psychopaths were paid €20 per hour and an extra sum proportional to their performance (maximum €10 per hour) during feedback training. The payments were made to ensure participation of this difficult-to-recruit group and also as a reward contingent on regulating brain activity. All participants signed informed consent and the study was approved by the local institutional review board and adhered to the Declaration of Helsinki.

fMRI Data Acquisition

Functional images were acquired on 3.0 T whole body scanner, with standard 12 channels head coil (Siemens Magnetom Trio Tim, Siemens, Erlangen, Germany). A standard echo-planar imaging sequence was used (EPI; TR = 1.5 s, matrix size = 64 x 64, echo time TE = 30 ms, flip angle α = 70°, bandwidth = 1.954 kHz/pixel). Sixteen slices (voxel size = 3.3 x 3.3 x 5.0 mm^3, slice gap = 1 mm), AC/PC aligned in axial orientation were acquired. For superposition of functional maps upon brain anatomy a high-resolution T1-weighted structural scan of the whole brain was collected from each subject (MPRAGE, matrix size = 256 x 256, 160 partitions, 1 mm^3 isotropic voxels, TR = 2300 ms, TE = 3.93 ms, TI = 1100 ms, α = 8°). In order to reduce head movement, two foam cushions were used to reduce unnecessary movement of the participant's head.

Experimental Protocol

The target region of interest (named ROI1), left anterior insula, was delineated in a localizer session for each participant. A block-based paradigm was used for the localizer session consisting of 4 blocks (22.5s each) during which the subjects had to use mental imagery to recall emotionally relevant personal experiences alternating with 5 resting blocks (22.5s each) during which they had to perform number counting in reverse order (for example, from 100 to 1). ROI1 was selected on the activation maps generated online during the task by means of the Turbo-BrainVoyager software (Goebel 2001) and stored for the following feedback training sessions. ROI1 consisted of a rectangular area encompassing 5 x 5 voxels (~20 x 20 mm) of the left anterior insula on a single slice of 5 mm thickness. The reference ROI (named ROI2) was another rectangular area selected from a slice positioned distant from ROI1 and selected to encompass a slice with the intent to cancel global changes in the BOLD signal.

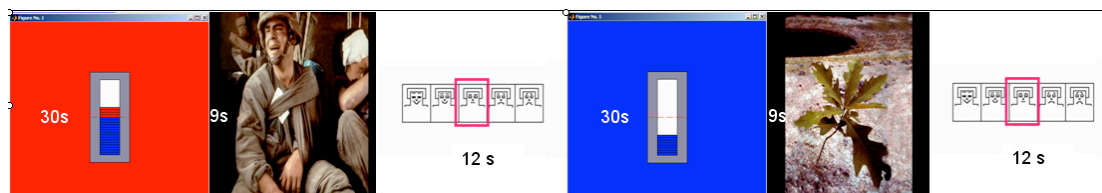***Figure 5.1.*** *Experimental design. A single run consisted of a 30s increase or decrease block followed by a 9s picture presentation block, that in turn was followed by a 12s rating block. There were 5 runs in each session. During rating blocks participants were shown the Self-Assessment Manikin, SAM [49], which allows them to evaluate emotional valence and arousal. Both valence and arousal dimensions vary*

along a 9-point scale. Selection of the subjective rating was performed by positioning a red outline on the chosen number on each of the two scales, presented in close succession. Subjects were provided with two buttons allowing movements of the cursor in the left and right direction.

Each participant took part in 3 different types of protocols: a pretest on the first day; 3-4 feedback runs per day after the pretest, for 2-3 days, depending on the availability of the subject; and a final day of 1-2 post-tests. Each feedback run consisted of 6 increase and 7 decrease blocks each of 30s duration. During the up- and down-regulation blocks subjects had to increase or decrease the BOLD response in the target ROI (left anterior insula) by watching the feedback presented in the form of an animated graphical thermometer. Normalized average BOLD signal from the left anterior insula was used to generate animated images of the varying thermometer bars. The up- and down-regulation blocks were cued with red and blue colour backgrounds, respectively (Figure 5.1). Each run of the feedback training took 6.75 minutes to complete. At the end of each training run monetary reward was computed and presented to the subject proportional to the aggregate valid differential BOLD increase or decrease at every time point with respect to the previous time points. A differential BOLD value is counted as valid only if there is a differential BOLD increase but not decrease during the increase condition, and a differential BOLD decrease but not increase during the decrease condition. Each valid differential increase and decrease of BOLD earned 10 European cents. Maximum reward for a feedback run was limited to 10 Euros.

The pretest and post-test were similar in structure and only differed in the stimulus material used. The intent of the tests was to measure the effect of volitional regulation of the left anterior insula on aversive and neutral picture evaluation. Each session of the pretest or post-test consisted of five alternating up- and down-regulation runs. Each run consisted of a 30s up- or down-regulation block performed by watching the feedback of the moving thermometer bars as described before, followed by a 9s emotional picture presentation block, that in turn was followed by a 12s evaluation block (Figure 5.1). During picture presentation blocks, one emotional or neutral picture from the International Affective Picture System (IAPS; (Lang, Bradley et al. NIMH Center for the Study of Emotion and Attention 1997) was presented. During the evaluation blocks subjects had to rate the picture for valence and arousal using a button-based control device inside the MRI scanner. Pictures were rated in terms of subjective emotional valence and arousal using the Self-Assessment Manikin (SAM, (Bradley and Lang 1994). The Self-Assessment Manikin is a non-verbal pictorial assessment for measuring pleasure, aversion and arousal associated with a person's affective reaction to a variety of stimuli. Valence and arousal dimensions vary along a 9-point scale. Before the experiment, participants were briefed about the experimental tasks, SAM ratings, and were also trained on how to rate the pictures using the two buttons.

During the picture rating blocks, subjects were shown the two SAM valence and arousal scales in close succession. Positioning a red outline on the chosen number on the scale denoted selection of the subjective rating. Subjects were provided with two buttons allowing movements of the cursor in the left and right direction. Cursor starting position was in the centre of the scale both for valence and arousal dimension. The pictures presented to the participants consisted of 20 aversive and 20 neutral pictures from IAPS (see Caria et al., in press for details). Valence and arousal ratings for aversive pictures were based on ratings from a large representative reference

sample (Lang, Bradley et al. NIMH Center for the Study of Emotion and Attention 1997) with mean values of 3.26± 0.78SD and 4.93±0.47SD, respectively. Valence and arousal ratings for neutral pictures had mean values of 4.84± 0.32SD and 2.33±0.40SD, respectively. Pictures were pseudo-randomized such that no significant difference in valence and arousal ratings was present between pictures after increase and decrease blocks and between sessions. Each session lasted about nine minutes.

Off-line Data Analysis

SPM Analysis

Off-line image post-processing, SPM analysis and ROI analyses were performed using SPM5 (Wellcome Department of Imaging Neuroscience, London) and Brain Voyager QX (Brain Innovations, Maastricht, the Netherlands) statistical parametric mapping software package. During signal preprocessing, the functional EPI images were realigned spatially, normalized into Montreal Neurological Institute (MNI) space, and smoothed spatially (9-mm Gaussian kernel) and temporally (0.0039 Hz, 2.5 times the duration of the activation and baseline block) to remove high frequency artifacts. Hemodynamic response amplitudes were estimated using standard regressors, constructed by convolving a boxcar function representing the block duration, with a canonical hemodynamic response function using standard SPM5 or Brain Voyager QX parameters. Motion parameters were also included in the general linear model (GLM) as covariates to account for variance caused by head motion. Signal change during up-regulation blocks with respect to the down-regulation blocks was evaluated. Areas showing training related changes were analysed with *t*-test comparison of BOLD magnitude over sessions.

Region of Interest Analysis

Hypothesis driven ROI analysis was performed using the ROI previously selected for each subject during the feedback training sessions. ROI time-series underwent the same preprocessing and model estimation using the General Linear Model (GLM) for whole brain analysis. The percent signal change during up-regulation blocks with respect to the down-regulation blocks was calculated for each session separately and then averaged across subjects. ROI analysis was also performed on the contralateral region positioned at the right anterior insular and a few other selected areas in emotional regulation. The training effect was evaluated by computing paired *t*-test on all subjects of percent signal changes in the target ROI session by session.

Functional Connectivity Analysis

Granger Causality Modeling (Granger 1969; Granger 1980) is a method originally developed in economics for causal interaction between multiple events from time-series data. Since then it has been applied in neuroscience research for analysing connectivity of neurons from their firing patterns, from local field potentials, from EEG data (Seth 2005; Seth 2007). More recently, GCM has been applied in conjunction with Vector Autoregressive Models (VAR) to fMRI data also (Abler, Roebroeck et al. 2006), (Roebroeck, Formisano et al. 2005) to investigate directed influences between neuronal populations. The strength of the method exists in its data driven nature and its non-reliance on a priori specification of a model. It is distinct from other approaches of effective connectivity, e.g. Dynamic Causal Modelling (DCM) (Kiebel, Kloppel et al.

2007), (Schlosser, Koch et al. 2007), (Van Horn and Ishai 2007) that aim at testing or contrasting specific hypotheses about neuronal interactions. Instead, GCM defines the existence and direction of influence from information in the data. Temporal precedence information is exploited to compute Granger causality maps that identify voxels that are sources or targets of directed influence from other voxels in the brain.

GCM is usually implemented as linear autoregressive models that predict the evolution of time-series. Univariate autoregressive models describe a single time-series in terms of linear combinations of the past values (lags) of the time-series. Multivariate vector autoregressive (VAR) models include lags of multiple time-series. For our implementation, let us consider 2 fMRI time-series $X_1(t)$ and $X_2(t)$ of length T, from 2 selected regions of the brain. Let us suppose that the temporal dynamics of the $X_1(t)$ and $X_2(t)$ can be described by a bivariate autoregressive model:

$$X_1(t) = \sum_{j=1}^{p} A_{11,j} X_1(t-j) + \sum_{j=1}^{p} A_{12,j} X_2(t-j) + E_1(t)$$

$$X_2(t) = \sum_{j=1}^{p} A_{21,j} X_1(t-j) + \sum_{j=1}^{p} A_{22,j} X_2(t-j) + E_2(t)$$

[

where p is the maximum number of lags included in the model (the model order, p < T), A contains the estimated coefficients of the model, E_1 and E_2 are residuals for each time-series. If the variance of the prediction error E_1 (or E_2) is reduced by the inclusion of the X_2 (or X_1) terms in the first (or second) equation, then it is said that X_2 (or X_1) *Granger-causes* X_1 (or X_2). X_2 Granger-causes X_1 if all the coefficients in A_{12} are significantly different from zero. This can be tested by performing a t-test or F-test of the null hypothesis that $A_{12} = 0$, with the assumption that X_1 and X_2 are covariance stationary. The magnitude of the Granger causality interaction can be estimated by taking the logarithm of the F-static. This concept can be extended to the multivariate case by estimating a multivariable VAR-model. In such a case, X_2 Granger-causes X_1 if knowing X_2 reduces X_1's prediction error when the time-series of all other variables (brain regions) $X_3 \ldots X_N$ are also taken into account. Multivariate analysis can improve robustness of the GCM results. For example, in a system in which X_1 and X_2 are both influenced by X_3 but are otherwise independent, a bivariate model of X_1 and X_2 may wrongly indicate that there is causal relationship between X_1 and X_2. A multivariate model would not have such a false positive, as knowing X_1 would not predict X_2 in the context of X_3. In this study, we incorporate the multivariate model for the above reason. Significant Granger causality interactions between variables can be represented as edges in a graph enabling graph-theoretic techniques to be used for further analysis and visualization.

GCM analysis was carried out to evaluate the network dynamics during self-regulation during three different training sessions: a session of weak regulation, a session of intermediate ability to regulate, and a session of strongest regulation. The criterion for considering a regulation session as weak, intermediate and strong was the magnitude of percent BOLD increase in each session; greater the percent BOLD increase, stronger is considered the regulation. Time-series of ROIs that passed the height threshold of P= 0.05 (Bonferroni corrected) and a cluster threshold of 50 voxels were used as input to the GCM analysis for each stage of regulation. We implemented a multivariate Granger Causality Model (GCM) by adapting the Causal Connectivity Matlab (Mathworks Inc., USA) Toolkit from (Seth 2005) to work with fMRI signals and our design protocols.

Multivariate GCM was applied to multiple time-series of selected ROIs (varying from 5-10) at 3 different stages of regulation under consideration.

Two important measures of connectivity, namely, *causal density* and *causal flow* are adapted from (Seth 2005; Seth 2007) for comparison of functional connectivity across feedback training sessions.

Causal Density: The *causal density* (*cd*) of a functional network defined as the fraction of interactions among ROIs that are causally significant. Causal density is given by the relation *cd = gc/(n(n-1)),* where *gc* is the total number of causal connections observed and *n* is the network size. A set of unconnected ROIs will have low *cd*.

Causal Flow: The *causal flow* (*cf*) of an ROI *i* in Granger-causality graph is defined as the difference between its outgoing connections and incoming connections. An ROI with highly positive *cf* exerts a strong causal influence over the network and so acts as a *causal source*. An ROI with a negative *cf* can be called a *causal sink* of the network.

Statistical Analysis of Picture Ratings

Ratings of the IAPS pictures presented after increase blocks were compared with the ratings of the pictures presented after decrease blocks across sessions using non-parametric Wilkoxon Signed Ranks test. Local brain activity was compared between pictures presented after increase blocks with respect to those presented after decrease blocks across sessions.

Results and Discussion

Experiment 1: Healthy individuals

The EG was guided by contingent BOLD feedback from the left anterior insula while the CG received a non-specific feedback corresponding to the BOLD activity of a large brain area. Both groups immediately after the modulation were required to observe and assess a selection of emotional pictures taken from the International Affective Picture System (IAPS) (Collins, Neelin et al. 1994) (Table. 5.1). The two groups of participants (EG n = 9, CG n = 7) underwent four fMRI-BCI scanning sessions in one day. Both ROI analysis and whole brain analysis showed a learned control of the left anterior insula activity in the EG only. The negative effect observed in the CG demonstrated the relevance of the contingent feedback to achieve control of the targeted brain area. Participants received written instructions of the experiment and guidelines for achieving control of the activity in the targeted brain. Experimental group reported that recalling positive and negative emotional personal episodes were used as strategies for successful regulation of insular activity. Control group reported using similar strategies but found them to be unsuccessful in consistently regulating the feedback signal.

77

Pictorial stimuli from the International Affective Pictures System (IAPS)

	Aversive Pictures				Neutral Pictures		
IAPS number	Description	Valence	Arousal	IAPS number	Description	Valence	Arousal
9421	Soldier	2,47	4,86	5740	Plant	5,07	2,36
9430	Burial	3,1	4,81	7175	Lamp	4,78	1,55
9432	Mastectomy	3,29	4,12	7002	Towel	4,91	2,99
9433	Dead man	2,39	5	7950	Tissue	4,62	2,3
9440	Skulls	4,42	4,71	7020	Fan	5,02	2,15
9452	Gun	3,62	4,5	7025	Stool	4,46	2,44
9470	Ruins	3,62	4,53	7031	Shoes	4,2	1,67
9480	Skull	4,06	5,15	7010	Basket	4,95	1,55
9490	Corpse	4,2	5,41	7004	Spoon	4,89	2,09
9500	Porpoises	2,85	5,65	7224	File cabinets	4,38	2,55
9520	Kids	2,14	5,45	7217	Clothes rack	4,63	2,31
9530	Boys	3,65	4,74	7705	Cabinet	4,75	2,4
9560	Duck in oil	2,07	5,46	7080	Fork	5,43	1,98
9561	Sick kitty	3,2	4,18	7009	Mug	4,96	2,69
9570	Dog	1,9	5,84	7030	Iron	4,82	2,76
9571	Cat	2,65	4,68	7035	Mug	4,81	2,56
9582	Dental Exam	4,09	5,15	7040	Dust pan	4,72	2,46
9584	Dental Exam	3,44	4,65	7050	Hair dryer	4,81	2,59
9592	Injection	4	5,11	7140	Bus	5,59	2,67
9594	Injection	4,08	4,55	7233	Plate	5,01	2,51

Table 5.1. Clusters of significant signal increase other than insulae during activation blocks from random effects analysis in the last session. Clusters exceeding the threshold of P<0.001 uncorrected and with a spatial extent large than 10 voxels were considered. Coordinates are in MNI stereotaxic space (Collins, Neelin et al. 1994) and labelled anatomically according to Tzourio-Mazoyer et al. (Tzourio-Mazoyer, Landeau et al. 2002).

Functional data

Single subject analysis without smoothing and averaging shows learned modulation of the activity in the target area (Figure. 5.2).
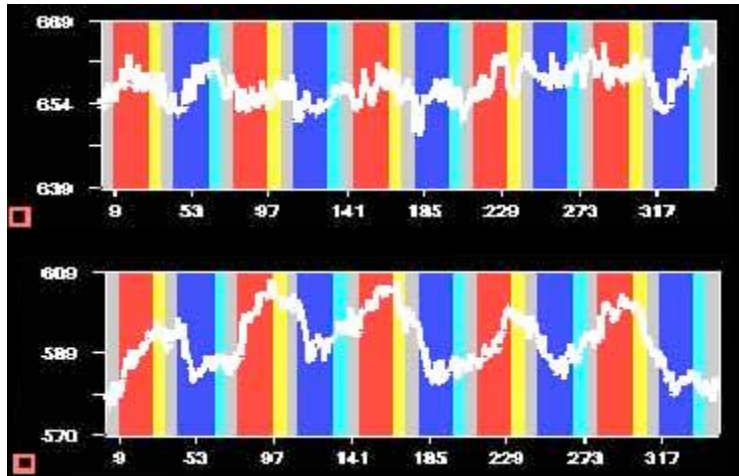
Figure 5.2 Single subject training performance. Example of single subject BOLD time-course of the left targeted area during the first session (top) and the last session (bottom). Each time-course shows BOLD response during increase (red bar) and decrease blocks (blue bar), picture presentation blocks after increase (yellow bar) and after decrease (light blue), and rating blocks (grey). Scan number is represented on the x-axis and the raw magnitude BOLD signal is represented on the y-axis. Improvement in control to increase and decrease activation with training is evident even without spatial smoothing and averaging.

ROI analysis in the EG showed a significant enhancement of the modulation of insular activity revealed by an increase across sessions of the percent BOLD signal change ($F_{(3,19)}$ = 129.86, P < 0.0001) in the this area (Figure 5.3). However, ROI analysis of the CG did not show increasing percent BOLD signal across sessions. Activity in the right anterior insula also showed increased percent signal change in the last session with respect to the first session ($t_{(19)}$ = 10.14, P < 0.001, two-tailed paired t-test), but the effect was lower than in the target area and did not increase monotonically (Figure 5.3).

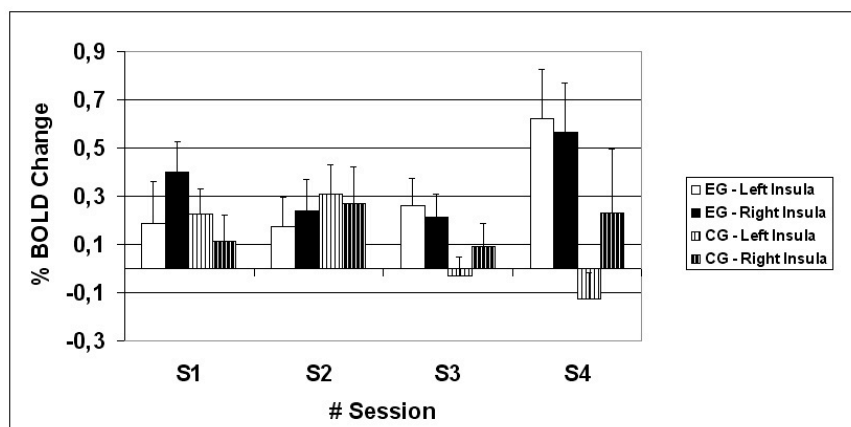*Figure 5.3. Brain activity in the left and right anterior insula in the experimental and control group during the task. % BOLD change in the experimental group and control group across training sessions. Percent signal change was calculated by computing the difference of the percent BOLD change of each time point during increase and decrease blocks for each participant, and these values were then averaged across all*

the participants. % BOLD increases across sessions in the target area in the experimental group only trained with contingent feedback (F(3,19) = 129.86, P < 0.0001, ANOVA). The control group trained with non-specific feedback showed an increase in the first two sessions only. Error bars represent standard deviations.

A lateralization index (LI), intended to assess whether brain activation was predominantly in the left or right hemisphere during training, showed an increased activity in the left insula across training sessions with a lateralization index of 0.46±0.27SD ($t_{(8)}$ = 2.64, P = 0.015, two-tailed paired t-test) in the last session (Figure 5.4).
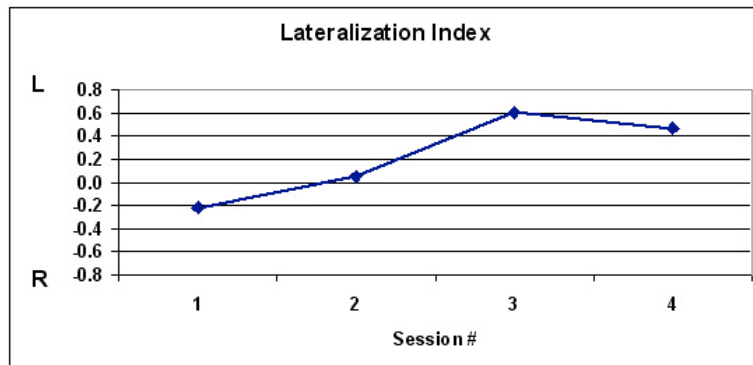

Figure 5.4. Lateralization Index. The LI was calculated based on the normalized difference between percent BOLD change extracted from the left anterior insula and the right anterior insula for each participant and then averaged across all participants as follows: (%L-%R)/(%L+%R) (L = positive values ; R = negative values). Activity during training was increasingly shifting to the left across sessions and reached a mean lateralization index of 0.46±0.27SD in the last session.

Random effect analysis of the whole brain activity during the modulation blocks confirmed ROI data analysis showing increased BOLD signal in the target area across sessions as indicator of learning. Activation in the left [-36,13,-5] (t = 9.80, P < 0.001 uncorrected) and in the right insula/ frontal operculum [43,13,-5] (t = 8.98, P < 0.001 uncorrected) were the most active in the third and the fourth sessions (coordinates refer to peak of activation in Montreal Neurological Institute – MNI space (Collins, Neelin et al. 1994) (Figure 5.5a). Additional active brain areas in the last two sessions were the right middle cingulate gyrus [3, 33, 30] (t = 8.07, P < 0.001), the left superior temporal gyrus [-59, -36,20] (t = 6.97, P < 0.001) and the right supplementary motor area [7,7,70] (t = 6.57, P < 0.001). A significant activated cluster was also observed in the target ROI during the third and the fourth training session compared to the second and the first ([-43,25,0] left insula/frontal operculum, t = 3.70, P < 0.001 uncorrected) (Figure 5.5b).
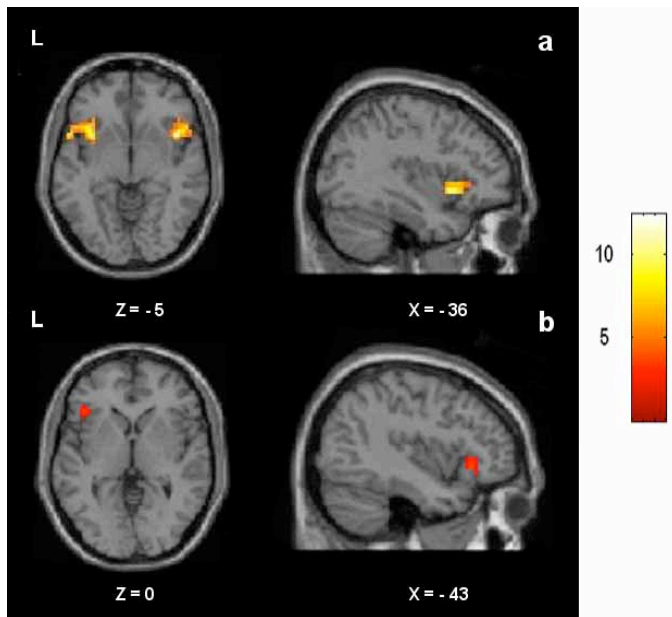
Figure 5.5. *Whole brain group analysis.* **a**. *Random effect analysis of the activity during the last two sessions at P < 0.001 uncorrected: both left [-36, 13, -5] and right [43, 13, -5] insula/ frontal operculum show increased BOLD signal. Activations network shows additional active areas: the right middle cingulate gyrus [3, 33, 30], the left superior temporal gyrus [-59, -36,20] and the right supplementary motor area [7,7,70].* **b**. *The contrast of the last training session with the first training session shows increased activity only* in the left insula/frontal operculm [-43, 25, 0], the targeted brain region.

Clusters of activity during the modulation blocks across all sessions were localized in the right anterior cingulate gyrus [7,20,35], the right supplementary motor area [3,13,70], the left superior temporal gyrus [-53,-36,20] and the left middle frontal gyrus [-26,43,20] (Table 2). Region of interest analysis of these additional active areas (Table 2) did not show a BOLD signal increase over training sessions ($F_{(3,19)}$ = 0.49 P < 0.48,) emphasizing the specificity of the measured effect (Figure 5.6).

BRAIN REGION	BROADMANN AREA (BA)	CLUSTER SIZE	t VALUE	MNI COORDINATES (x,y,z)
R anterior cingulate gyrus	BA 24	100	11.91	7 20 35
R supplementary motor area	BA 6	47	9.89	3 13 70
L middle frontal gyrus	BA 46	61	9.58	-26 43 20
L superior temporal gyrus	BA 42/22	15	7.21	-53 -36 20

Table 5.2. *Additional active brain regions.*

The CG showed a small increase of BOLD signal activity in the left and right ROI during the first two sessions only. They both reached significance when the BOLD

amplitude was compared with respect to the first session ($t_{(19)}$ = 3.27, P < 0.004, left; $t_{(19)}$ = 5.12, P < 0.001, right). The analysis of the interaction effect of ROI time course per group reached significance ($F_{(1,15)}$ = 18,49, P < 0.001).
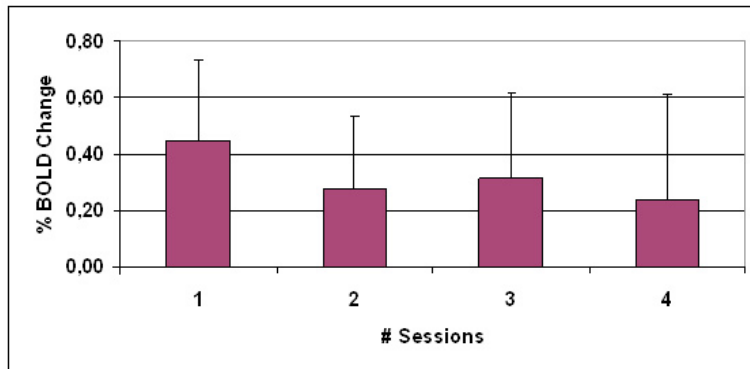
Figure 5.6. ROI analysis of all significantly activated clusters from statistical maps, excluding left and right anterior insular region. No increase across sessions was observed during the feedback training.

Behavioral data

To exclude variability across subjects and pictures the ratings of the emotional pictures presented after increase blocks were compared to those presented after decrease blocks. The EG showed a difference of the aversive pictures ratings in the valence and arousal dimensions in the last session; valence reached significance (z = 2.13, P = 0.033, Wilkoxon signed rank test) while arousal did not (z = 1.10, P = 0.271) (Figure. 5.7).
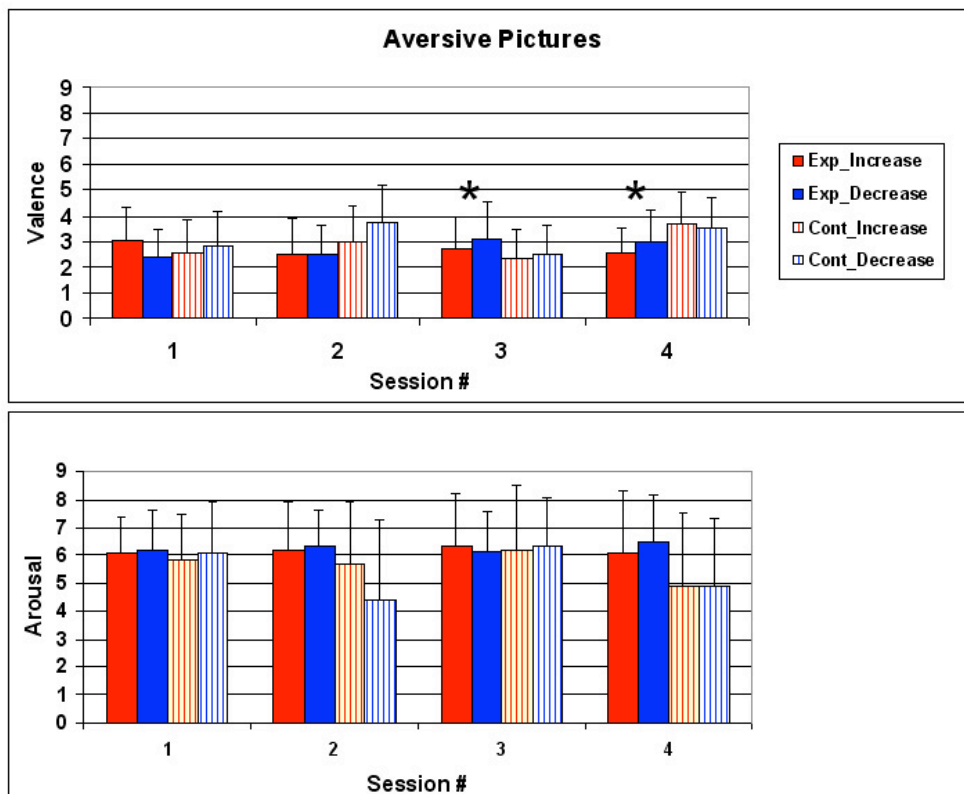
Figure 5.7. Aversive pictures ratings. SAM valence (top) and arousal (bottom) ratings for aversive pictures for the experimental (Exp) and control group (Cont) (* P < 0.05 two-tailed). During the last two training sessions when the participants in the experimental group had acquired sufficient control, aversive pictures presented after the increase condition were rated as significantly more negative (lower valence) than after the decrease condition.

A smaller significant difference of ratings only in the valence dimension was also measured in the third session ($z = 2.02$, $P = 0.043$). Valence ratings significantly decreased when pictures were presented after increase blocks with respect to decrease blocks in the last two sessions. Ratings of the neutral pictures were not significantly different in both dimensions (over all sessions (Figure. 5.8). During the third and the fourth training session when the EG had increased the activity in the left anterior insula, aversive pictures presented after the increase condition were perceived more negative than after the decrease condition (linear regression, $P < 0.05$) (Figure 5.9). Interestingly, the CG showed a trend to significance in valence and arousal ratings of aversive pictures during the second session (valence, $z = 1.725$, $P = 0.084$; arousal, $z = 1.786$, $P = 0.088$) (Figure 5.7). Differences of ratings of neutral pictures failed significance both in valence and arousal dimension across all sessions (Figure 5.8).
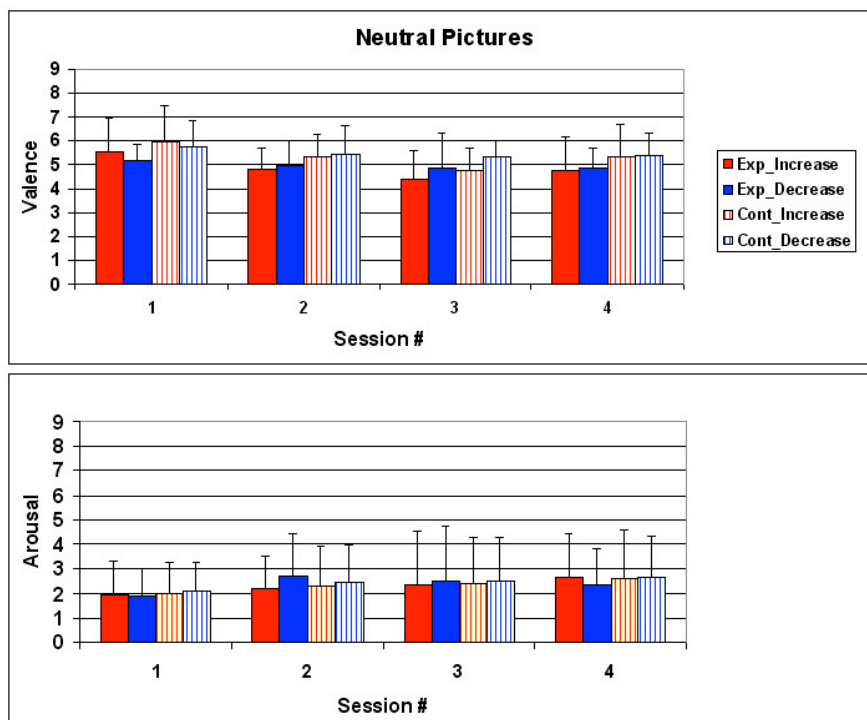
Figure 5.8. Neutral pictures ratings. SAM valence (top) and arousal (bottom) ratings for neutral pictures. No significant differences were found comparing ratings of the pictures presented after increase blocks with those presented after decrease blocks.

A correlation analysis was also conducted to show a relationship between BOLD percent signal change in the anterior insula and ratings of the emotional stimuli. Changes in valence ratings of the aversive pictures were significantly correlated with changes in the left anterior insula activity ($F_{(1,33)} = 4.90$, $P < 0.05$); the correlation with the right anterior insula was almost significant ($F_{(1,33)} = 4.012$, $P = 0.053$).
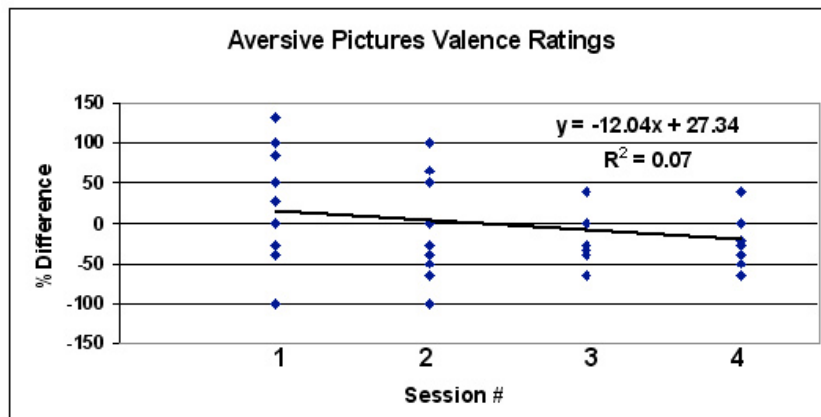
Figure 5.9 *Single subject percentage difference ratings of aversive pictures. Single subject percentage difference index of SAM valence ratings for aversive pictures between increase and decrease blocks across sessions. Lower value indicates more aversion. Percentage difference of affective ratings between increase and decrease conditions could be a better indicator than actual values, as it rules out inter-subject variability and baseline drift during the experiment.*

The time course of the hemodynamic response both during regulation and emotional stimuli presentation blocks across sessions was analyzed for the purpose of correlating the volitional modulation of target brain activity and the behavioural effects. The amplitude of the BOLD signal in the targeted left anterior insula insular maintained higher BOLD levels in the subsequent picture presentation condition, indicating a prolonged effect on picture processing (Figure 5.10). This effect was greater in the last two training sessions compared to the first two ($t_{(53)} = 5.37$, $P < 0.0001$).
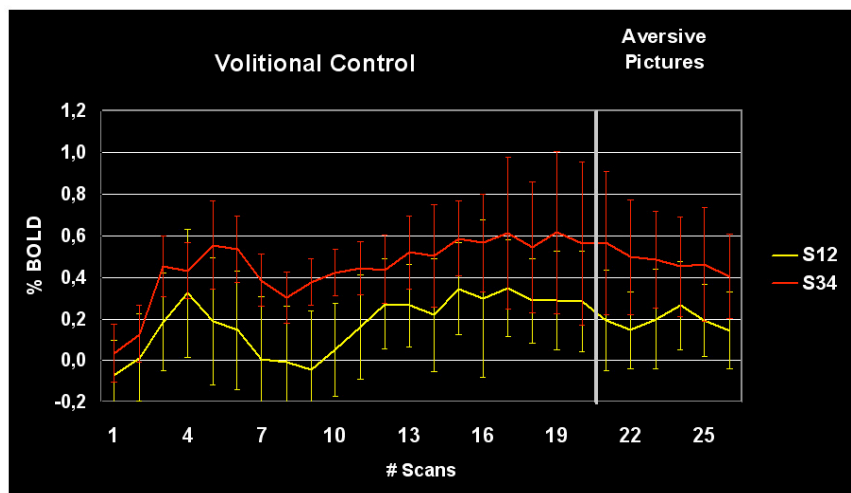
Figure 5.10. *Percentage BOLD signal change progression. Time-course of percent BOLD change computed as difference between increase and decrease conditions in the left anterior insula during the volitional control and aversive picture presentation conditions for first two training sessions (S1 and S2; yellow line) and last two training sessions (S3 and S4; red line). Percent difference of BOLD between volitional increase and decrease conditions in the region of interest maintained significantly larger values during subsequent picture presentation in the last two training sessions compared to the first two sessions indicating a clear effect of volitional control over emotional picture processing.*

Experiment 1: Discussion

Our findings demonstrate that subjects can achieve volitional control of the left anterior insula activity through an fMRI-BCI training. The learned control was specific for the target area and not an effect of general arousal and/or global unspecific brain activation as demonstrated by the inability of the control group to achieve volitional control due to the non-contingent feedback. Furthermore, we reported a modulation of the emotional response, specific to aversive stimuli but not to neutral stimuli, which correlated with the modulation of the left anterior insular activity. Although the contribution of the right homologous area for successful regulation is less significant, the similar pattern of activity indicates that the right insula could subserve a complementary function. Results in the control group are also quite intriguing. The small increase of BOLD signal in the left and right insula and a close to significant difference in valence ratings during the second session might suggest an effect generated by the adopted strategy. However, as here and previously demonstrated, mental imagery alone is not sufficient to achieve a focal and stable activity in the target area. A combination of mental strategies and real-time fMRI information drives subjects to achieve successful control (Caria, Veit et al. 2007).

Experiment 2: Results

Functional Data

Psychopathic criminals learned to control BOLD–magnitude in the left anterior insula to different extents when compared among the participants (Birbaumer, Sitaram et al. 2008). The ability to regulate differed among participants. Training resulted in a significantly increased activation cluster in the anterior portion of the left insula across sessions. Participants reported the following recall of emotional episodes and imageries during the regulation blocks: fight with the landlord, death of parents, experience in jail, memories of grand mother, and negative memories of a stay in a detention centre and pronouncement of judgement in the courtroom. Online analysis of each participant's BOLD signal without smoothing and averaging clearly shows learned modulation of the activity in the targeted area. Figure 5.11 shows the results of online analysis of a subject in early and late training sessions, respectively.
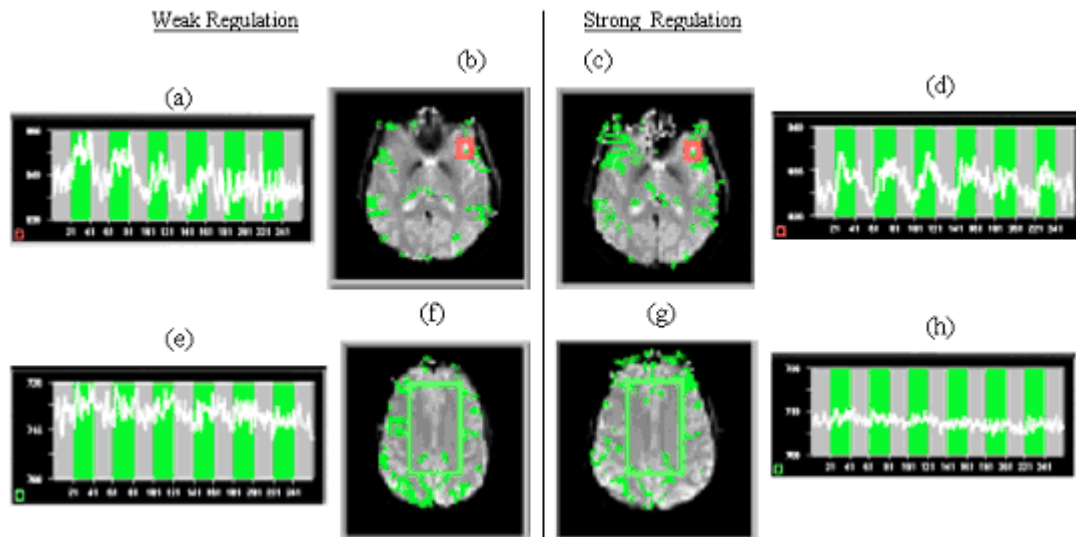
Figure 5.11. *Results of online analysis of self-regulation of left anterior insula from early and late training sessions, respectively. Figures (a)-(b) show the transversal slices in which the left anterior insula, the target ROI (red rectangle), and reference ROI (large green rectangle) were selected, respectively. Difference between the BOLD signals of target ROI and the reference ROI was used to compute the feedback signal to improve the specificity of the signal from the target ROI by removing general effects of arousal on the BOLD signal. Figures (c)-(d) show corresponding views for a session when a stronger regulation was achieved. Figures (e)-(f) show time-courses of BOLD activation in the target and reference ROIs, respectively, for weak regulation. Figures (g)-(h) show similar time-courses for the strong regulation session. With feedback training subjects learn to regulate the target ROI by consistently increasing and decreasing the BOLD activity in time while maintaining the BOLD activity in the reference ROI constant.*

We used the difference in the percent BOLD between volitional increase and decrease conditions rather than absolute values in order to rule out effects of baseline drift and inter-subject differences, and more importantly to arrive at a combined measure of volitional control. Continued training enhances the percent differential BOLD in the up-regulation condition compared to the down-regulation condition. Percent BOLD difference increases with contingent feedback from an early weak regulation session, to an intermediate medium regulation session, to a late strong regulation session. Whole brain analysis for each participant showed an increased activated cluster in the ROI at a later session when the subject had learned to regulate strongly in comparison to an early session when self-regulation was not yet learned (Figure 5.12).
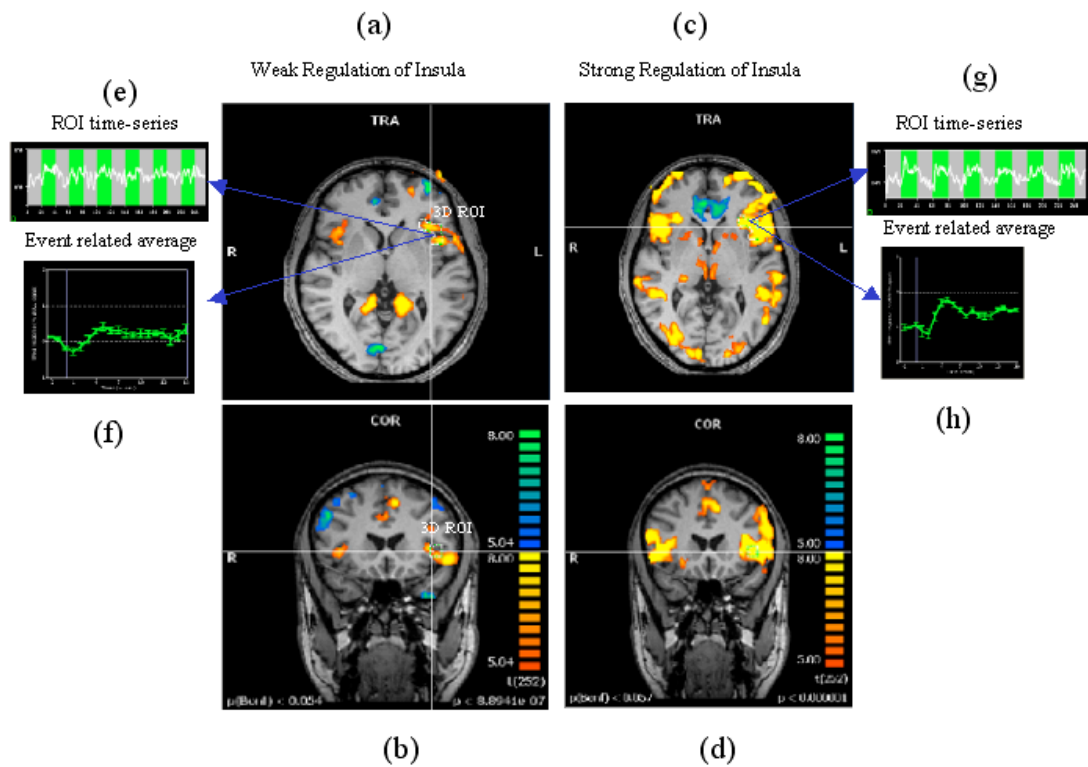
Figure 5.12. *Results of offline SPM analysis for representative subject AK. Statistical parametric maps showing the contrast up-regulation vs down-regulation during early and late sessions. Figures (a)-(b) show the transversal and coronal views of the contrast during an early session when the regulation was still weak. Figures (c)-(d) show the same views for a later session when a stronger regulation was achieved. Maps are all obtained at the same height threshold (P = 0.05, Bonferroni corrected). A precise, 3-dimensional ROI was delineated in the left anterior insula. Figures (e)-(f) show the time-series of BOLD signal and its event related average (ERA) in the ROI during weak regulation. The up- and down-regulation blocks are shown as alternating green and gray rectangles in the time-series. The ERA plots the percent BOLD change in the up-regulation block with respect to the down-regulation block after averaging across all the blocks of the session. The Figures (g)-(h) show similar plots for the stronger regulation.*

Figure 5.13 plots the percent BOLD increase and the network density (*cd*) for the three sessions for a representative subject AK. The plot shows that the performance of self-regulation of a session is proportional to the *causal density*, i.e., the number of interactions that are causally significant of the brain network involved in the function of emotion regulation out of the total number of possible interactions among ROIs. The figure shows results of connectivity analysis for 3 different strengths of regulation. Left column of the figure contains schematic depictions of the directed influences among different ROIs; the right column shows bar charts of causal flow (*cf*) for the ROIs.
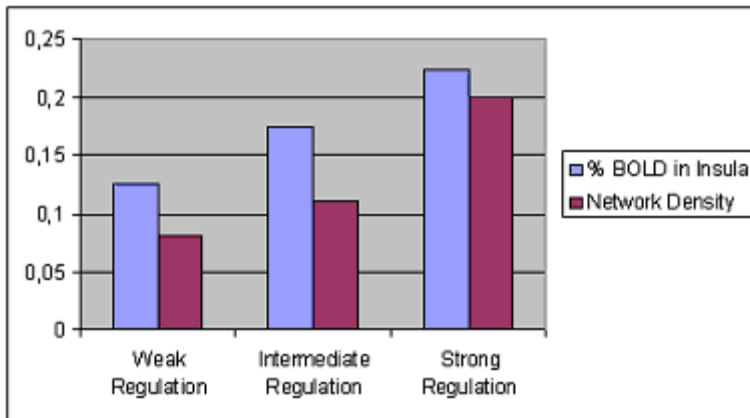
Figure 5.13. *Bar chart showing percent BOLD increase in insula and the corresponding values for density of the functional connectivity of the network computed by the Granger Causality Mapping (GCM) method. As the strength of regulation increases, the density of the network (defined as the ratio of number of directed connections between regions to the total number of possible connections) also increases.*

Connectivity during weak regulation of insula

Figures 5.14a and 5.14d show the brain network and the *causal flow*, respectively, during weak regulation. Regulation at this stage is driven by the posterior part of the brain, mainly involving the posterior cingulate which has significant directed influences to left insula, anterior cingulate cortex and hippocampus. The posterior cingulate is the major *causal source* in the weak regulation condition followed by the left medial prefrontal cortex. At this stage one can see a very sparse network involving interactions among very few ROIs in the emotional network indicated by the low *causal density*.
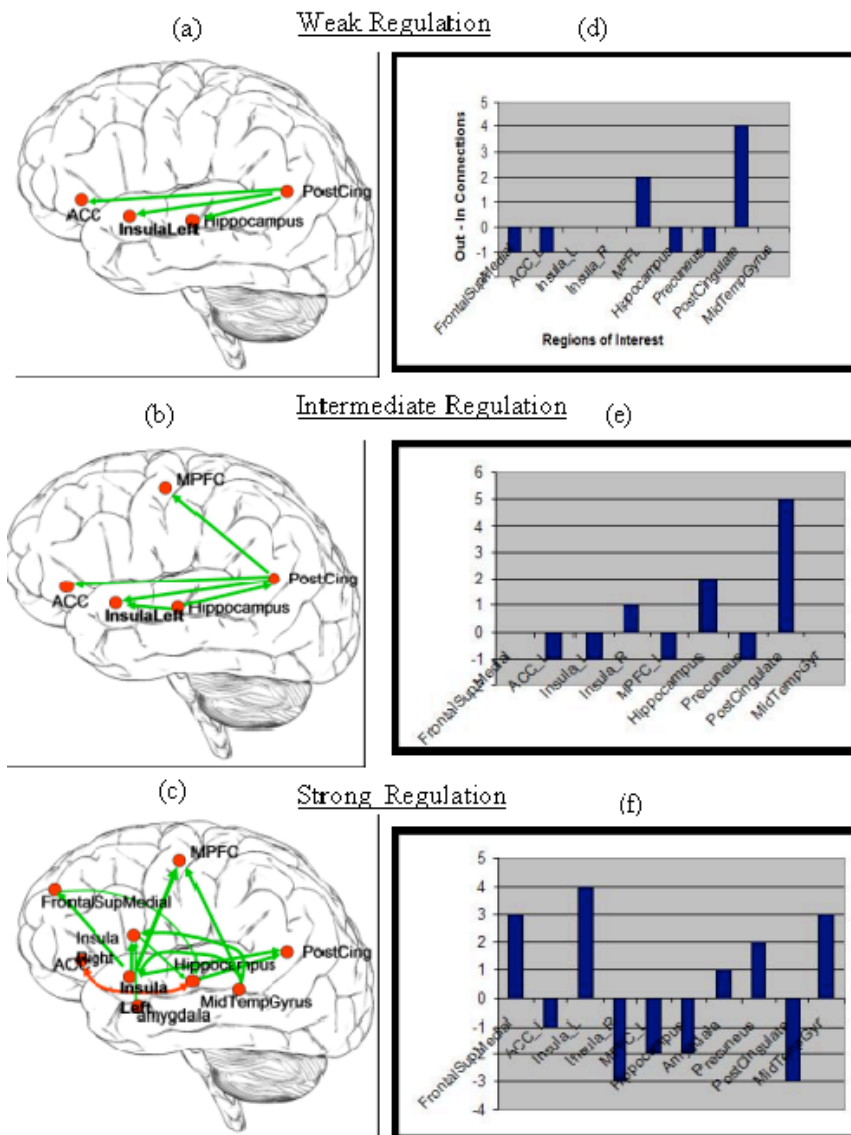
Figure 5.14. *Representative results (from Subject AK) of functional connectivity analysis of self-regulation of insula. Figures (a)-(c) show directed influence maps (DIMS) and figures (d)-(f) show the bar charts of the causal flow (CF; defined as the net difference between outgoing and incoming connections) in the brain regions (the emotional network) involved in the self-regulation of insula. Figures are arranged from top to bottom in terms of their increasing strength of regulation: from weak regulation (top), intermediate regulation (middle) to strong regulation (bottom). It is clear that as the strength of regulation increases, the number of directed influences in the emotional network also increases as shown by the DIMs. During strong self-regulation, many regions in the emotional network, including medial prefrontal cortex (MPFC), right insula, anterior cingulate cortex (ACC), amygdala and posterior cingulate cortex are seen to become connected with insula. The CF diagrams of the weak regulation shows that the activations at this stage are driven predominantly from the posterior portion of the brain (especially by the posterior cingulate cortex) and that the causal flow in the left insula is close to zero. However, with increasing strength of regulation, insula and the anterior regions of the brain seem to drive the network activation to a greater extent as shown by their increasing causal flow.*

Connectivity during intermediate regulation of insula

Figures 5.14b and 5.14e show the brain network and the *causal flow*, respectively, during intermediate regulation. Regulation at this stage continues to be driven by the posterior cingulate which has significant directed influences to left insula, anterior cingulate cortex, medial prefrontal cortex and hippocampus. In addition, the hippocampus directs its influence to the left insula. The posterior cingulate is still the major *causal source* followed by hippocampus in the intermediate regulation condition. The *causal density* of the network has slightly increased compared to the weak regulation stage.

Connectivity during strong regulation of insula

Figures 5.14c and 5.14f show the brain network and the *causal flow*, respectively, during strong regulation. Now, the anterior portion of the brain drives the network, with left insula taking a major share. Left insula is the predominant *causal source* with directed influences to superior medial frontal cortex, right insula, medial prefrontal cortex and posterior cingulate. Right insula and the posterior cingulate are the major *causal sinks*. At this stage, a great number of ROIs in the network (high *causal density*) have been recruited into the regulation function, mainly mediated by the left insula, superior medial frontal cortex and hippocampus. The anterior cingulate has reciprocal connections with hippocampus. New influences from midtemporal gyrus and amygdale towards insula are also observed.

Behavioural data (figure 5.15) were assessed by comparing the valence and arousal ratings of aversive and neutral pictures presented after up-regulation blocks and those presented after down-regulation blocks to exclude variability across subjects. Ratings were collected once before the self-regulation training was started (Pretest) and twice after a predetermined number of training sessions were completed (Posttest1 and Posttest2).

Figure 5.15. *Behavioural results for subject AK. Subject rated aversive and neutral pictures taken from the International Affective Picture System (IAPS) inside the scanner immediately after every up- and down-regulation block using the Self Assessment Manikin (SAM). Ratings were collected once before the self-regulation training was*

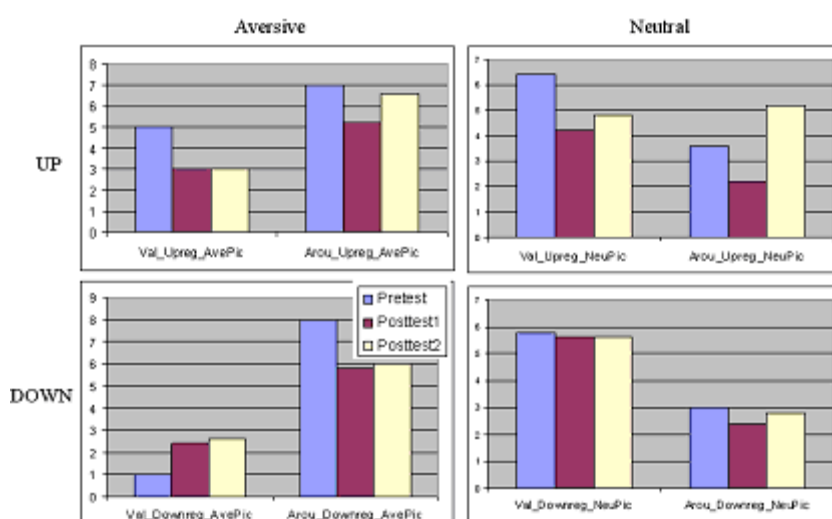*started (Pretest) and twice after a predetermined number of training sessions were completed (Posttest1 and Posttest2). (a) Subject AK aversive pictures as more negative (lower valence value) in the posttests compared to the pretest after up-regulation. (c) Inversely, subject AK rated versive pictures as less negative (higher valence value) in the posttests compared to the pretest after down-regulation. Aversive pictures were rated slightly more arousing after up-regulation than after down-regulation in the posttests compared to the pretests (a and c). No consistent differences were observed with arousal ratings for both aversive and neutral pictures (b and d).*

Experiment 2: Discussion

The present study (Birbaumer, Sitaram et al. 2008) demonstrates for the first time that criminal psychopaths can learn volitional regulation of left anterior insula with the help of an fMRI Brain-Computer Interface developed in our laboratory (Sitaram, Caria et al. 2007; Weiskopf, Sitaram et al. 2007; Sitaram, Weiskopf et al. 2008). Subjects learned to regulate insula by employing negative emotional imageries taken from previous episodes in their lives, in conjunction with contingent feedback. Our previous studies with healthy volunteers (Caria, Veit et al. 2007) had already shown that learned control was specific to the target region, and not a result of general arousal and global unspecific brain activation, as demonstrated by a control group trained with a non-contingent feedback. From another previous study, we had reported that regulation of left anterior insula modulates the emotional response specific to aversive picture stimuli but not neutral picture stimuli. Both studies had shown that mental imagery alone is not sufficient, and that real-time feedback of the BOLD signal extracted from the target region enhances subjects' ability to achieve regulation. In the present study we have extended the experimental protocol by providing monetary reward after every session. Monetary reward was computed proportional to the percent BOLD increase in the target region to motivate these difficult-to-recruit experimental subjects to continue feedback training. We show that continued training enhances the percent differential BOLD in the up-regulation condition compared to the down-regulation condition. Remarkably, subjects with higher Psychopathic Checklist-Revised (PCL-R) scores are less successful at self-regulation than their lower PCL-R counterparts, supporting the existing notion that psychopaths are emotionally detached and have deficient emotional processing (Lykken 1957).

Although, the statistical analysis of the ratings of valence and arousal of the aversive and neutral pictures from the International Affective Picture System (IAPS) did not turn up significant results, a trend similar to the previous study on healthy normals (Caria et al., in press) in the form of increased negativity (lower valence ratings) of aversive pictures compared to neutral pictures was apparent. We attribute the lack of significance to fewer experimental subjects and consequently a smaller rating data set substantially reducing the statistical power. Furthermore, not all criminal psychopaths achieved equal level of percent BOLD increase, potentially leading to inconsistent and diluted effects of regulation on emotional processing and hence picture ratings. This indicates the need for a future extended study involving more psychopathic subjects undergoing longer training and a more sensitive rating system for measurement of behavioral effects of regulation.

The main purpose of the present study was not only to ascertain whether criminal psychopaths can learn to regulate the BOLD signal in the left anterior insula but also to

investigate the changes in functional connectivity in the brain of criminal psychopaths due to successful regulation. In particular, we wanted to compare the functional connectivity changes with varying strength of the regulation. To this end, we employed the multivariate Granger Causality Model (GCM) adapted from the Causal Connectivity Toolkit from Seth (Seth 2005) to work with fMRI data. Multivariate GCM was applied to time-series of 8-10 ROIs from the emotional network separately for 3 different levels of regulation, namely, weak, intermediate and strong, determined based on the average percent BOLD increase in up-regulation blocks compared down-regulation blocks. The results show that, firstly, the strength of regulation is proportional to the *causal density* of the network, in other words, the amount of 'connectedness' of the functional network purportedly involved in the regulation process. Secondly, the results show that weak regulation is driven mainly from the posterior cingulate, which acts as the main *causal source,* while right insula and the posterior cingulate are the major *causal sinks*. As regulation gets stronger, the source of the network moves towards the anterior of the brain finally settling in the left anterior insula at the strongest regulation. During strong regulation, left insula directs its influence outwardly to superior medial frontal cortex, right insula, medial prefrontal cortex and posterior cingulate, indicated by the high value of *causal flow*. In addition, the hippocampus, amygdala and midtemporal gyrus are introduced into the causal network during strong regulation. Our results are supported by previous reports of emotional regulation and processing. Ochsner et al., (Ochsner, Ray et al. 2004) have shown that up- and down-regulating negative emotion recruited prefrontal and anterior cingulate regions implicated in cognitive control. Further, they reported that self-focussed regulation recruited medial prefrontal regions implicated in internally focused processing, whereas situation-focussed regulation recruited lateral prefrontal regions implicated in externally focused processing. In our study, predominance of medial prefrontal activation and its involvement in the causal network, and in addition the self-report of regulation strategies by subjects (e.g., fight with the landlord, death of parents, experience in jail, memories of grand mother, negative memories of a stay in a detention centre and pronouncement of judgement in the courtroom) indicate the employment of self-focussed imagery and thus further corroborate Ochsner's (Ochsner, Ray et al. 2004) conclusion.

Chapter 6.

Discussion

In this thesis, we have presented first our technical implementation of metabolic brain-computer interfaces based on fNIRS and fMRI. We have demonstrated the capability of metabolic BCIs to decode brain states in real-time based on fNIRS and fMRI signals by the application of pattern recognition technology. We have shown preliminary results of applying fNIRS-BCI for brain state classification of motor imagery and execution (Sitaram, Hoshi et al. 2005; Sitaram, Zhang et al. 2007), and a word speller application as a potential technology to enable communication for locked-in patients. We have also demonstrated our new developments in real-time decoding and detection of multiple emotional states in the brain using fMRI signals (Sitaram, Lee et al. 2008). Subsequent to these technical developments, we have demonstrated three preliminary results of applying fMRI-BCI: 1) self-regulation of emotion with feedback from anterior insula in healthy individuals (Caria, Sitaram et al. 2006; Caria, Veit et al. 2007); 2) self-regulation of right inferior frontal gyrus and the influence of regulation on language processing of prosody in healthy individuals (Rota, Sitaram et al. 2008); and 3) self-regulation of ventrolateral premotor cortex in healthy individuals and stroke patients (in preparation). Encouraged by the above results, we conducted a more intensive study to investigate the emotional influences of self-regulation of anterior insula in a number of healthy individuals and psychopathic criminals (Birbaumer, Sitaram et al., 2008). Our results show that healthy individuals and psychopathic criminals can learn to regulate the BOLD response in the anterior insula by the help of mental imagery of emotional episodes in their lives aided by contingent feedback from the fMRI-BCI system. In the case of psychopathic criminals, we have also reported first evidence that the ability to self-regulate is inversely proportional the severity of psychopathy. We have, shown that the immediate effect of up-regulation of the signal is to enhance the negative aspect (i.e., reduction in the valence dimension) of emotion. This specific effect of self-regulation on emotion processing is also shown to be associated with a reorganisation of the functional network of emotion (involving insula, ACC, prefrontal cortex, hippocampus, etc.) with training, leading to an optimal network that utilizes cognitive resources in an efficient fashion in performing the regulation task.

Logothetis (2008) pointed out that without simultaneous measurement of BOLD and neurophysiological response for the same area, it is impossible to conclude whether a BOLD increase or decrease is excitatory or inhibitory. In addition, a correct interpretation of the functional role of BOLD activity needs simulataneous recording of the relevant behaviour. FMRI-BCI is the method of choice to overcome this problem in human experiments because specific behaviour effects can be studied as dependent variable of a learned circumscribed BOLD response. Non-invasive experimentation with people in fMRI-BCI allows recording of EEG, ECoG and NIRS together with BOLD.

While this work has indicated the potential role that metabolic BCIs could play in neuroscientific research and clinical applications, it has, however, left one important question open. How do individuals learn to volitionally regulate the metabolic response from a circumscribed brain region, and how does this self-regulation influence behaviour. The hemo-neural hypothesis (Moore and Cao 2008) looks at the vascular and molecular processes involved in blood flow and oxygen consumption, and how these in turn lead to changes in neural activation and hence behaviour. We propose a model of regulation based on the hemo-neural hypothesis.

Hemo-neural Model of Regulation

The brain contains a rich and interdependent network of neurons, whose activity is well correlated with information processing (Moore and Cao 2008). The brain also contains a rich and interdependent vascular network, whose activity, i.e., blood flow, is typically well correlated with neural activity. The standard modern view of blood flow is that it serves a physiological function unrelated to information processing, such as bringing oxygen to active neurons, eliminating "waste" generated by neural activity, or regulating temperature. Realistic computational models of brain function do not include blood flow as a component, and neurophysiologists do not consider it as a regressor to explain variance in their data. In contrast to this position, the hemo-neural hypothesis (Moore and Cao 2008) states that hemodynamics play a role in information processing, through modulation of neural activity by blood flow. This hypothesis predicts that the modulation of flow of blood to a brain region during neural activity provides a spatially and temporally correlated source of regulation, modulating the excitability of the local circuit. This shaping of the neural response will, in turn, impact representation and behavior. We do have evidence to support this hypothesis.

Firstly, the vascular pathways that regulate blood flow are finely interleaved with neural architecture. These anatomical vascular patterns are not uniform, and in many cases reflect the information processing functionality of a given brain area. In the neocortex, capillary density shows specificity in the vertical dimension through enhanced concentration in specific layers, such as layer IV of primary sensory areas (Patel 1983; Zheng, LaMantia et al. 1991; Woolsey, Rovainen et al. 1996), in contrast to the flat laminar profile in the entorhinal cortex (Michaloudi, Grivas et al. 2005). Subcortical structures show similar apparent principles of distribution, as the striatum of the basal ganglia shows enhanced capillary density in the matrix as compared with the striosomes (Feekes and Cassell 2006). Hence, the anatomy and physiological regulatory mechanisms can position hemodynamic signals spatially and temporally to have an impact on neural activity.

Secondly, when local populations of neurons are active, they recruit increased blood flow and volume to the activated region, a process known as "functional hyperemia" (Kong, Zheng et al. 2004; Hoge, Franceschini et al. 2005; Martin, Martindale et al. 2006). Functional hyperemia can be induced and modulated by a variety of mechanisms. Relaxation of smooth muscles around arteries and arterioles leads to changes in blood flow and volume. Further, astrocytes are believed to be a primary route for detecting neural activity and engaging the vasculature. Recent evidence has also implicated neurons in the direct control of blood flow. In neocortex, interneurons

directly contact vascular processes. Intracellular electrical stimulation in vitro of interneurons adjacent to vessels can evoke dilation or constriction. Hence, there are known correlations between information processing and changes in blood flow. This suggests that the anatomy and physiology of these two networks are positioned to function synergistically in information processing.

Thirdly, there could be mechanisms by which changes in hemodynamics in the normal range of function can impact neural activity. Moore and Cao (Moore and Cao 2008) propose an alternative explanation for functional hyperemia, beyond an exclusively metabolic account. Functional hyperemia is spatially and temporally precisely directed to the neural processing. Under hemo-neural hypothesis, functional hyperemia is not the overdelivery of oxygenated blood for metabolism but rather the targeted regulation of neural processing. In support of this hypothesis, Moore and Cao (2008) describe evidence for different possible mechanisms: 1) direct hemo-neural interactions via diffusible messengers that freely cross the blood-brain barrier; mechanical engagement of blood on tissue; and temperature change due ion exchanges, and 2) indirect mechanisms such as astrocyte-mediated hemo-to-neural signaling. Further studies need to provide concrete evidence for the mechanisms suggested under this hypothesis.

Under the hemo-neural hypothesis, blood flow would anticipate the acquisition of information, helping transform cortical circuits to more optimally represent the incoming sensory signals. In many cognitive paradigms, blood flow modulation occurs in anticipation of or independent of the receipt of sensory input. One example of a context in which hemo-neural modulation of cortical dynamics may impact information processing is through enhancement of evoked responses during selective attention (Moore and Cao, 2008). A wide variety of studies have shown that attention to a region of input space (e.g., a body area) is correlated with enhanced evoked action potential of cortical neurons with receptive fields overlapping the attended region (Bichot and Desimone 2006). These effects typically emerge 100–500 ms after the onset of attentional focus (Khayat, Spekreijse et al. 2006).

Moore and Cao (2008) suggest that there are several potential clinical implications of the prediction that functional hyperemia modulates neural activity. Diseases that impact the vasculature and cognitive function may in part be operating through a failure in hemo-neural interactions and the loss or alteration of neuromodulatory function that results. The negative outcome of stroke is commonly believed to arise only from localized cell death in the focus of the lesion and the metabolic losses and stresses associated with deprived flow. Under the hemo-neural hypothesis, the altered blood supply in itself, and the subsequent loss of normal functionality in a given neural circuit, may be cause behavioral symptoms. A prediction of the hemo-neural hypothesis is that decreased blood flow could induce an increase in the excitability of neural tissue and that this loss of a suppressive mechanism could contribute to this posttraumatic response.

Based on the hemo-neural hypothesis, we propose that if participants learn to volitionally regulate the hemodynamic activity of a brain region by instrumental conditioning with contingent feedback, such a modulation would in turn change neural activity in the region. We further propose that this change in neural activation brought about indirectly by the modulation of hemodynamics in the region could also

change behavior. Future multimodal studies using fMRI, EEG and TMS should investigate the above hypotheses.

References

Abler, B., A. Roebroeck, et al. (2006). "Investigating directed influences between activated brain areas in a motor-response task using fMRI." <u>Magn Reson Imaging</u> **24**(2): 181-5.

Adam, G. (1998). <u>Visceral perception: understanding internal cognition</u>. New York, Plenum Press.

Adolphs, R. (2003). "Cognitive neuroscience of human social behaviour." <u>Nat Rev Neurosci</u> **4**(3): 165-78.

Adolphs, R. (2003). "Investigating the cognitive neuroscience of social behavior." <u>Neuropsychologia</u> **41**(2): 119-26.

Anders, S., N. Birbaumer, et al. (2004). "Parietal somatosensory association cortex mediates affective blindsight." <u>Nat Neurosci.</u> **7**(4): 339-40. Epub 2004 Mar 14.

Anokhin, A. P., W. Lutzenberger, et al. (2000). "Complexity of electrocortical dynamics in children: developmental aspects." <u>Dev Psychobiol.</u> **36**(1): 9-22.

Atsumori, H., M. Kiguchi, et al. (2007). "Development of a multi-channel, portable optical topography system." <u>Conf Proc IEEE Eng Med Biol Soc</u> **2007**: 3362-4.

Augustine, J. R. (1985). "The insular lobe in primates including humans." <u>Neurol. Res.</u> **7**: 2-10.

Augustine, J. R. (1996). "Circuitry and functional aspects of the insular lobe in primates including humans." <u>Brain Res Brain Res Rev</u> **22**(3): 229-44.

Babiloni, F., F. Cincotti, et al. (2001). "Recognition of imagined hand movements with low resolution surface Laplacian and linear classifiers." <u>Med Eng Phys</u> **23**(5): 323-8.

Bagarinao, E., K. Matsuo, et al. (2003). "Estimation of general linear model coefficients for real-time application." <u>Neuroimage</u> **19**(2 Pt 1): 422-9.

Bandettini, P. A., E. C. Wong, et al. (1992). "Time course EPI of human brain function during task activation." <u>Magn Reson Med</u> **25**(2): 390-7.

Barber, T. X., J. Kamiya, et al., Eds. (1971–78). <u>Biofeedback and Self-Control</u>. Chicago, Aldine Series.

Beisteiner, R., Hollinger, P., Lindinger, G., Lang, W., Berthoz, A. (1995). "Mental representation of movements. Brain potentials associated with imagination of hand movements." <u>Electroencephalogr Clin Neurophysiol</u>(96): 183-193.

Benaron, D. A., S. R. Hintz, et al. (2000). "Noninvasive functional imaging of human brain using light." <u>J Cereb Blood Flow Metab</u> **20**(3): 469-77.

Bichot, N. P. and R. Desimone (2006). "Finding a face in the crowd: parallel and serial neural mechanisms of visual selection." <u>Prog Brain Res</u> **155**: 147-56.

Binkofski, F., G. Buccino, et al. (1999). "Mirror agnosia and mirror ataxia constitute different parietal lobe disorders." <u>Ann Neurol</u> **46**(1): 51-61.

Birbaumer, N. (2006). "Brain-computer-interface research: Coming of age." <u>Clin Neurophysiol.</u> **117**(3): 479-83. Epub 2006 Feb 2.

Birbaumer, N. (2006). "Breaking the silence: brain-computer interfaces (BCI) for communication and motor control." <u>Psychophysiology</u> **43**(6): 517-32.

Birbaumer, N. and L. G. Cohen (2007). "Brain-computer interfaces: communication and restoration of movement in paralysis." <u>J Physiol</u> **579**(Pt 3): 621-36.

Birbaumer, N., T. Elbert, et al. (1990). "Slow potentials of the cerebral cortex and behavior." <u>Physiol Rev.</u> **70**(1): 1-41.

Birbaumer, N., N. Ghanayim, et al. (1999). "A spelling device for the paralysed." <u>Nature.</u> **398**(6725): 297-8.

Birbaumer, N., T. Hinterberger, et al. (2003). "The thought-translation device (TTD):

neurobehavioral mechanisms and clinical outcome." <u>IEEE Trans Neural Syst Rehabil Eng.</u> **11**(2): 120-3.

Birbaumer, N. and H. Kimmel, Eds. (1979). <u>Biofeedback and Self-regulation</u>. Erlbaum, Hillsdale FL, USA.

Birbaumer, N., R. Sitaram, et al. (2008). <u>Operant conditioning of the anterior insula in criminal psychopaths</u> Society for Neurosience, Washington Convention Center: Hall A-C.

Birbaumer, N., R. Veit, et al. (2005). "Deficient fear conditioning in psychopathy: a functional magnetic resonance imaging study." <u>Arch Gen Psychiatry.</u> **62**(7): 799-805.

Birbaumer, N., C. Weber, et al. (2006). "Physiological regulation of thinking: brain-computer interface (BCI) research." <u>Prog Brain Res</u> **159**: 369-91.

Birn, R. M., J. B. Diamond, et al. (2006). "Separating respiratory-variation-related fluctuations from neuronal-activity-related fluctuations in fMRI." <u>Neuroimage</u> **31**(4): 1536-48.

Blair, R. J., K. S. Peschardt, et al. (2006). "The development of psychopathy." <u>J Child Psychol Psychiatry</u> **47**(3-4): 262-76.

Blankertz, B., G. Curio, et al. (2001). <u>Classifying single trail EEG: Toward brain computer interfacing</u>. Cambridge, MA, MIT Press.

Bradley, M. M. and P. J. Lang (1994). "Measuring emotion: the Self-Assessment Manikin and the Semantic Differential." <u>J Behav Ther Exp Psychiatry</u> **25**(1): 49-59.

Brambilla, P., R. Cerini, et al. (2007). "Assessment of cerebral blood volume in schizophrenia: A magnetic resonance imaging study." <u>J Psychiatr Res</u> **41**(6): 502-10.

Brass, M., S. Zysset, et al. (2001). "The inhibition of imitative response tendencies." <u>Neuroimage</u> **14**(6): 1416-23.

Breitenstein, C., I. Daum, et al. (1996). "Erfassung der Emotionswahrnehmung bei zentralnervösen Läsionen und Erkrankungen: Psychometrische Gütekriterien der "Tübinger Affekt Batterie"." <u>Neurol & Rehab</u> **2**: 93-101.

Buccino, G., F. Binkofski, et al. (2001). "Action observation activates premotor and parietal areas in a somatotopic manner: an fMRI study." <u>Eur J Neurosci</u> **13**(2): 400-4.

Buccino, G., A. Solodkin, et al. (2006). "Functions of the mirror neuron system: implications for neurorehabilitation." <u>Cogn Behav Neurol</u> **19**(1): 55-63.

Buchel, C., J. Morris, et al. (1998). "Brain systems mediating aversive conditioning: an event-related fMRI study." <u>Neuron</u> **20**(5): 947-57.

Calder, A. J., J. Keane, et al. (2000). "Impaired recognition and experience of disgust following brain injury." <u>Nat Neurosci</u> **3**(11): 1077-8.

Caria, A., R. Sitaram, et al. (2006). <u>Can We Learn to Increase Our Emotional Involvement? Real-Time fMRI of Anterior Cingulate Cortex During Emotional Processing.</u> Human Brain Mapping, Florence, Italy.

Caria, A., R. Veit, et al. (2007). "Regulation of anterior insular cortex activity using real-time fMRI." <u>Neuroimage</u> **35**(3): 1238-46.

Castiello, U. (2003). "Understanding other people's actions: intention and attention." <u>J Exp Psychol Hum Percept Perform</u> **29**(2): 416-30.

Chang, C. C. and C. J. Lin (2001). LIBSVM - A Library for Support Vector Machines. http://www.csie.ntu.edu.tw/cjlin/libsvm/.

Chua, P., M. Krams, et al. (1999). "A functional anatomy of anticipatory anxiety." <u>Neuroimage</u> **9**(6 Pt 1): 563-71.

Cleckley, H. M. (1951). "The mask of sanity." <u>Postgrad Med</u> **9**(3): 193-7.

Coghill, R. C., C. N. Sang, et al. (1999). "Pain intensity processing within the human brain: a bilateral, distributed mechanism." <u>J Neurophysiol</u> **82**(4): 1934-43.

Cohen, M. S. (2001). "Real-time functional magnetic resonance imaging." <u>Methods</u> **25**(2): 201-20.

Collins, D. L., P. Neelin, et al. (1994). "Automatic 3D intersubject registration of MR volumetric data in standardized Talairach space." <u>J Comput Assist Tomogr</u> **18**(2): 192-205.

Cox, R. W., A. Jesmanowicz, et al. (1995). "Real-time functional magnetic resonance imaging." <u>Magn Reson Med</u> **33**(2): 230-6.

Coyle, S., T. Ward, et al. (2004). "On the Suitability of Near-Infrared Systems for Next Generation Brain Computer Interfaces." <u>Physiological Measurement</u> **25**: 815–822.

Coyle, S. M., T. E. Ward, et al. (2007). "Brain-computer interface using a simplified functional near-infrared spectroscopy system." <u>J Neural Eng</u> **4**(3): 219-26.

Craig, A. D. (2002). "How do you feel? Interoception: the sense of the physiological condition of the body." <u>Nat Rev Neurosci</u> **3**(8): 655-66.

Craig, A. D. (2003). "Interoception: the sense of the physiological condition of the body." <u>Curr Opin Neurobiol</u> **13**(4): 500-5.

Craighero, L., A. Bello, et al. (2002). "Hand action preparation influences the responses to hand pictures." <u>Neuropsychologia</u> **40**(5): 492-502.

Cramer, S. C. (1999). "Stroke recovery. Lessons from functional MR imaging and other methods of human brain mapping." <u>Phys Med Rehabil Clin N Am</u> **10**(4): 875-86, ix.

Critchley, H. D., S. Wiens, et al. (2004). "Neural systems supporting interoceptive awareness." <u>Nat Neurosci</u> **7**(2): 189-95.

Damasio, A. R. (2000). "Eighth C.U. Ariens Kappers Lecture. The fabric of the mind: a neurobiological perspective." <u>Prog Brain Res</u> **126**: 457-67.

Damasio, A. R., T. J. Grabowski, et al. (2000). "Subcortical and cortical brain activity during the feeling of self-generated emotions." <u>Nat Neurosci</u> **3**(10): 1049-56.

Davare, M., M. Andres, et al. (2006). "Dissociating the role of ventral and dorsal premotor cortex in precision grasping." <u>J Neurosci</u> **26**(8): 2260-8.

Davatzikos, C., K. Ruparel, et al. (2005). "Classifying spatial patterns of brain activity with machine learning methods: application to lie detection." <u>Neuroimage</u> **28**(3): 663-8.

Day, R. and S. Wong (1996). "Anomalous perceptual asymmetries for negative emotional stimuli in the psychopath." <u>J Abnorm Psychol</u> **105**(4): 648-52.

deCharms, R. C., K. Christoff, et al. (2004). "Learned regulation of spatially localized brain activation using real-time fMRI." <u>Neuroimage.</u> **21**(1): 436-43.

deCharms, R. C., F. Maeda, et al. (2005). "Control over brain activation and pain learned by using real-time functional MRI." <u>Proc Natl Acad Sci U S A.</u> **102**(51): 18626-31. Epub 2005 Dec 13.

Dogil, G., I. Frese, et al. (2004). "Where and how does grammatically geared processing take place-and why is Broca's area often involved. A coordinated fMRI/ERBP study of language processing." <u>Brain Lang.</u> **89**(2): 337-45.

Donoghue, J. P. (2002). "Connecting cortex to machines: recent advances in brain interfaces." <u>Nat Neurosci.</u> **5 Suppl**: 1085-8.

Egner, T. and J. H. Gruzelier (2003). "Ecological validity of neurofeedback: modulation of slow wave EEG enhances musical performance." <u>Neuroreport.</u> **14**(9): 1221-4.

Ehrsson, H. H., A. Fagergren, et al. (2000). "Cortical activity in precision- versus power-grip tasks: an fMRI study." J Neurophysiol **83**(1): 528-36.

Ehrsson, H. H., E. Fagergren, et al. (2001). "Differential fronto-parietal activation depending on force used in a precision grip task: an fMRI study." J Neurophysiol **85**(6): 2613-23.

Elbert, T., B. Rockstroh, et al. (1980). "Biofeedback of slow cortical potentials. I." Electroencephalogr Clin Neurophysiol. **48**(3): 293-301.

Fallgatter, A. J., M. Roesler, et al. (1997). "Loss of functional hemispheric asymmetry in Alzheimer's dementia assessed with near-infrared spectroscopy." Brain Res Cogn Brain Res **6**(1): 67-72.

Feekes, J. A. and M. D. Cassell (2006). "The vascular supply of the functional compartments of the human striatum." Brain **129**(Pt 8): 2189-201.

Feinberg, T. E. and M. J. Farah, Eds. (2003). Behavioral Neurology and Neuropsychology. New York, McGraw-Hill.

Fernandez, B., D. Cardebat, et al. (2004). "Functional MRI follow-up study of language processes in healthy subjects and during recovery in a case of aphasia." Stroke **35**(9): 2171-6.

Fetz, E. E. (1969). "Operant conditioning of cortical unit activity." Science **163**(870): 955-8.

Fox, P. T. and M. E. Raichle (1986). "Focal physiological uncoupling of cerebral blood flow and oxidative metabolism during somatosensory stimulation in human subjects." Proc Natl Acad Sci U S A **83**(4): 1140-4.

Franceschini, M. A., V. Toronov, et al. (2000). "On-line optical imaging of the human brain with 160-ms temporal resolution." Optical Society of America.

Francis, S., E. T. Rolls, et al. (1999). "The representation of pleasant touch in the brain and its relationship with taste and olfactory areas." Neuroreport **10**(3): 453-9.

Friederici, A. D. and K. Alter (2004). "Lateralization of auditory language functions: a dynamic dual pathway model." Brain Lang **89**(2): 267-76.

Friederici, A. D., S. A. Kotz, et al. (2003). "Syntactic comprehension in Parkinson's disease: investigating early automatic and late integrational processes using event-related brain potentials." Neuropsychology **17**(1): 133-42.

Friston, K. J., A. P. Holmes, et al. (1995). "Analysis of fMRI time-series revisited." Neuroimage **2**(1): 45-53.

Gelnar, P. A., B. R. Krauss, et al. (1999). "A comparative fMRI study of cortical representations for thermal painful, vibrotactile, and motor performance tasks." Neuroimage **10**(4): 460-82.

Gembris, D., J. G. Taylor, et al. (2000). "Functional magnetic resonance imaging in real time (FIRE): sliding-window correlation analysis and reference-vector optimization." Magn Reson Med. **43**(2): 259-68.

Glover, G. H., T. Q. Li, et al. (2000). "Image-based method for retrospective correction of physiological motion effects in fMRI: RETROICOR." Magn Reson Med. **44**(1): 162-7.

Goebel, R. (2001). "Cortex-based real-time fMRI." Neuroimage **13**(S129).

Gorno-Tempini, M. L., S. Pradelli, et al. (2001). "Explicit and incidental facial expression processing: an fMRI study." Neuroimage **14**(2): 465-73.

Granger, C. (1969). "Investigating causal relations by econometric models and cross-spectral methods." Econometrica **37**: 424–38.

Granger, C. (1980). "Testing for causality: a personal viewpoint. J Econ Dyn Control." **2**: 329 – 52.

Haihong, Z. and G. Cuntai (2006). <u>Kernel-based Signal Localization Method for NIRS</u>

<u>Brain-computer Interfaces</u>. International Conference on Pattern Recognition, Hong Kong.

Hanakawa, T., S. Parikh, et al. (2005). "Finger and face representations in the ipsilateral precentral motor areas in humans." <u>J Neurophysiol</u> **93**(5): 2950-8.

Hare, R. D. (1978). "Psychopathy and electrodermal responses to nonsignal stimulation." <u>Biol Psychol</u> **6**(4): 237-46.

Hare, R. D., S. D. Hart, et al. (1991). "Psychopathy and the DSM-IV criteria for antisocial personality disorder." <u>J Abnorm Psychol</u> **100**(3): 391-8.

Haynes, J. D. and G. Rees (2006). "Decoding mental states from brain activity in humans." <u>Nat Rev Neurosci</u> **7**(7): 523-34.

Heim, S. (2005). "The structure and dynamics of normal language processing: insights from neuroimaging." <u>Acta Neurobiol Exp (Wars)</u> **65**(1): 95-116.

Hock, C., K. Villringer, et al. (1997). "A role for near infrared spectroscopy in psychiatry?" <u>Adv Exp Med Biol</u> **413**: 105-23.

Hoekert, M., R. S. Kahn, et al. (2007). "Impaired recognition and expression of emotional prosody in schizophrenia: review and meta-analysis." <u>Schizophr Res</u> **96**(1-3): 135-45.

Hoge, R. D., M. A. Franceschini, et al. (2005). "Simultaneous recording of task-induced changes in blood oxygenation, volume, and flow using diffuse optical imaging and arterial spin-labeling MRI." <u>Neuroimage</u> **25**(3): 701-7.

Horovitz, S. G. and J. C. Gore (2004). "Simultaneous event-related potential and near-infrared spectroscopic studies of semantic processing." <u>Hum Brain Mapp</u> **22**(2): 110-5.

Hoshi, Y. (2007). "Functional near-infrared spectroscopy: current status and future prospects." <u>J Biomed Opt</u> **12**(6): 062106.

Hoshi, Y., N. Kobayashi, et al. (2001). "Interpretation of near-infrared spectroscopy signals: a study with a newly developed perfused rat brain model." <u>J Appl Physiol</u> **90**(5): 1657-62.

Hoshi, Y., I. Oda, et al. (2000). "Visuospatial imagery is a fruitful strategy for the digit span backward task: a study with near-infrared optical tomography." <u>Brain Res Cogn Brain Res</u> **9**(3): 339-42.

Hoshi, Y. and M. Tamura (1993). "Dynamic multichannel near-infrared optical imaging of human brain activity." <u>J Appl Physiol</u> **75**(4): 1842-6.

Hoshi, Y. and M. Tamura (1997). "Near-infrared optical detection of sequential brain activation in the prefrontal cortex during mental tasks." <u>Neuroimage</u> **5**(4 Pt 1): 292-7.

Huppert, T. J., R. D. Hoge, et al. (2006). "A temporal comparison of BOLD, ASL, and NIRS hemodynamic responses to motor stimuli in adult humans." <u>Neuroimage</u> **29**(2): 368-82.

Jackson, A., J. Mavoori, et al. (2006). "Correlations between the same motor cortex cells and arm muscles during a trained task, free behavior and natural sleep in the macaque monkey." <u>J Neurophysiol</u>.

Jackson, P. L., A. N. Meltzoff, et al. (2005). "How do we perceive the pain of others? A window into the neural processes involved in empathy." <u>Neuroimage</u> **24**(3): 771-9.

Jobsis, F. F. (1977). "Non-invasive, infra-red monitoring of cerebral O2 sufficiency, bloodvolume, HbO2-Hb shifts and bloodflow." <u>Acta Neurol Scand Suppl</u> **64**: 452-3.

Josephs, O., A. M. Howseman, et al. (1997). "Physiological noise modelling for multi-slice EPI fMRI using SPM."

Kamiya, J. (1971). "Biofeedback Training in Voluntary Control of EEG Alpha Rhythms." Calif Med **115**(3): 44.

Kan, Y., M. Mimura, et al. (2004). "Recognition of emotion from moving facial and prosodic stimuli in depressed patients." J Neurol Neurosurg Psychiatry **75**(12): 1667-71.

Kato, T., A. Kamei, et al. (1993). "Human visual cortical function during photic stimulation monitoring by means of near-infrared spectroscopy." J Cereb Blood Flow Metab **13**(3): 516-20.

Kennan, R. P., S. G. Horovitz, et al. (2002). "Simultaneous recording of event-related auditory oddball response using transcranial near infrared optical topography and surface EEG." Neuroimage **16**(3 Pt 1): 587-92.

Khayat, P. S., H. Spekreijse, et al. (2006). "Attention lights up new object representations before the old ones fade away." J Neurosci **26**(1): 138-42.

Kiebel, S. J., S. Kloppel, et al. (2007). "Dynamic causal modeling: a generative model of slice timing in fMRI." Neuroimage **34**(4): 1487-96.

Kiguchi, M., N. Ichikawa, et al. (2007). "Comparison of light intensity on the brain surface due to laser exposure during optical topography and solar irradiation." J Biomed Opt **12**(6): 062108.

Kim, J. J. and M. W. Jung (2006). "Neural circuits and mechanisms involved in Pavlovian fear conditioning: a critical review." Neurosci Biobehav Rev **30**(2): 188-202.

Kimbrell, T. A., M. S. George, et al. (1999). "Regional brain activity during transient self-induced anxiety and anger in healthy adults." Biol Psychiatry **46**(4): 454-65.

Kleinschmidt, A., H. Obrig, et al. (1996). "Simultaneous recording of cerebral blood oxygenation changes during human brain activation by magnetic resonance imaging and near-infrared spectroscopy." J Cereb Blood Flow Metab **16**(5): 817-26.

Kong, Y., Y. Zheng, et al. (2004). "A model of the dynamic relationship between blood flow and volume changes during brain activation." J Cereb Blood Flow Metab **24**(12): 1382-92.

Kotchoubey, B., U. Strehl, et al. (1999). "Control of cortical excitability in epilepsy." Adv Neurol. **81**: 281-90.

Kotz, S. A., S. Frisch, et al. (2003). "Syntactic language processing: ERP lesion data on the role of the basal ganglia." J Int Neuropsychol Soc **9**(7): 1053-60.

LaConte, S., S. Strother, et al. (2005). "Support vector machines for temporal classification of block design fMRI data." Neuroimage. **26**(2): 317-29. Epub 2005 Mar 24.

Laconte, S. M., S. J. Peltier, et al. (2006). "Real-time fMRI using brain-state classification." Hum Brain Mapp.

Lang, P. J., M. M. Bradley, et al. (NIMH Center for the Study of Emotion and Attention 1997). International Affective Picture System (IAPS): Technical Manual and Affective Ratings, NIMH Center for the Study of Emotion and Attention.

Liang, K. C., J. L. McGaugh, et al. (1982). "Post-training amygdaloid lesions impair retention of an inhibitory avoidance response." Behav Brain Res **4**(3): 237-49.

Logothetis, N. K. (2002). "The neural basis of the blood-oxygen-level-dependent functional magnetic resonance imaging signal." Philos Trans R Soc Lond B

Biol Sci. **357**(1424): 1003-37.

Logothetis, N. K. (2003). "The underpinnings of the BOLD functional magnetic resonance imaging signal." J Neurosci. **23**(10): 3963-71.

Logothetis, N. K. (2007). "The ins and outs of fMRI signals." Nat Neurosci **10**(10): 1230-2.

Logothetis, N. K. (2008). "What we can do and what we cannot do with fMRI." Nature **453**(7197): 869-78.

Logothetis, N. K., J. Pauls, et al. (2001). "Neurophysiological investigation of the basis of the fMRI signal." Nature. **412**(6843): 150-7.

Logothetis, N. K. and J. Pfeuffer (2004). "On the nature of the BOLD fMRI contrast mechanism." Magn Reson Imaging. **22**(10): 1517-31.

Lykken, D. T. (1957). "A study of anxiety in the sociopathic personality." J Abnorm Psychol **55**(1): 6-10.

Martin, C., J. Martindale, et al. (2006). "Investigating neural-hemodynamic coupling and the hemodynamic response function in the awake rat." Neuroimage **32**(1): 33-48.

Mathiak, K. and S. Posse (2001). "Evaluation of motion and realignment for functional magnetic resonance imaging in real time." Magn Reson Med. **45**(1): 167-71.

McGaugh, J. L., J. L. Martinez, Jr., et al. (1982). "Role of neurohormones as modulators of memory storage." Adv Biochem Psychopharmacol **33**: 123-30.

Meng, M. and M. Bader (2000). "Mode of disambiguation and garden path strength: an investigation of subject- object ambiguities in German." Lang Speech **43**: 43-74.

Mesulam, M. and E. Mufson (1982). "Insula of the old world monkey. III: Efferent cortical output and comments on function." J. Comp. Neurol **212**: 38-52.

Mesulam, M. M. and E. J. Mufson (1982). "Insula of the old world monkey. I. Architectonics in the insulo-orbito-temporal component of the paralimbic brain." J. Comp. Neurol **212**: 1-22.

Michaloudi, H., I. Grivas, et al. (2005). "Areal and laminar variations in the vascularity of the visual, auditory, and entorhinal cortices of the developing rat brain." Brain Res Dev Brain Res **155**(1): 60-70.

Mitchell, T. M., R. Hutchinson, et al. (2003). "Classifying instantaneous cognitive states from FMRI data." AMIA Annu Symp Proc: 465-9.

Miyai, I., H. C. Tanabe, et al. (2001). "Cortical mapping of gait in humans: a near-infrared spectroscopic topography study." Neuroimage **14**(5): 1186-92.

Mochizuki, H., Y. Ugawa, et al. (2006). "Cortical hemoglobin-concentration changes under the coil induced by single-pulse TMS in humans: a simultaneous recording with near-infrared spectroscopy." Exp Brain Res **169**(3): 302-10.

Moonen, C. T. W. and P. A. Bandettini, Eds. (2000). Functional MRI. Berlin, Springer.

Moore, C. I. and R. Cao (2008). "The hemo-neural hypothesis: on the role of blood flow in information processing." J Neurophysiol **99**(5): 2035-47.

Morris, J. S., K. J. Friston, et al. (1998). "A neuromodulatory role for the human amygdala in processing emotional facial expressions." Brain **121 (Pt 1)**: 47-57.

Morris, J. S., A. Ohman, et al. (1998). "Conscious and unconscious emotional learning in the human amygdala." Nature **393**(6684): 467-70.

Mourao-Miranda, J., A. L. Bokde, et al. (2005). "Classifying brain states and determining the discriminating activation patterns: Support Vector Machine on

functional MRI data." <u>Neuroimage.</u> **28**(4): 980-95. Epub 2005 Nov 4.

Murphy, F. C., I. Nimmo-Smith, et al. (2003). "Functional neuroanatomy of emotions: a meta-analysis." <u>Cogn Affect Behav Neurosci</u> **3**(3): 207-33.

Naito, M., Y. Michioka, et al. (2007). "A Communication Means for Totally Locked-in ALS Patients Based

on Changes in Cerebral Blood Volume Measured with

Near-Infrared Light." <u>IEICE TRANS. INF. & SYST.</u> **E90-D**(No.7).

Nicolelis, M. A. (2003). "Brain-machine interfaces to restore motor function and probe neural circuits." <u>Nat Rev Neurosci.</u> **4**(5): 417-22.

Nicolelis, M. A. and J. K. Chapin (2002). "Controlling robots with the mind." <u>Sci Am.</u> **287**(4): 46-53.

Noguchi, Y., E. Watanabe, et al. (2003). "An event-related optical topography study of cortical activation induced by single-pulse transcranial magnetic stimulation." <u>Neuroimage</u> **19**(1): 156-62.

Norman, K. A., S. M. Polyn, et al. (2006). "Beyond mind-reading: multi-voxel pattern analysis of fMRI data." <u>Trends Cogn Sci</u> **10**(9): 424-30.

Obermaier, B., C. Guger, et al. (2001). "Hidden Markov models for online classification of single trial EEG data." <u>Pattern Recognition Letters</u>(22): 1299-1309.

Obermaier, B., C. Guger, et al. (1999). "Hidden Markov models used for the offline classification of EEG data." <u>Biomed Tech (Berl)</u> **44**(6): 158-62.

Ochsner, K. N., R. D. Ray, et al. (2004). "For better or for worse: neural systems supporting the cognitive down- and up-regulation of negative emotion." <u>Neuroimage</u> **23**(2): 483-99.

Ogawa, S., T. M. Lee, et al. (1990). "Brain magnetic-resonance-imaging with contrast dependent on blood oxygenation." <u>Proceedings of National Academy of Science, USA</u> **87**: 9868--9872.

Okada, M., Firbank, M., Schweiger, S., Arridge, M., Delpy, C.D. (1997). "Theoretical and experimental investigation of the near-infrared light propogation in a model of the adult head." <u>Applied Optics</u> **36**(1): 21-31.

Oppenheimer, S. M., A. Gelb, et al. (1992). "Cardiovascular effects of human insular cortex stimulation." <u>Neurology</u> **42**(9): 1727-32.

Ostrowsky, K., J. Isnard, et al. (2000). "Functional mapping of the insular cortex: clinical implication in temporal lobe epilepsy." <u>Epilepsia</u> **41**(6): 681-6.

Parks, T. W., Burrus, C.S. (1987). <u>Digital Filter Design</u>. New York, John Wiley & Sons.

Patel, U. (1983). "Non-random distribution of blood vessels in the posterior region of the rat somatosensory cortex." <u>Brain Res</u> **289**(1-2): 65-70.

Patrick, C. J. (1994). "Emotion and psychopathy: startling new insights." <u>Psychophysiology</u> **31**(4): 319-30.

Patrick, C. J., B. N. Cuthbert, et al. (1994). "Emotion in the criminal psychopath: fear image processing." <u>J Abnorm Psychol</u> **103**(3): 523-34.

Paulus, M. P., J. S. Feinstein, et al. (2004). "Anterior cingulate activation in high trait anxious subjects is related to altered error processing during decision making." <u>Biol Psychiatry</u> **55**(12): 1179-87.

Paulus, M. P. and M. B. Stein (2006). "An insular view of anxiety." <u>Biol Psychiatry</u> **60**(4): 383-7.

Penfield, W. and M. E. Faulk, Jr. (1955). "The insula; further observations on its function." <u>Brain</u> **78**(4): 445-70.

Peyron, R., B. Laurent, et al. (2000). "Functional imaging of brain responses to pain.

A review and meta-analysis (2000)." <u>Neurophysiol Clin</u> **30**(5): 263-88.

Pfurtscheller, G., B. Graimann, et al. (2004). "Brain-computer communication based on the dynamics of brain oscillations." <u>Suppl Clin Neurophysiol</u> **57**: 583-91.

Pfurtscheller, G., C. Guger, et al. (2000). "Brain oscillations control hand orthosis in a tetraplegic." <u>Neurosci Lett</u> **292**(3): 211-4.

Pfurtscheller, G., G. R. Muller-Putz, et al. (2006). "15 years of BCI research at Graz University of Technology: current projects." <u>IEEE Trans Neural Syst Rehabil Eng</u> **14**(2): 205-10.

Pfurtscheller, G., C. Neuper, et al. (2000). "Current trends in Graz Brain-Computer Interface (BCI) research." <u>IEEE Trans Rehabil Eng</u> **8**(2): 216-9.

Phan, K. L., D. A. Fitzgerald, et al. (2006). "Association between amygdala hyperactivity to harsh faces and severity of social anxiety in generalized social phobia." <u>Biol Psychiatry</u> **59**(5): 424-9.

Phan, K. L., T. Wager, et al. (2002). "Functional neuroanatomy of emotion: a meta-analysis of emotion activation studies in PET and fMRI." <u>Neuroimage</u> **16**(2): 331-48.

Phillips, M. L., A. W. Young, et al. (1997). "A specific neural substrate for perceiving facial expressions of disgust." <u>Nature</u> **389**(6650): 495-8.

Pollock, D. S. G. (1999). <u>A Handbook of Time-Series Analysis, Signal Processing and Dynamics.</u> San Diego,CA, Academic Press.

Polyn, S. M., V. S. Natu, et al. (2005). "Category-specific cortical activity precedes retrieval during memory search." <u>Science</u> **310**(5756): 1963-6.

Posse, S., F. Binkofski, et al. (2001). "A new approach to measure single-event related brain activity using real-time fMRI: feasibility of sensory, motor, and higher cognitive tasks." <u>Hum Brain Mapp.</u> **12**(1): 25-41.

Rabiner, L. and B. H. Juang (1993). <u>Fundamentals of Speech Recognition</u>. Englewoord Cliffs, NJ, Prentice-Hall.

Rabiner, L. R. (1989). "A tutorial on hidden Markov models and selected applications in speech recognition." <u>Proceedings of the IEEE</u> **77**(2): 257-286.

Rabiner, L. R. (1989). "A tutorial on hidden Markov models and selected applications in speech recognition." <u>Proceedings of the IEEE</u> **vol. 77**(no. 2): pp. 257-286.

Reiman, E. M., M. J. Fusselman, et al. (1989). "Neuroanatomical correlates of anticipatory anxiety." <u>Science</u> **243**(4894 Pt 1): 1071-4.

Reiman, E. M., R. D. Lane, et al. (1997). "Neuroanatomical correlates of externally and internally generated human emotion." <u>Am J Psychiatry</u> **154**(7): 918-25.

Roberts, L. E., N. Birbaumer, et al. (1989). "Self-report during feedback regulation of slow cortical potentials." <u>Psychophysiology.</u> **26**(4): 392-403.

Rockstroh, B., T. Elbert, et al. (1990). "Biofeedback-produced hemispheric asymmetry of slow cortical potentials and its behavioural effects." <u>Int J Psychophysiol.</u> **9**(2): 151-65.

Roebroeck, A., E. Formisano, et al. (2005). "Mapping directed influence over the brain using Granger causality and fMRI." <u>Neuroimage</u> **25**(1): 230-42.

Rolls, E. T. (1996). "The orbitofrontal cortex." <u>Philos Trans R Soc Lond B Biol Sci</u> **351**(1346): 1433-43; discussion 1443-4.

Rolls, E. T. (2004). "The functions of the orbitofrontal cortex." <u>Brain Cogn</u> **55**(1): 11-29.

Rota, G., R. Sitaram, et al. (2008). "Self-regulation of regional cortical activity using real-time fMRI: The right inferior frontal gyrus and linguistic processing." <u>Hum Brain Mapp</u>.

Schienle, A., R. Stark, et al. (2002). "The insula is not specifically involved in disgust

processing: an fMRI study." Neuroreport **13**(16): 2023-6.

Schlosser, R. G., K. Koch, et al. (2007). "Assessing the state space of the brain with fMRI: an integrative view of current methods." Pharmacopsychiatry **40 Suppl 1**: S85-92.

Schroeter, M. L., M. M. Bucheler, et al. (2004). "Towards a standard analysis for functional near-infrared imaging." Neuroimage **21**(1): 283-90.

Schwartz, M. S. and Associates, Eds. (1995). Biofeedback: A Practitioner's Guide, Published by Guilford Press.

Serruya, M. D., N. G. Hatsopoulos, et al. (2002). "Instant neural control of a movement signal." Nature **416**(6877): 141-2.

Seth, A. K. (2005). "Causal connectivity analysis of evolved neural networks during behavior." Network: Computation in Neural Systems **16**: 35-55.

Seth, A. K. (2007). "Distinguishing causal interactions in neural populations." Neural Comput. **19**(4): 910-933.

Shiga, T., K. Yamamoto, et al. (1997). "Study of an algorithm based on model experiments and diffusion

theory for a portable tissue oximeter." J. Biomed. Opt. **2**: 154–161.

Shinba, T., M. Nagano, et al. (2004). "Near-infrared spectroscopy analysis of frontal lobe dysfunction in schizophrenia." Biol Psychiatry **55**(2): 154-64.

Shmuel, A., M. Augath, et al. (2006). "Negative functional MRI response correlates with decreases in neuronal activity in monkey visual area V1." Nat Neurosci. **9**(4): 569-77. Epub 2006 Mar 19.

Simmons, A., S. C. Matthews, et al. (2004). "Anticipation of emotionally aversive visual stimuli activates right insula." Neuroreport **15**(14): 2261-5.

Simmons, A., I. Strigo, et al. (2006). "Anticipation of aversive visual stimuli is associated with increased insula activation in anxiety-prone subjects." Biol Psychiatry **60**(4): 402-9.

Singer, T., B. Seymour, et al. (2004). "Empathy for pain involves the affective but not sensory components of pain." Science **303**(5661): 1157-62.

Sitaram, R. (2007). fMRI Brain-Computer Interfaces. 15th Annual Conference of International Society for Neurofeedback & Research, Current Perspectives in Neuroscience: Neuroplasticity & Neurofeedback, San Diego (USA).

Sitaram, R., A. Caria, et al. (2007). "fMRI Brain-Computer Interface: A Tool for Neuroscientific Research and Treatment." Computational Intelligence and Neuroscience 2007,Article ID 25487, 10 pages, 2007. doi:10.1155/2007/25487.

Sitaram, R., A. Caria, et al. (2005). Real-time fMRI based Brain-computer Interface enhanced by Interactive Virtual Worlds. 45th Annual Meeting Society for Psychophysiological Research, Lisbon, Portugal.

Sitaram, R., A. Caria, et al. (2006). "Functional Magnetic Resonance Imaging based BCI for

Neurorehabilitation." 3rd International Brain-Computer Interface Workshop and Training Course.

Sitaram, R., Y. Hoshi, et al., Eds. (2005). Near Infrared Spectroscopy based Brain-Computer Interface. Fundamental Problems of Optoelectronics and Microelectronics II, Proceedings of the SPIE.

Sitaram, R., S. Lee, et al. (2008). Real-time pattern classification and neurofeedback of emotion states in the brain in a fMRI brain-computer interface. Society for Neuroscience, Washington Convention Center: Hall A-C.

Sitaram, R., S. Lee, et al. (2008). Real-time Classification of Emotional States in an

fMRI Brain-Computer Interface. Society for Neuroscience, Washington DC.

Sitaram, R., N. Weiskopf, et al. (2008). "fMRI brain-computer interfaces: A tutorial on methods and applications." IEEE Signal Processing Magazine, Special Issue on BCI.

Sitaram, R., H. Zhang, et al. (2007). "Temporal classification of multichannel near-infrared spectroscopy signals of motor imagery for developing a brain-computer interface." Neuroimage **34**(4): 1416-27.

Snitz, B. E., A. MacDonald, 3rd, et al. (2005). "Lateral and medial hypofrontality in first-episode schizophrenia: functional activity in a medication-naive state and effects of short-term atypical antipsychotic treatment." Am J Psychiatry **162**(12): 2322-9.

Sprengelmeyer, R., A. W. Young, et al. (1996). "Loss of disgust. Perception of faces and emotions in Huntington's disease." Brain **119 (Pt 5)**: 1647-65.

Stein, M. B., A. N. Simmons, et al. (2007). "Increased amygdala and insula activation during emotion processing in anxiety-prone subjects." Am J Psychiatry **164**(2): 318-27.

Suto, T., M. Fukuda, et al. (2004). "Multichannel near-infrared spectroscopy in depression and schizophrenia: cognitive brain activation study." Biol Psychiatry **55**(5): 501-11.

Thulborn, K. R., P. A. Carpenter, et al. (1999). "Plasticity of language-related brain function during recovery from stroke." Stroke **30**(4): 749-54.

Toronov, V., M. A. Franceschini, et al. (2000). "Near-infrared study of fluctuations in cerebral hemodynamics during rest and motor stimulation: temporal analysis and spatial mapping." Med Phys **27**(4): 801-15.

Tremblay, M., F. Tam, et al. (2005). "Retrospective coregistration of functional magnetic resonance imaging data using external monitoring." Magn Reson Med **53**(1): 141-9.

Triantafyllou, C., R. D. Hoge, et al. (2005). "Comparison of physiological noise at 1.5 T, 3 T and 7 T and optimization of fMRI acquisition parameters." Neuroimage **26**(1): 243-50.

Tzourio-Mazoyer, N., B. Landeau, et al. (2002). "Automated anatomical labeling of activations in SPM using a macroscopic anatomical parcellation of the MNI MRI single-subject brain." Neuroimage **15**(1): 273-89.

van Gelderen, P., J. A. de Zwart, et al. (2007). "Real-time shimming to compensate for respiration-induced B0 fluctuations." Magn Reson Med **57**(2): 362-8.

Van Horn, J. D. and A. Ishai (2007). "Mapping the human brain: new insights from FMRI data sharing." Neuroinformatics **5**(3): 146-53.

Vapnik, V. N. (1998). Statistical Learning Theory. New York, Wiley.

Veit, R., H. Flor, et al. (2002). "Brain circuits involved in emotional learning in antisocial behavior and social phobia in humans." Neurosci Lett. **328**(3): 233-6.

Villringer, A. and B. Chance (1997). "Non-invasive optical spectroscopy and imaging of human brain function." Trends Neurosci **20**(10): 435-42.

Villringer, A. and H. Obrig (2002). Near Infrared Spectroscopy and Imaging, Elsevier Science (USA).

Villringer, A. and H. Obrig (2002). Near Infrared Spectroscopy and Imaging. In: Brain Mapping: The Methods, Elsevier Science (USA).

Wager, T. D., K. L. Phan, et al. (2003). "Valence, gender, and lateralization of functional brain anatomy in emotion: a meta-analysis of findings from neuroimaging." Neuroimage **19**(3): 513-31.

Ward, H. A., S. J. Riederer, et al. (2000). "Prospective multiaxial motion correction for fMRI." <u>Magn Reson Med</u> **43**(3): 459-69.

Weiskopf, N., C. Hutton, et al. (2006). "Optimal EPI parameters for reduction of susceptibility-induced BOLD sensitivity losses: a whole-brain analysis at 3 T and 1.5 T." <u>Neuroimage</u> **33**(2): 493-504.

Weiskopf, N., C. Hutton, et al. (2007). "Optimized EPI for fMRI studies of the orbitofrontal cortex: compensation of susceptibility-induced gradients in the readout direction." <u>Magma</u> **20**(1): 39-49.

Weiskopf, N., U. Klose, et al. (2005). "Single-shot compensation of image distortions and BOLD contrast optimization using multi-echo EPI for real-time fMRI." <u>Neuroimage.</u> **24**(4): 1068-79. Epub 2004 Dec 8.

Weiskopf, N., K. Mathiak, et al. (2004). "Principles of a brain-computer interface (BCI) based on real-time functional magnetic resonance imaging (fMRI)." <u>IEEE Trans Biomed Eng</u> **51**(6): 966-70.

Weiskopf, N., F. Scharnowski, et al. (2004). "Self-regulation of local brain activity using real-time functional magnetic resonance imaging (fMRI)." <u>J Physiol Paris</u> **98**(4-6): 357-73.

Weiskopf, N., R. Sitaram, et al. (2007). "Real-time functional magnetic resonance imaging: methods and applications." <u>Magn Reson Imaging</u>.

Weiskopf, N., R. Sitaram, et al. (2007). "Real-time functional magnetic resonance imaging: methods and applications." <u>Magn Reson Imaging</u> **25**(6): 989-1003.

Weiskopf, N., R. Veit, et al. (2003). "Physiological self-regulation of regional brain activity using real-time functional magnetic resonance imaging (fMRI): methodology and exemplary data." <u>Neuroimage.</u> **19**(3): 577-86.

Wieser, H. (1983). <u>Electroclinical features of the psychomotor seizure.</u> Stuttgart, Gustav Fisher.

Wolf, M., U. Wolf, et al. (2002). "Functional frequency-domain near-infrared spectroscopy detects fast neuronal signal in the motor cortex." <u>Neuroimage</u> **17**(4): 1868-75.

Wolf, M., U. Wolf, et al. (2003). "Detection of the fast neuronal signal on the motor cortex using functional frequency domain near infrared spectroscopy." <u>Adv Exp Med Biol</u> **510**: 193-7.

Wolf, M., U. Wolf, et al. (2003). "Fast cerebral functional signal in the 100-ms range detected in the visual cortex by frequency-domain near-infrared spectrophotometry." <u>Psychophysiology</u> **40**(4): 521-8.

Wolpaw, J. R. (2004). "Brain-computer interfaces (BCIs) for communication and control: a mini-review." <u>Suppl Clin Neurophysiol</u> **57**: 607-13.

Wolpaw, J. R., N. Birbaumer, et al. (2000). "Brain-computer interface technology: a review of the first international meeting." <u>IEEE Trans Rehabil Eng.</u> **8**(2): 164-73.

Wolpaw, J. R., N. Birbaumer, et al. (2002). "Brain-computer interfaces for communication and control." <u>Clin Neurophysiol</u> **113**(6): 767-91.

Wolpaw, J. R., N. Birbaumer, et al. (2002). "Brain-computer interfaces for communication and control." <u>Clin Neurophysiol.</u> **113**(6): 767-91.

Wolpaw, J. R., G. E. Loeb, et al. (2006). "BCI Meeting 2005--workshop on signals and recording methods." <u>IEEE Trans Neural Syst Rehabil Eng</u> **14**(2): 138-41.

Woolsey, T. A., C. M. Rovainen, et al. (1996). "Neuronal units linked to microvascular modules in cerebral cortex: response elements for imaging the brain." <u>Cereb Cortex</u> **6**(5): 647-60.

Wright, P., G. He, et al. (2004). "Disgust and the insula: fMRI responses to pictures of

mutilation and contamination." Neuroreport **15**(15): 2347-51.

Yoo, S. S., T. Fairneny, et al. (2004). "Brain-computer interface using fMRI: spatial navigation by thoughts." Neuroreport. **15**(10): 1591-5.

Yoo, S. S. and F. A. Jolesz (2002). "Functional MRI for neurofeedback: feasibility study on a hand motor task." Neuroreport. **13**(11): 1377-81.

Young, S. J., P. C. Woodland, et al. (1993). HTK Version 1.5: User, Reference and Programmer Manual. Washington DC, Entropic Research Laboratories.

Zheng, D., A. S. LaMantia, et al. (1991). "Specialized vascularization of the primate visual cortex." J Neurosci **11**(8): 2622-9.